ABSTRACT

TANG, WENXING. New Solid-State NMR Methodologies for Structure Determination of Membrane Proteins: Sensitivity Enhancement, Spectroscopic Assignment, and Macroscopic Alignment. (Under the direction of Professor Alexander A. Nevzorov.)

Oriented-sample NMR (OS NMR) has emerged as a powerful tool for structure determination of membrane proteins in their native lipid environment. In the present work, we address three issues of critical importance for OS NMR of membrane proteins: sensitivity enhancement, spectroscopic assignment, and macroscopic alignment. (i). A repetitive-contact cross-polarization (REP-CP) scheme was developed that allows one to fully transfer the thermodynamic limit of polarization from the abundant protons to low-gamma nuclei. As a result, a factor of two (2) enhancement in sensitivity was gained over the single-contact traditional CP, whereas 45% average intensity gain is achieved as compared to CP-MOIST, currently the most widely used CP scheme in OS NMR. (ii). We have also developed a strategy for assigning solid-state NMR spectra of Pf1 coat protein reconstituted in magnetically aligned bicelles, and obtained a two-dimensional spin-exchanged version of the SAMPI4 spectrum correlating ^{15}N chemical shift and ^{15}N-^{1}H dipolar couplings. Combining the spin-exchanged version with the original SAMPI4 experiment makes it possible to establish sequence-specific assignments, and this technique is generally applicable to other membrane proteins. Notably, only a single uniformly labeled protein sample is required as opposed to multiple selectively labeled samples currently employed for spectroscopic assignment. Using sensitivity enhancement techniques such as REP-CP assists in further elucidating cross peaks and allows the establishment of correlations between the adjacent residue along the backbone. Simulation accurately predicts the optimal MMHH condition as well as explains experimental trends. (iii). Finally, we also successfully applied a new

method to align membrane proteins into the lipid bilayers and obtained high-resolution OS NMR spectra of the uniformly ^{15}N labeled transmembrane domain of Pf1 coat protein. Nanoporous anodic aluminum oxide (AAO) sheets have been proven to be an alternative alignment system for the study of membrane proteins in their native environments by means of solid-state NMR. AAO-supported bilayers have the potential of providing an alternative membrane mimic of highly flexible composition for the structure-function studies of membrane proteins.

New Solid-State NMR Methodologies for Structure Determination of Membrane Proteins: Sensitivity Enhancement, Spectroscopic Assignment, and Macroscopic Alignment

by
Wenxing Tang

A dissertation submitted to the Graduate Faculty of
North Carolina State University
in partial fulfillment of the
requirements for the degree of
Doctor of Philosophy

Chemistry

Raleigh, North Carolina

2013

APPROVED BY:

_____	_____
Professor Alexander A. Nevzorov Committee Chair	Professor Edmond F. Bowden
_____	_____
Professor Tatyana I. Smirnova	Professor Reza A. Ghiladi

DEDICATION

To my family.

BIOGRAPHY

Early in one morning in February, 1982, a new born child took his first look at this world in a city called Tianjin in northern China. His overjoyed parents were both majored in Literature and hence named him Wenxing, which direct translates as “a rising star in literature”. None of them know at that point that, some day he will go to the United States. Neither did they expect that, he will major in Chemistry and focus on solid-state NMR.

Time flies. At the age of 18, Wenxing was accepted by one of the oldest university in China, Tianjin University. He applied to be majored in Architecture or Civil Engineering, but was, somehow, enrolled by the Department of Chemistry.

Wenxing was really depressed, and his way of fighting back was to skip all the classes. Till the 4th year. One of the mandatory classes, Biochemistry, was offered by Prof. Wang, who received his Ph.D at Columbia University and was the vice dean of Department of Pharmaceutical Science. Wenxing became so fascinated by his class that, he, for the first time, found bio-related subject interesting. It was also at that time that, he made up his mind to go to the United States.

The summer of 2008 will always be remembered, because it was when Wenxing’s dream finally came true: he was enrolled by the Department of Chemistry, again. Only this time it was by his own will. He chose to join Prof. Nevzorov’s group to study membrane proteins with solid-state NMR, which he had absolutely no idea about.

During the years, he made a lot of friends, had a lot of fun. He met with a beautiful girl on his first visit to DMV and married her.

He loves his group. He loves research. He loves his life here.

And now, after 4 years of study, he thinks he could finally say he knows a little bit about what he’s been doing, even though he’s still trying to pick up quantum mechanics.

What next? We’ll see.

ACKNOWLEDGMENTS

This work would not have been possible without the support of many people. First and foremost, I would like to express my deep and sincere gratitude to my adviser, Professor Alexander A. Nevzorov. He patiently trained me when I first joined the group, and gradually guided me into the field of solid-state NMR. Throughout the years, his enlightening discussion over different topics has truly broadened my knowledge and outlook. His unique way of thinking not only helped me in solving research related problems, but also appreciating more on what's normally viewed as basic. It was his encouragement, motivation and support that made my Ph.D. experience productive and joyful. His clear vision both in research and life inspires me. I could not have asked for a better mentor and friend.

Many people on the faculty and staff of the Department of Chemistry assisted and encouraged me in various ways during my course of studies. I am especially grateful to Prof. Tatyana I. Smirnova, Prof. Reza A. Ghiladi, Prof. Edmond F. Bowden and Prof. Hanna Gracz for being my committee members.

My deepest gratitude is also due to other group members for their constant support and laughs. They provided a great atmosphere for research and study.

Last but not least, I would like to thank my family and friends for their constant love and support. They have always been there at every turn of my life. And I must thank my wife for all the delicious food she cooked.

TABLE OF CONTENTS

LIST OF TABLES

APPENDICES

LIST OF FIGURES

CHAPTER 1 INTRODUCTION

CHAPTER 1

INTRODUCTION

1.1 Membrane proteins and the challenges in their structure determination

The proteins that span the cell membrane perform an array of functions that are vital to our lives. These functions include, but are not limited to: ion transport, signal transduction, energy regulation, pathway activation, and molecular recognition. It has been proven that, the misfolding of the secondary structure generally leads to the malfunction of the membrane protein, some of which are directly related to serious diseases such as cancer. In addition, the vital role of membrane proteins could also be reflected by the fact that they are the targets of more than 50% of the modern drugs (1). However, despite their critical importance and the fact that ~30% of all proteins in eukaryotic cells are membrane proteins (2), only 371 unique membrane protein structures have been solved to date (http://blanco.biomol.uci.edu/mpstruc/query), which accounts for less than 1% of the total protein structures deposited in the Protein Data Bank (PDB). This is mainly due to the fact that high-resolution structures of integral membrane proteins in phospholipid bilayers have been notoriously difficult to obtain by either X-ray diffraction or solution NMR methods.

Despite its success in solving the structures of soluble proteins, X-ray crystallography (XRC) of membrane proteins, which is generally achieved with the aid of detergents, might still be considered a high art. And the reason is that, the method itself requires the sample to be trapped in a crystal conformation. However, this requirement introduces a few complications. First, the dynamic regions of a protein cannot be efficiently studied as they

would either get trapped in some energetically favorable intermediate conformations, or would result in a blurred region representing the average of all possible conformations. Second, potential loss of structural lipids, due to the existence of detergents, may lead to protein misfolding or denaturation (3). Finally, many membrane proteins are extremely difficult or even impossible to be crystallized due to their amphiphilic nature of having both the hydrophobic and hydrophilic regions (4).

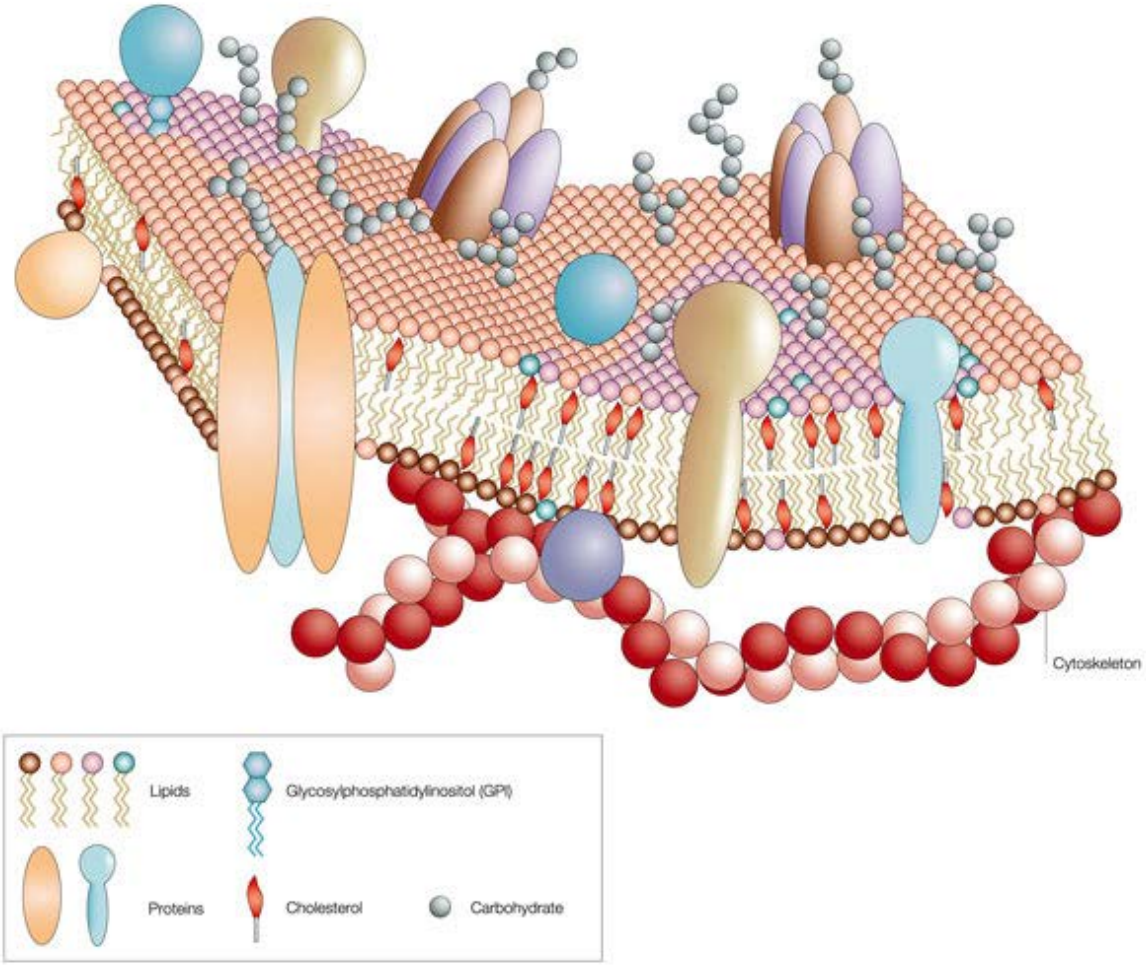

Figure 1.1 A cartoon representation of the cell membrane showing its essential components. (http://www.nature.com/scitable/topicpage/protein-function-14123348)

Solution-state NMR is another highly utilized experimental method; however, it requires the proteins to rapidly reorient in solution. Large vesicular assemblies such as liposomes have proven to be much too large for their reorientation time to be fast enough for the solution-state NMR time scale (5). Nevertheless, some progress has been made in the structural studies of membrane proteins by utilizing phospholipid micelles, which rapidly reorient in aqueous solutions (6). However, micelles represent less than an ideal structure since their highly curved geometry significantly differs from that of the biological membranes. Furthermore, many membrane proteins require a full bilayer in order to be reconstituted in a native-like conformation (7,8) and their structure in micelles can be considerably different from that in bicelles which mimic more closely the native lipid environment (9,10).

In contrast, solid-state NMR (SSNMR) spectroscopy has become an effective alternative approach for studying membrane proteins in their native-like functional environment. There are two different approaches in the realm of SSNMR: magic-angle spinning (MAS) and oriented-sample (OS) NMR. The first involves spinning the sample at a specific angle, which is 54.7°, with regard to the external magnetic field B_0, to average out the anisotropic terms such as dipolar couplings, and obtain spectra at high resolution. Whereas the latter approach involves macroscopic sample alignment, either mechanically or magnetically, the OS NMR spectrum directly contains structural information of the target protein. Proteins whose structures have been successfully investigated by SSNMR include, but are not limited to, gramicidin (11), rhodopsin (12), Pf1 phage-coat protein (13), AchR

M2 domain (14), M2 domain of the influenza A virus (15), phospholamban (16), Vpu from HIV-1(17), and MerF (18).

1.2 Most widely used pulse sequences by oriented-sample NMR

1.2.1 Polarization Inversion Spin Exchange at the Magic Angle (PISEMA)

Ever since its introduction in 1994 by C. H. Wu, A. Ramamoorthy and S. J. Opella (19), PISEMA has become one of the most powerful tools for high-resolution SSNMR of membrane proteins. The main idea is to combine polarization inversion of the *S* spin (e.g. nitrogens) with the flip-flop Lee-Goldburg homonuclear decoupling on the abundant *I* spins (e.g. protons) following spin-lock cross polarization to the dilute *S* spins during the t_1 evolution. In this way, the experiment yields a two-dimensional correlation of the chemical shift of the sparse spin *S* with the heteronuclear *IS* dipolar coupling. As a result, linewidths are remarkably reduced in the dipolar dimension compared to that of the conventional separated-local-field (SLF) spectrum. Pulse sequences for the conventional SLF experiment as well as the PISEMA experiments are depicted in Figure 1.2. Furthermore, dipolar splitting and chemical-shift frequencies could also be used in combination in three-dimensional spectra to enhance resolution even further.

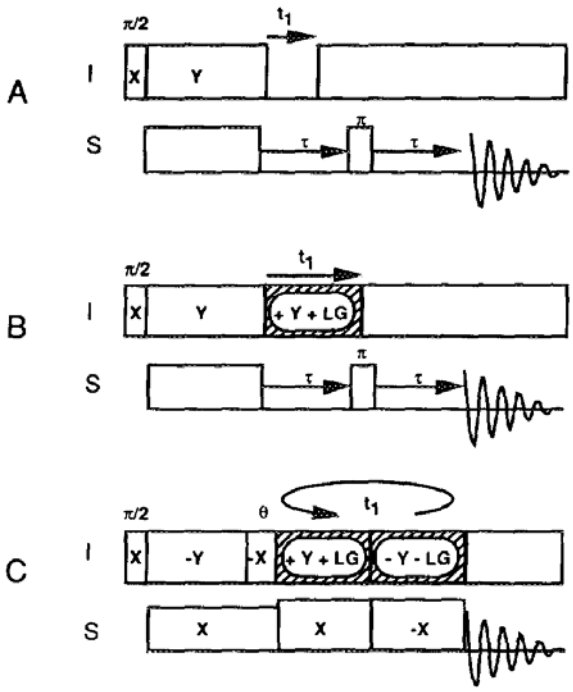

Figure 1.2 Pulse sequences for two-dimensional heteronuclear dipolar/chemical-shift spectroscopy. (A) Simplest version of the SLF experiment. (B) SLF experiment with Lee-Goldburg homonuclear decoupling applied during the t_1 period. (C) PISEMA experiment. Figure taken from Ref. (19).

1.2.2 SAMMY pulse sequence with π/4 pulse correction (SAMPI4)

Though providing heteronuclear dipolar coupling spectra with higher resolution compared to conventional separated local-field experiments, PISEMA, being sensitive to the choice of ^{1}H carrier frequency, suffers from unstable performance when the range of ^{1}H frequencies is broad. This is intrinsic to PISEMA because it is based on the off-resonance Lee-Goldburg (20) irradiation for ^{1}H homonuclear decoupling. Consequently, PISEMA is not ideal to be used for the study of membrane proteins refolded in their native like

environments, since such a complex system would give rise to a wide range of ^{1}H resonance frequencies.

To overcome this problem, a pulse sequence based on the Average Hamiltonian Theory (AHT) was implemented by Nevzorov and Opella in 2003 (21). In order to remove the homonuclear interactions between various ^{1}H spins, a "magic sandwich" pulse scheme was incorporated (hence the name "SAMMY"), instead of the frequency-switched Lee-Goldburg irradiation. The pulse program is diagrammed in Figure 1.3.

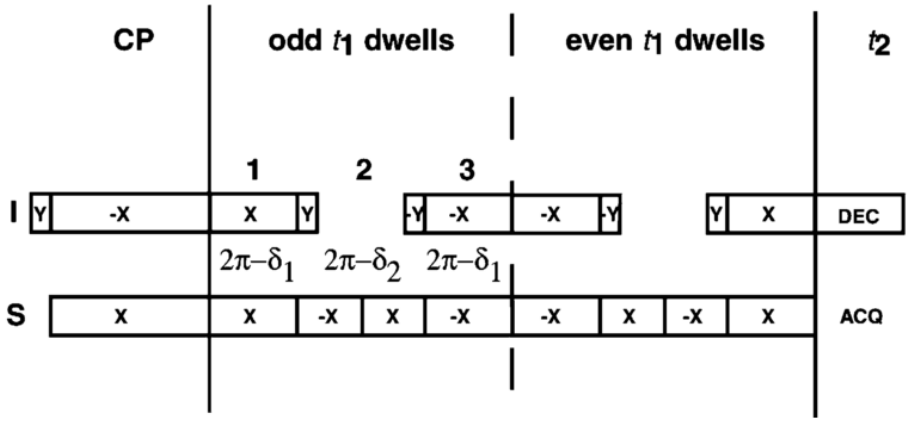

Figure 1.3 The pulse sequence of SAMMY. The heteronuclear interaction evolves during section 1 and 3. During section 2, the *S* spins are decoupled from the abundant *I* spins. To achieve optimal decoupling, the duration of section 1, 2 and 3 requires experimental adjustments. Figure taken from Ref. (21)

Unfortunately, spectroscopic studies have shown that the linewidths for most resonances in the heteronuclear dipolar coupling dimension of two-dimensional SAMMY spectra, although more uniform, are typically about 50% greater than that of PISEMA.

Combining the broadband capability of SAMMY with the line-narrowing ability of PISEMA in a single experiment has then become the next goal.

In 2007, an improved version of SAMMY, which is termed as SAMPI4, pulse scheme was proposed (22). And the pulse diagram is depicted in Figure 1.4. Generally, it yields sub-200 Hz linewidths in the heteronuclear dipolar coupling dimension while covering the broad ranges of frequencies given rise from the aligned samples of membrane proteins reconstituted in lipid bilayers under high magnetic fields.

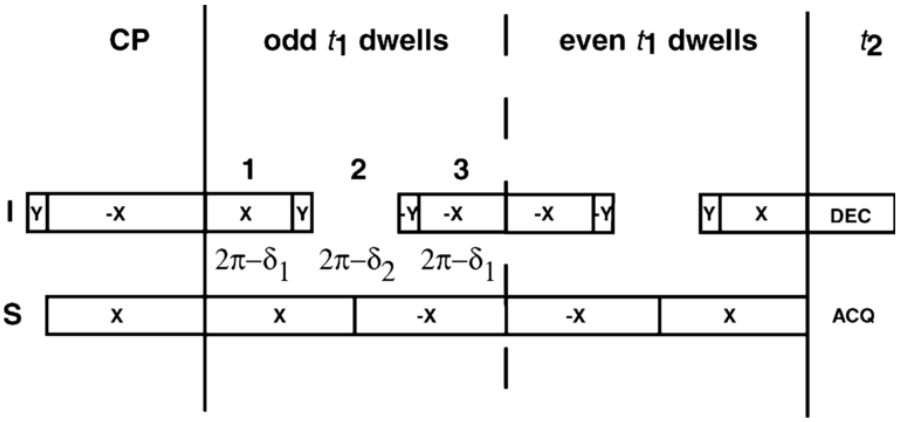

Figure 1.4 The SAMPI4 pulse sequence. Compared with SAMMY in Figure 1.3, only one phase alteration on the S spin channel is used. A $\pi/4$ pulse correction is applied to δ_1 and δ_2. Figure taken from Ref.(22).

1.3 Polarity Index Slant Angle (PISA) Wheels

Resonance patterns observed in two-dimensional Oriented-Sample NMR spectra provide structural details of the protein molecule. As was introduced in the previous section,

the PISEMA sequence gives high-resolution ^{1}H-^{15}N dipolar coupling/^{15}N chemical shift separated-local-field (SLF) spectra where the individual resonances contain orientational constraints for structure determination (19). It has been shown that the PISEMA spectra of membrane proteins reconstituted in the magnetically aligned lipid bilayers are good indicators of α-helical structure (23,24). For helical proteins, these spectra exhibit characteristic wheel-like patterns of resonances, which are termed as "Polar Index Slant Angle" (PISA) wheels, and reflect helical wheel projections of residues (25). These wheels are useful both in assigning the resonances and in determining the general orientation of α-helices, as well as β-sheets (26), with respect to the magnetic field.

Figure 1.5 is a demonstration of the calculated PISA wheels caused by the variation of the helix tilt angle with respect to the bilayer normal. One could easily tell that the resonance frequencies dramatically depend on the helical orientation.

Together with the high resolution of PISEMA or SAMPI4 spectra, these achievements make Oriented-Sample NMR a powerful tool for obtaining structural information about membrane proteins, which are generally difficult to study using X-ray crystallography or solution NMR.

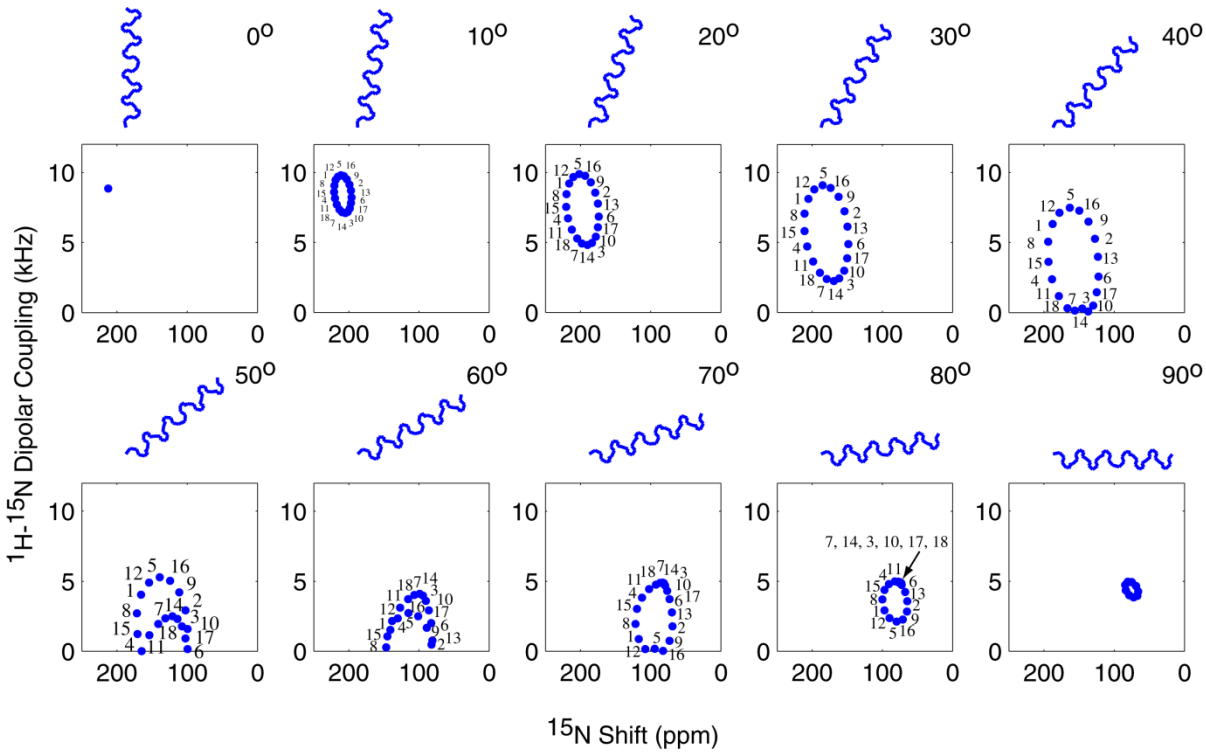

Figure 1.5 PISEMA spectra calculated for a 19-residue α-helix with 3.6 residues per turn and uniform dihedral angles (φ= -65, ψ= -40) at various helix tilt angles relative to the bilayer normal.

1.4 Sample alignment in the study of membrane proteins by OSNMR

1.4.1 The use of glass plates

Pioneered by Seelig and Gally (27), the use of glass plates as a media to mechanically align NMR sample could be dated back to the 1970s, and is now widely used in the study of membrane proteins in their native environments. The idea is to refold membrane proteins into the lipid bilayers supported on the surface of glass plates, so that most, if not all, the protein

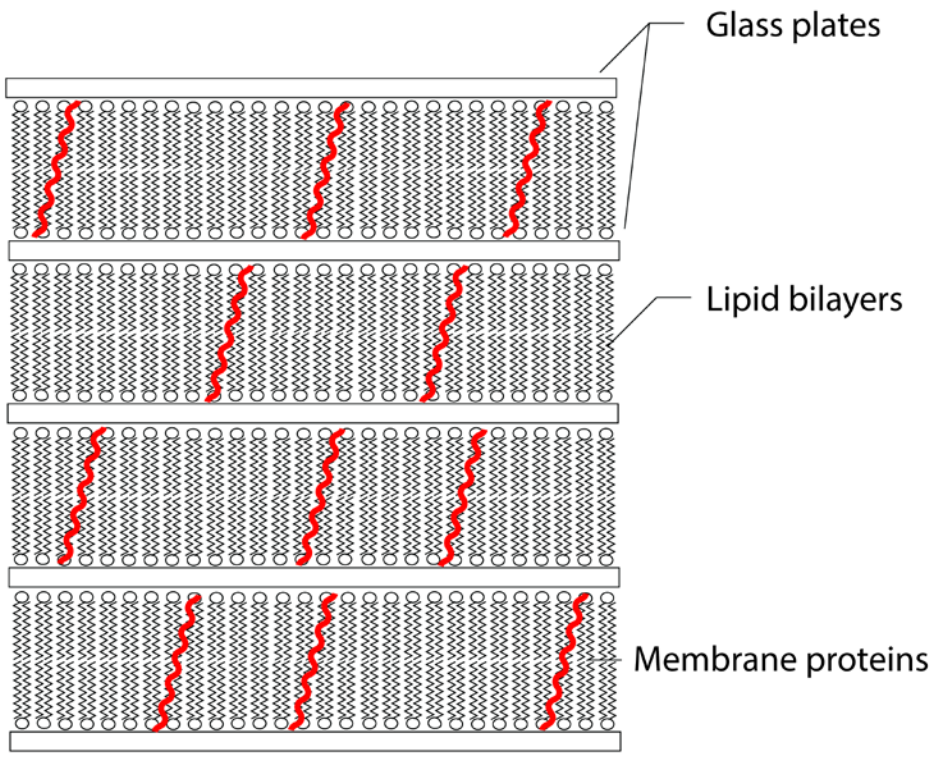

Figure 1.6 A demonstration of reconstituting membrane proteins into lipid bilayers supported by glass plates

molecules are oriented in the same way with regard to the external magnetic field. By doing so, the uniformity of the alignment, instead of molecular motions, narrows down the spectroscopic linewidths, and hence benefits the structural study of membrane proteins with SSNMR. Figure 1.6 is a demonstration of such a scheme. One of the greatest advantages of mechanically aligned samples on glass plates is that, NMR spectra can be acquired as a function of sample orientation when necessary. However, the drawbacks of such a design are quite obvious. First of all, the majority of the limited volume in the NMR tube is occupied by

the glass plates, which limits the maximum amount of lipid molecules as well as the target proteins that could be deposited. On the other hand, it's hard to maintain the surface of a sample fully hydrated since it is directly exposed to the environment.

1.4.2 The use of bicelles

In the past decades, researchers have developed various models to investigate the structure and dynamics of membrane proteins in their native-like environments such as micelles (6), multilamellar vesicles (28), unilamellar vesicles (29) or mechanically oriented bilayers between glass plates (30,31). Recently, an alternative system, which represents a combination of micelles and vesicles, became widely used. The foundation for this system was laid in the pioneering work of Roberts and co-workers on "bilayered micelles" in the early 1980s (32). In 1992, Sanders and Schwonek have made an interesting discovery that the mixture of DMPC and DHPC has the ability to spontaneously align in an external magnetic field (33). This phenomenon makes the system extremely valuable for the NMR study of membrane proteins. Further improvement of this model system has lead to a change in the terminology to "bicelles" (7) in 1995.

Nowadays, bicelles are normally referred to as the aqueous suspension of the mixture of aliphatic long chain lipids (between 12 and 16 carbons) and short chain lipids (6–8 carbons). The most recognized organization is a nanodisc with the long chain lipids forming the disc plane and the short chain lipids mainly distributed in the torus of the disc.

The reason that bicelles align in the presence of the external magnetic field is mainly due to the diamagnetic susceptibility anisotropy of phospholipids, $\Delta\chi$ (which is the difference

between the parallel ($\chi_{\parallel}$) and the perpendicular ($\chi_{\perp}$) magnetic susceptibility to the long lipid axis: $\Delta\chi = \chi_{\parallel} - \chi_{\perp}$). Hence, it is possible to "flip" the bicelles by adding a component with a positive $\Delta\chi$.

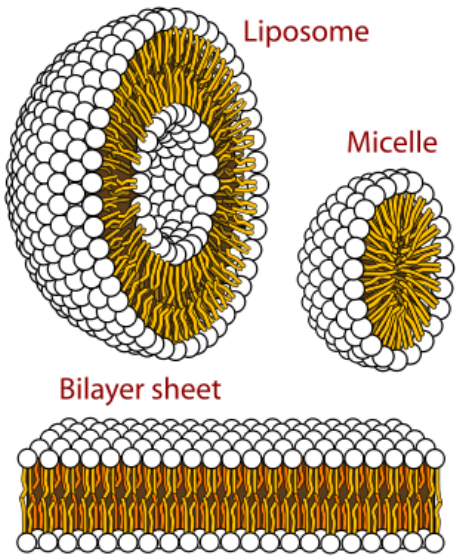

Figure 1.7. Structures that can be formed by phospholipids in aqueous solutions. (http://en.wikipedia.org/wiki/Micelle)

The most widely used method now is the addition of a small amount of lanthanide ions, Yb^{3+} for example. Spectra studies of various proteins reconstituted in magnetically aligned bicelles in both orientations have been published (18,34). A comparison of the spectra obtained for the perpendicular and parallel bicelle orientations are useful in cross-validating the results

and, in some cases, can even provide a method for assigning solid-state NMR spectra of membrane proteins (35).

The use of magnetically aligned bicelles in the structural studies of membrane proteins provides numerous benefits, the most important one being relatively easy sample preparation. In addition, the use of a sealed tube containing a liquid sample not only prolongs the life-time of the sample but also enables its placement inside a solenoid coil, which allows for optimal NMR probe performance. Furthermore, the availability of instant control over different sample parameters, such as pH and solvent composition, makes it possible to perform many standard procedures, such as hydrogen/deuterium exchange experiments (17,36). However, bicelles are not perfect; they also have their disadvantages. First, the choices of lipid combinations are limited, since not all lipids align in an external magnetic field. Second, each lipid combination has its own restricted temperature range. However, experimental solutions to these problems have been found by introducing mixed long-chain lipid combinations (37).

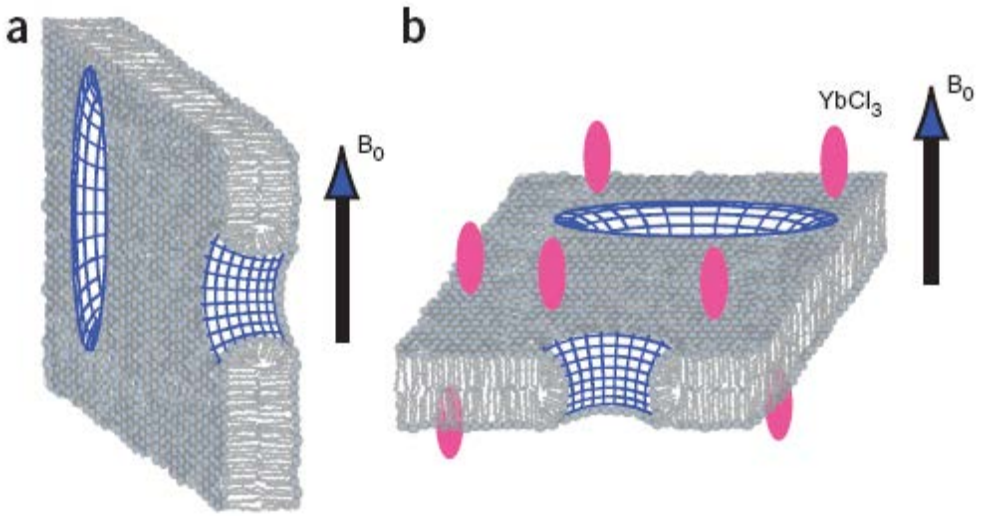

Figure 1.8 Schematic representations of magnetically aligned bicelles. (a) Perpendicular or "unflipped" bicelles: the bilayer normal is perpendicular to the direction of the external static magnetic field. (b) Parallel or "flipped" bicelles: in the presence of YbCl3, the bilayer normal is parallel to the main magnetic field. Figure taken from Ref. (38).

1.5 Filamentous bacteriophages and Pf1 coat protein

A bacteriophage (also called phage or bacterial virus) is a virus that infects and multiplies within bacteria, and is mainly composed of coat proteins encapsulating a DNA or RNA genome. Their discovery could be dated back to the beginning of the 20th century. Bacteriophages are categorized based on their morphology and the nucleic acid within the core by the International Committee on Taxonomy of Viruses (ICTV). Of all the known bacteriophages, filamentous bacteriophages are of special interest due to their relatively simple structures and broad applications (39,40).

Although their DNA genomes could be dramatically different from one to another, filamentous bacteriophage assemblies share a similar configuration of virion as well as live

cycle. Such a virion is a flexible protein rod that is normally 800-2000 nm in length with a diameter of around 6 nm, comprised of thousands of identical α-helical major coat protein subunits, with a circular single-stranded DNA (ssDNA) in the core. Each of these subunits is about 7 nm long by 1 nm diameter, with their long axes oriented at a small angle to the virion axis. Shown in Figure 1.9 is an illustrative demonstration of a filamentous bacteriophage

Figure 1.9 An illustrative demonstration of a phage assembly. The thin eclipse in red represents the circular viral DNA, whereas the small eclipses in dark gray represent the main coat protein subunits. The rectangles on the bottom are other proteins related to the phage life cycles.

assembly. Upon infection, viral DNA enters the host cell cytoplasm with the help of the major coat protein subunits after virion uncoating, and is converted to a double-stranded replicative form by host enzymes. It is then replicated and assembled with a viral replication-assembly protein. The replication-assembly protein is then replaced by capsid proteins at the cell membrane as the virion is extruded without killing the host.

The most widely used strains of filamentous bacteriophage in scientific research are f1, fd, M13 in class I, which are almost identical filamentous phages that infect bacteria with F-pili, due to their ease to cultivate and high reproductive rate. Pf1 in class II, on the other hand, gives by far the highest resolution X-ray diffraction patterns known for filamentous bacteriophage, and is very well studied not only by XRD, but also by solid-state NMR.

The structure of the main coat protein of Pf1 bacteriophage has been thoroughly studied in not only intact virus particle but also membrane-bound form by different groups (41-45). Figure 1.10 is a demonstration of the structure of the main coat protein of Pf1 bacteriophage in different environments. Hence, it is a perfect system to test newly developed NMR methodologies.

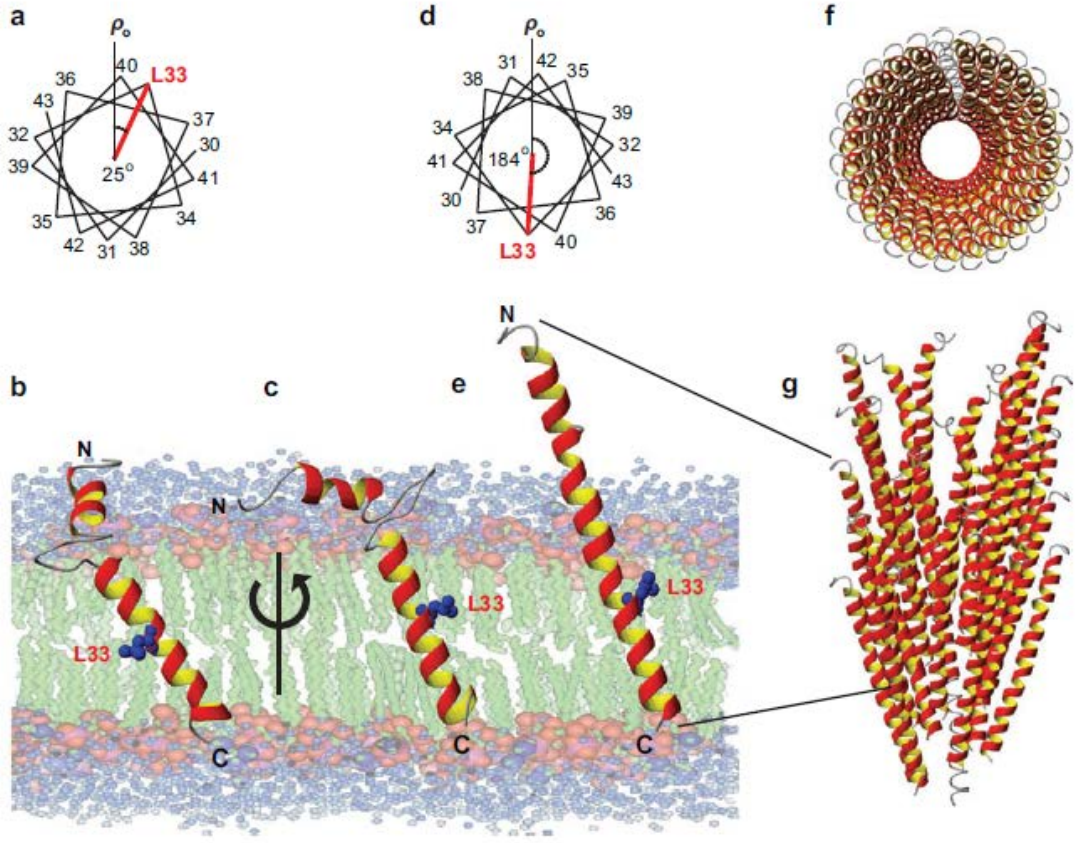

Figure 1.10 A demonstration of the structure of the coat protein in Pf1 bacteriophage in its different forms. (a) and (d) on the top shows the phase difference mapped on the helical wheel diagrams of the C-terminal region of the protein in bicelles (a) and bacteriophage particles (d). (b) demonstrates the Pf1 coat protein in a membrane environment. (c) 159° rotation of panel (b) to the vertical axis. (e) is the monomer structure of Pf1 coat protein in intact bacteriophage particles. (f) and (g) are the top and side views of a model structure of Pf1 bacteriophage particles. (Figure taken from Opella, et al, 2008)

In summary, in the present Dissertation, three (3) issues of critical importance of OSNMR of membrane proteins will be addressed. The first one is the intrinsic low sensitivity of SSNMR. To circumvent the problem, a pulse sequence termed as REP-CP is developed. A more than 2 fold sensitivity enhancement is gained compared to the normal CP. This pulse

sequence will be discussed in Chapter 2. The second issue is to develop a strategy to assign the OSNMR spectra of membrane proteins. Unlike the conventional method which requires multiple selectively labeled samples and assumes ideal secondary structure of the protein, a novel spectroscopic assignment scheme is proposed, which requires only one single uniformly labeled sample. Last but not least, an alternative approach for macroscopic sample alignment is established. The first two-dimensional SSNMR study of a uniformly ^{15}N labeled membrane protein reconstituted in lipid bilayers of various composition supported by AAO nanopores is accomplished. More details are covered in Chapter 4. It will be demonstrated that these achievement have considerably increased the utility of the OSNMR for the structure-activity studies of membrane proteins in their native lipid environments.

CHAPTER 2

REPETITIVE CROSS-POLARIZATION CONTACTS VIA EQUILIBRATION-RE-EQUILIBRATION OF THE PROTON BATH: SENSITIVITY ENHANCEMENT FOR NMR OF MEMBRANE PROTEINS RECONSTITUTED IN MAGNETICALLY ALIGNED BICELLES*

*This chapter is based on the publication entitled “Repetitive cross-polarization contacts via equilibration-re-equilibration of the proton bath: Sensitivity enhancement for NMR of membrane proteins reconstituted in magnetically aligned bicelles” by Wenxing Tang and Alexander A. Nevzorov.

2.1 Abstract

Thermodynamic limit of magnetization corresponding to the intact proton bath often cannot be transferred in a single cross-polarization contact. This is mainly due to the finite ratio between the number densities of the high- and low-gamma nuclei, quantum-mechanical bounds on spin dynamics, and Hartmann-Hahn mismatches due to rf field inhomogeneity. Moreover, for fully hydrated membrane proteins refolded in magnetically oriented bicelles, short spin-lock relaxation times ($T_{1\rho}$) and rf heating can further decrease cross polarization efficiency. Here we show that multiple equilibrations-re-equilibrations of the high- and low-spin reservoirs during the preparation period yield an over two-fold gain in the magnetization transfer as compared to a single-contact cross polarization (CP), and up to 45% enhancement

as compared to the mismatch-optimized CP-MOIST scheme for bicelle-reconstituted membrane proteins. This enhancement is achieved by employing the differences between the spin-lattice relaxation times for the high- and low-gamma spins. The new technique is applicable to systems with short $T_{1\rho}$'s, and speeds up acquisition of the multidimensional solid-state NMR spectra of oriented membrane proteins for their subsequent structural and dynamic studies.

2.2 Introduction

As for virtually every spectroscopic measurement, signal-to-noise ratio plays perhaps the most critical role in the acquisition and interpretation of solid-state NMR spectra of macroscopically aligned samples. This method has recently demonstrated the capability of providing remarkable detail about the conformations of membrane proteins in their native-like, fully hydrated lipid environment at nearly atomic resolution (46). Magnetically aligned bicelles (47,48) have the potential of advancing this technique even further since they provide superior spectral resolution as compared to glass plates (49-51). However, the necessity to detect dilute spins in such strongly proton-coupled systems is inherently connected with the problem of low sensitivity. As a result, the acquisition of multidimensional solid-state NMR spectra can take several days. Usually, magnetization enhancement for the dilute spins during the preparation period is achieved via the cross-polarization (CP) method (52) under the Hartmann-Hahn matching conditions (53). Numerous improvements of the method have been proposed, including ramped CP (54), CP-

MOIST (55,56), CP involving simultaneous phase inversion (57), variable-amplitude CP (58), selective-excitation RELOAD-CP technique (59), frequency-modulated CP (60), and CP-COMPOZER (61). The latter two techniques have shown their robustness with respect to Hartmann-Hahn mismatches and the capability of improving the signal to noise ratio by up to 20-25% for aligned samples (60,62). However, only a part of the overall magnetization is transferred from the abundant proton bath to the dilute spins in a single cross-polarization contact (63). This can be due to the finite ratio of the total number of protons with respect to that of the low-gamma spins, as well as relaxation effects. In addition, universal or quantum-mechanical bounds on spins dynamics (64) may play a role, thus further limiting the amount of the maximum transferred quasi-stationary magnetization (55,65). The classical multiple-contact scheme (52) can be employed to further enhance the magnetization transfer from the protons to the dilute spins in static and spinning solids. However, for membrane proteins reconstituted in magnetically aligned bicelles (49), this scheme may not be appropriate due to the relatively short $T_{1\rho}$ relaxation times (66) (typically up to several milliseconds) inherent to the liquid-like bilayers and uniaxially rotating membrane proteins (67,68). In such samples, the proton spin-lock responsible for the successive enhancement of magnetization would be lost during the 10 ms of the first acquisition period. Moreover, substantial heating of the sample would take place if the protons are irradiated for 30 ms or longer. Therefore, CP-MOIST and ramped CP currently remain the most widely used methods to enhance ^{15}N magnetization in uniaxially aligned membrane protein systems. Here we employ an alternative scheme (69) based on repetitive short CP contacts during the preparation period that circumvents the above thermodynamic and quantum-mechanical bounds and the issue of

short $T_{1\rho}$'s. This pulse sequence (which we term here as REP-CP) yields more than a factor 2 enhancement of magnetization as compared to a single-contact CP for membrane proteins refolded in bicelles, and up to 45% on average improvement as compared to CP-MOIST.

2.3 Materials and Methods

Uniformly ^{15}N-labeled Pf1 phage sample was purchased from Hyglos GmbH (Regensburg, Germany). To isolate the protein, the sample was dissolved in 1 ml of TFE (50%)/TFA (0.1%) in order to remove the DNA, and the soluble fraction was isolated and lyophilized. About 6 mg of pure lyophilized protein was reconstituted in DMPC/DHPC (at 3:1 molar ratio) bicelles as previously described (38). All experiments have been performed on a Bruker Avance II spectrometer operating at 500 MHz ^{1}H frequency with Topspin 2.0 software. A commercial Bruker 5 mm round low-E coil probe was used. For the bicelle-reconstituted protein, the sample temperature was maintained at 38^{o}C, 6 sec recycle delay and 40.3 kHz B_1 fields were used. The z-filter time was chosen as short as possible to shorten the overall length of the experiment, on the one hand, and to minimize the losses of ^{15}N magnetization due to proton-driven spin diffusion, on the other. At the same time, however, the z-filter should be sufficiently long to let the proton bath equilibrate to the lattice temperature after each flip-back pulse. Optimal z-filter times of less than 1 sec have been found. Increasing the z-filter time to greater than 1 sec yielded considerable loss in intensity due to proton-driven spin diffusion (results not shown).

The REP-CP sequence is based on multiple equilibration-re-equilibrations of the two spin reservoirs, and is depicted in Fig. 2.1. Consider N_I abundant and N_S dilute spins (e.g. ^{15}N nitrogens) with the gyromagnetic ratios γ_I and γ_S, respectively. After each CP-contact followed by two flip-back pulses and the z-filter, the protons are re-equilibrated to the lattice temperature. After two simultaneous 90-degree pulses followed by the application of radiofrequency irradiation with the amplitude B_{1I} for the protons and B_{1S} for the nitrogens,

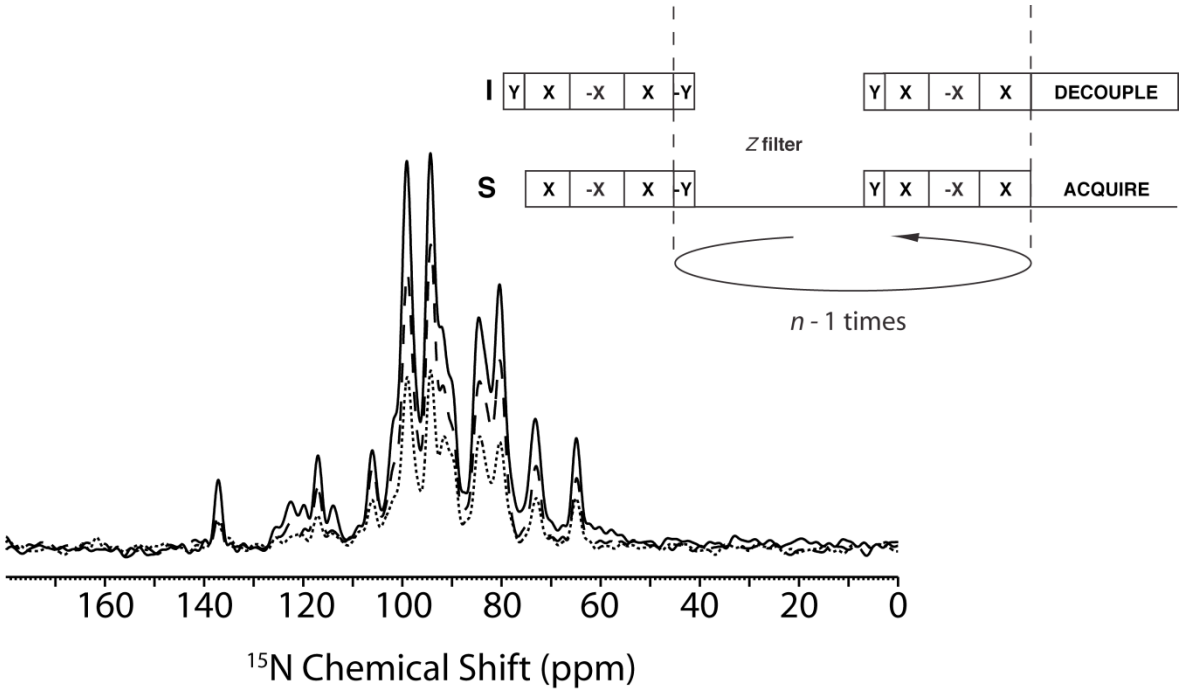

Figure 2.1 The REP-CP pulse sequence employing repetitive CP contacts during the preparation period and experimentally observed enhancement for NMR spectra for Pf1 coat protein reconstituted in magnetically aligned bicelles. Single-contact CP (dotted line); CP-MOIST (dashed line); REP-CP (solid line). A two-fold gain in the signal-to-noise ratio is obtained for the case of REP-CP as compared to the conventional CP, and a 45% gain over CP-MOIST. All experiments have equal total experimental times; 50 Hz exponential linebroadening has been applied.

the spin temperature of the latter equilibrates with that of the proton bath, initially at the temperature T_0 (in the tilted frame). Assuming that the two spin systems are at thermodynamic equilibrium at all times, we write for the conservation of energy in the doubly tilted rotating frame (63) after each contact:

$$-\beta_0 C_I B_{1I}^2 - \beta_{n-1} C_S B_{1S}^2 = -\beta_n (C_I B_{1I}^2 + C_S B_{1S}^2) \qquad \text{(Eqn. 2.1)}$$

Here the symbol β_n denotes the inverse spin temperature in the tilted frame after the *n*-th contact, $\beta_0 = \hbar/k_B T_0$, and $C_I = 1/3\gamma_I^2\hbar I(I+1)N_I$ and $C_S = 1/3\gamma_S^2\hbar S(S+1)N_S$ are the Curie constants for the *I* and *S* spins, respectively. In establishing the above relation, we have also assumed that the spin-lattice relaxation time of the dilute spins is much longer than that of the high-gamma abundant spins. Consequently, the inverse spin temperature of the low-gamma spins, β_{n-1}, remains constant after the previous contact if the z-filter is sufficiently short. At the exact Hartmann-Hahn match for $S = I = 1/2$, $\gamma_I B_{1I} = \gamma_S B_{1S}$, the above equation can be rewritten as:

$$\beta_n = \frac{\beta_0 + \varepsilon\beta_{n-1}}{1+\varepsilon} \qquad \text{(Eqn. 2.2)}$$

where $\varepsilon = N_S / N_I < 1$. The final spin temperature of the *I*-*S* system after *n* contacts can be obtained by summing up a geometric progression, which yields:

$$\beta_n = \frac{\beta_0}{1+\varepsilon}\sum_{k=0}^{n-1}\left(\frac{\varepsilon}{1+\varepsilon}\right)^k = \beta_0\left[1-\left(\frac{\varepsilon}{1+\varepsilon}\right)^n\right] \to \beta_0, n \to \infty \qquad \text{(Eqn. 2.3)}$$

In contrast to the original multiple-contact experiment (52), the convergence (albeit a very fast one for small values of ε) is achieved to the inverse spin temperature β_0 instead of being proportional to β_0/ε (which would have been a much more desirable behavior since $\varepsilon < 1$).

This simplified thermodynamic treatment implies that even if the ratio between the number of protons and that of the dilute spins is finite, one can nevertheless equilibrate them to the same spin temperature corresponding to the intact proton bath. Having equal amounts of magnetization on both nitrogen and protons is advantageous for multidimensional separated local field (SLF) experiments in order to minimize the positive or negative zero-frequency peaks such as those observed in PISEMA (19) or SAMPI4 (22). For instance, if $\varepsilon = 0.13$ (7-8 protons per nitrogen spin, the ratio typical for proteins), after one CP contact resulting in the nitrogen spin-locking temperature $\beta_0(1+\varepsilon)^{-1}$ only 88% of the intact proton bath temperature will be transferred. However, after just two re-equilibrations this number will increase to 99%. It should be noted that $T_{1\rho}$ relaxation and Hartmann-Hahn mismatches due to rf field inhomogeneity have not been explicitly taken into account by Eqn. 2.1, which may yield even lower magnetization transferred in each contact. Moreover, there is an additional factor that may limit the final amount of magnetization. A recent many-body quantum-mechanical treatment (69) has shown that a single nitrogen spin never achieves full thermodynamic contact with the proton bath even under perfect Hartmann-Hahn matching conditions. Briefly, for a system consisting of a single nitrogen spin and N_I protons, the density matrix $\rho(t)$ obeys unitary evolution in the doubly tilted rotating frame:

$$\rho(t) = e^{-iH_T t} I_z e^{iH_T t} \qquad \text{(Eqn. 2.4)}$$

Here the truncated CP Hamiltonian for the *IS* system, H_T, is given by:

$$H_T = \frac{1}{4}\sum_{n=1}^{N_I} a_n (S_+ I_-^{(n)} + S_- I_+^{(n)}) - \frac{1}{2}\sum_{i<j}^{N_I} b_{ij}\left[\frac{3}{2} I_z^{(i)} I_z^{(j)} - \frac{1}{2}\mathbf{I}^{(i)}\mathbf{I}^{(j)}\right] \qquad \text{(Eqn. 2.5)}$$

where the a_n are the coupling constants describing the dipolar interactions between the *S* spin (nitrogen) and the *I* spins (protons), and b_{ij} are the coupling constants for the homonuclear interactions. The quasistationary amount of normalized transferred magnetization is calculated as (69):

$$M_S(\infty) = \lim_{t\to\infty} \frac{Tr(S_z e^{-iH_T t} I_z e^{iH_T t})}{Tr(S_z^2)} = 1 - 2^{-N_I+1} \sum_k \left| \langle k' | S_z | k \rangle \right|^2 < 1 \qquad \text{(Eqn. 2.6)}$$

where the summation is carried over the values of *k* together with the indices *k*' that correspond to the same degenerate eigenvalues of the Hamiltonian, H_T. Many-spin simulations have shown that the quasi-stationary limit of the transferred magnetization, Eq. (6), converges to a value of around 0.84 (69). Therefore, the nitrogen spin temperature as given by Eqn. 2.2 should be corrected by this factor at each transfer step. The combination of the above quantum-mechanical (84%) and thermodynamic bounds (88%) would result in the single-step CP enhancement of around 74% relative to the "ideal" (i.e. γ_H / γ_N) value. Hartmann-Hahn mismatches and loss of spin-lock due to $T_{1\rho}$ relaxation could lower this amount even further. Disregarding the additional losses, the theoretical gain factor for REP-CP is thus estimated to be 1.35 relative to a single-contact CP.

2.4 Results and Discussion

The method of multiple equilibrations of high- and low-gamma spins has been applied to Pf1 coat protein both in the phage form and reconstituted in magnetically aligned bicelles (50). As expected for biological samples having $T_{1\rho}$'s of several milliseconds (66), which is

shorter than the acquisition period (typically about 10 ms), the original multiple-contact scheme (52) is not very efficient. Experiments on ^{15}N-labeled Pf1 phage, as is shown in Figure 2.2, have demonstrated that for the same number of transients, the signal-to-noise ratio is even less than for the single-contact CP-MOIST experiment (55,56) since more noise than signal is acquired during the subsequent contacts. For Pf1 coat protein reconstituted in magnetically aligned bicelles, ^{15}N-detected proton $T_{1\rho}$ experiment (see Figure 2.3) has yielded the $T_{1\rho}$ relaxation time of 4.3 msec, which would make the multiple contacts also prohibitive for such systems. The spin-lattice relaxation time for the protons has been determined by an ^{15}N-detected proton inversion recovery, which yielded T_{1Z} = 1.3 sec. While the experimentally found optimal time of the z-filter for the bicelle-reconstituted protein

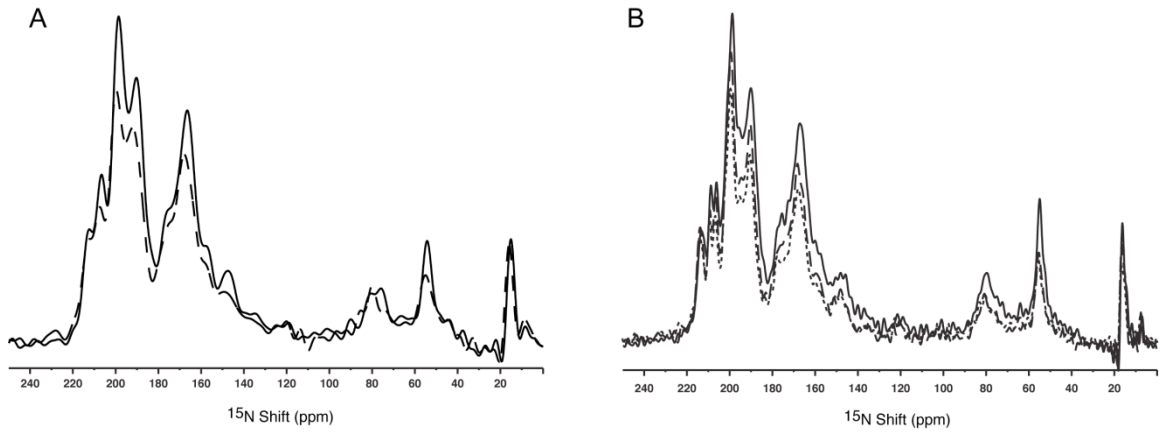

Figure 2.2 A. ^{15}N Spectra of Pf1 phage: CP-MOIST (solid line) and multiple contacts (dashed line). All phage spectra were measured at -4 ^{o}C, 1 ms single contact time was used and three (3) CP contacts were employed for the multiple contact experiment; 64 transients with a 6 sec recycle delay were acquired for each spectrum, and the acquisition time was 5 ms. The signal-to-noise ratio for the CP-MOIST experiment is 48:1; whereas for the multiple contacts it is 38:1. B. ^{15}N Spectra of Pf1 phage: single-contact CP (dotted line, 256 scans, 1 ms contact, 10 ms acquisition time); CP-MOIST (dashed line, all parameters are the same as for the single-contact CP); REP-CP (solid line, 6 contacts, 200 μs each, 1 sec z-filter delay, other parameters are the same). About 50% intensity gain is obtained for the case of REP-CP as compared to the conventional CP, and 25% relative to CP MOIST.

(0.15 sec) is much shorter than ^{1}H T_{1Z}, in combination with the flip-back pulses it appears to be sufficient to re-equilibrate the proton bath to the lattice temperature, and thus achieve the successive ^{15}N magnetization enhancement. This is due to the fact that the amide protons, which donate most of the magnetization to the nitrogen spins, are quickly re-equilibrated by the rest of the proton bath by spin diffusion. A very similar mechanism of an accelerated T_1 relaxation was observed for the carbonyl carbons in the RELOAD-CP experiment employing selective excitation pulses (59). Figure 2.1 shows an overlay of the REP-CP experiment (5 CP-MOIST contacts each having 300 μs contact time, 0.15 sec z-filter time), CP-MOIST, and CP (with a 300 μs contact time). (The parameters for REP-CP may need to be optimized

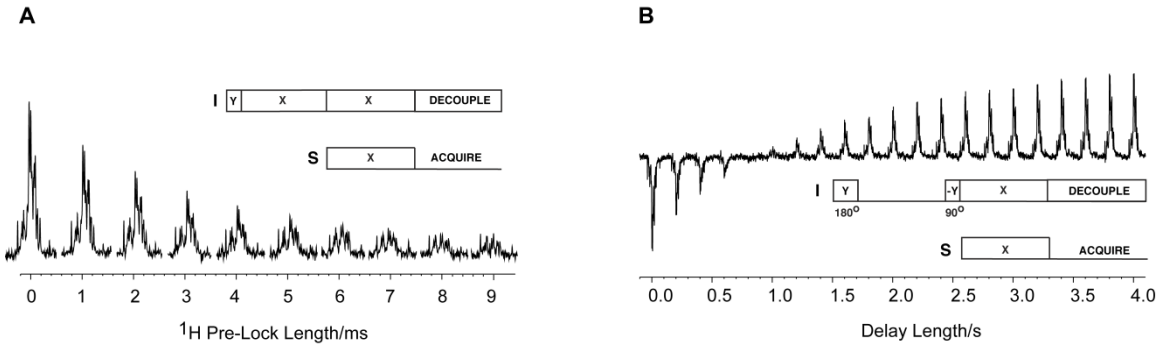

Figure 2.3 A. ^{15}N-detected proton $T_{1\rho}$ experiment for Pf1 coat protein reconstituted in magnetically aligned bicelles. The protons have been pre-locked for variable durations and then the ^{15}N spins were cross-polarized and detected. The $T_{1\rho}$ relaxation time was determined by fitting the integrals of the spectra corresponding to the transmembrane region of Pf1 coat protein (from 55 to 110 ppm) yielding $T_{1\rho} = 4.3$ msec. B. ^{15}N-detected proton T_{1Z} experiments for Pf1 coat protein reconstituted in magnetically aligned bicelles using the inversion recovery pulse sequence as shown. A 1.3 sec spin-lattice relaxation time for the protons was determined from the crossover.

depending on the type of sample; fewer numbers of contacts can also be used since most of the magnetization is transferred from the protons to the nitrogen spins after as little as 3-4 contacts.) One thousand twenty-four transients were acquired in the conventional CP and CP-MOIST experiments; whereas 930 scans were acquired for the REP-CP experiment (resulting in equal total times for each experiment of 1 hour and 42 minutes). It should be noted that the single-contact CP-MOIST sequence (55,56) already yields an over 50% enhancement as compared to the conventional CP (the integral ratio between the two spectra is 1.55). This observation may indicate that in magnetically aligned bicelles it is difficult to satisfy the exact Hartmann-Hahn match for every protein species present in the sample, possibly due to rf field inhomogeneity and/or sample heating (62). Notably, more than a factor-two gain in intensity is achieved by the REP-CP experiment as compared to the single-contact CP experiment (the integral ratio between the two spectra is 2.2), and about a 45% gain in the signal-to-noise ratio when compared to the CP-MOIST. A comparison of the REP-CP spectrum with direct-excitation ^{15}N spectrum for the transmembrane helix region, as is shown in Figure 2.4, has yielded from 9 to 13-fold intensity enhancement depending on the spectral position, with the integral ratio taken over the helical regions equal to 9.8. Taking into account the very low sensitivity obtainable by direct ^{15}N excitation, these gain values on average correspond to the ratio γ_H / γ_N. It should also be noted that for Pf1 phage the enhancement factor for the REP-CP was only 1.51 as compared to a single-contact CP, and 1.25 as compared to CP-MOIST (cf. Fig 2.2). This would mean that, for the more rigid phage samples, a single-contact CP is more efficient than for the more dynamic bicelle-reconstituted proteins which are rapidly re-orienting about the axis perpendicular to the main

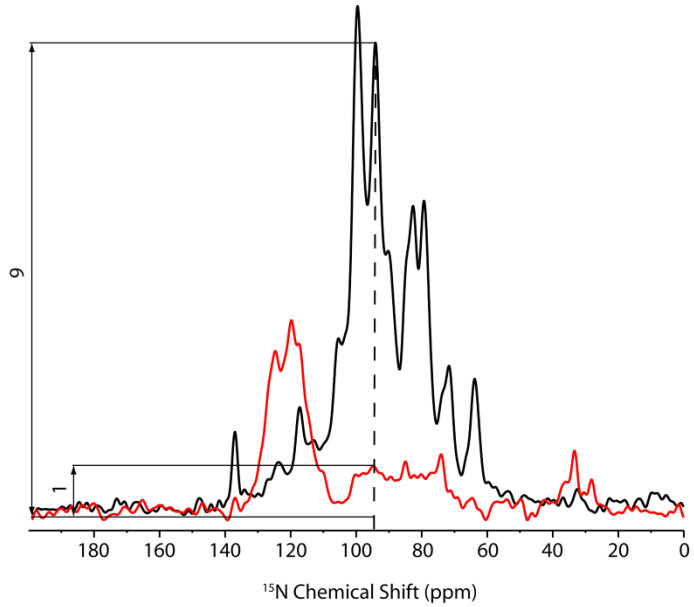

Figure 2.4 Comparison of REP-CP spectrum (black) vs. direct-excitation echo-detected ^{15}N spectrum (red). 990 scans were used for the REP-CP experiment with 6 contacts each having 200 µs contact time, and the z-filter was set to 0.04 s. For the direct-excitation echo-detected ^{15}N spectrum, the number of scans was 1024, and a 300 s relaxation delay was utilized. The peaks at 75 and 85 ppm are due to the mobile Arg side-chains which exhibit small dipolar couplings in the 2D spectrum (cf. Fig. 2.5), and can interfere with the assessment of the enhancement factor for this spectral range. The enhancement effect for the transmembrane helical region (105 to 65 ppm) varies from 9 to 14 depending on the position of the peak in the spectrum due to a very low signal-to-noise ratio. Note that the peaks between 110 and 130 ppm, which correspond to the more dynamic N-terminal residues (1-18), are efficiently excited by a single pulse, but are absent from the CP spectrum where only residues 19-43 are observed.

magnetic field. An even lower (<20%) enhancement was previously observed for a single crystal of *n*-aceyl Leucine (69), which has a much higher proton-to-nitrogen ratio (15:1), on the one hand, and virtually no dynamics on the other, thus yielding greater single-contact CP efficiencies. This issue merits additional investigation as it may allow one to study semi-quantitatively the dynamics of membrane proteins by comparing the relative amounts of the

transferred cross-polarization as compared to the single-contact CP and, whenever feasible, to direct excitation of the low-gamma nuclei.

Such an enhancement can appreciably speed up the acquisition of multidimensional NMR data. Figure 2.5 shows two-dimensional SAMPI4 (22) spectra for the bicelle-reconstituted Pf1 coat protein acquired with only 14 transients per each of the 64 t_1 increments for the REP-CP and 16 scans for the CP-MOIST enhanced SAMPI4 (resulting in less than 2 hour total time per experiment). It can be seen that the application of repetitive CP contacts during the preparation period is sufficient to detect all peaks in the spectrum;

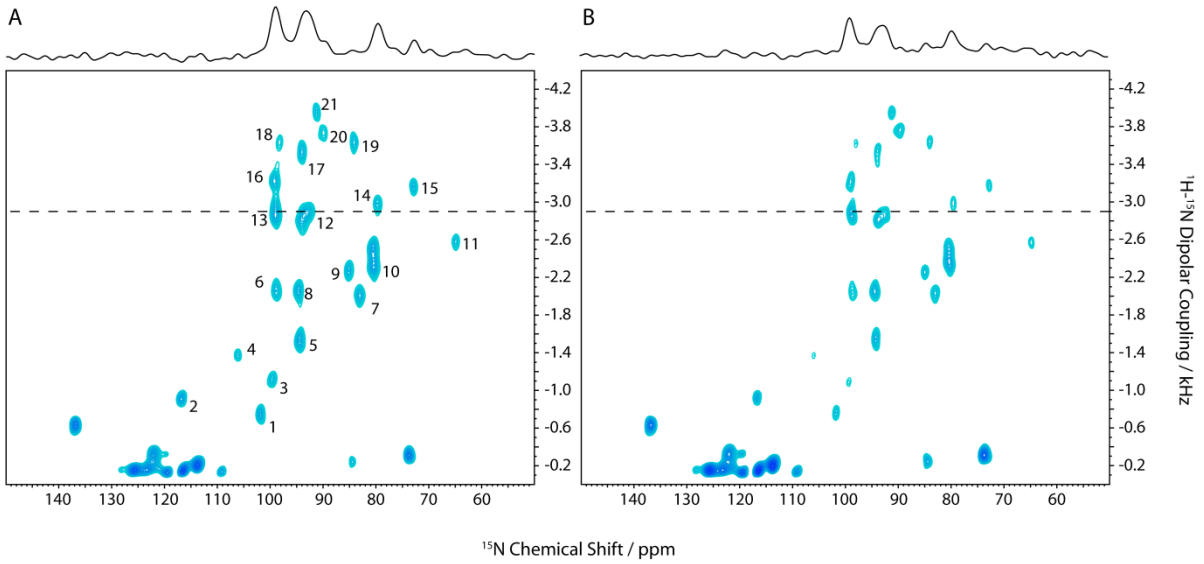

Figure 2.5 SAMPI4 experiments for Pf1 coat protein reconstituted in magnetically aligned bicelles acquired at 500 MHz proton frequency. (A) REP-CP enhanced SAMPI4 (14 scans for each t_1 increment); (B) CP-MOIST enhanced SAMPI4 (16 scans). Representative slice along 3 kHz in the dipolar dimension shows that that superior sensitivity is obtained in part A (with 6 REP-CP contacts, 300 μs each, 0.15 sec z-filter time) as compared to CP-MOIST with a single 1 ms contact (part B). The experimental time was 1 hour and 42 minutes for each experiment.

whereas if the initial enhancement is made via CP-MOIST more scans would be necessary. A comparison of the signal-to-noise ratios for 21 fully resolved resonances in the transmembrane alpha-helical region (50) of the Pf1 protein (performed at 128 scans) is shown in Fig. 2.6. As can be seen, the use of the REP-CP scheme of Fig. 2.1 has yielded up to 60% technique (70,71) even greater signal-to-noise enhancements can be expected in the SLF experiments. In addition, the use of the above methods in combination with paramagnetic T_1 relaxation enhancers (72) may considerably reduce the z-filter lengths and the overall acquisition time for NMR of oriented membrane proteins.

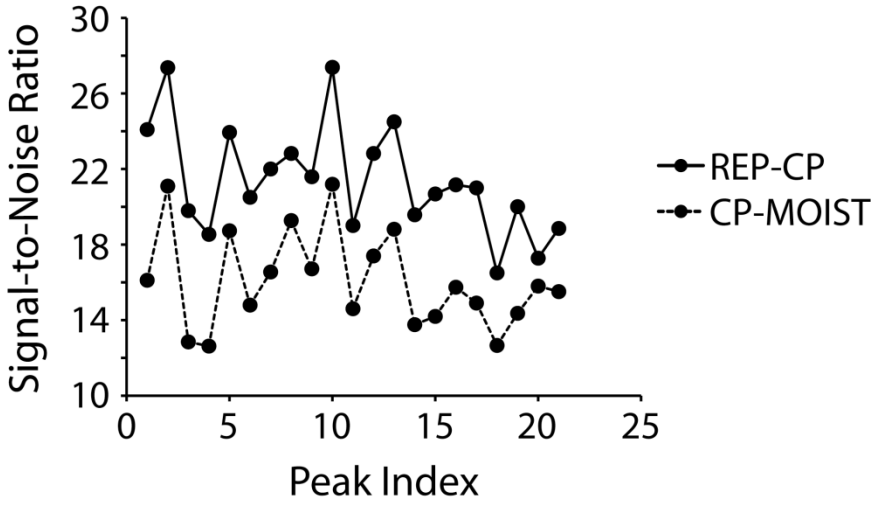

Figure 2.6 Comparison of the signal-to-noise ratios for 21 resolved residues in the α-helical transmembrane region of Pf1 coat protein. Solid line: REP-CP enhanced SAMPI4 (128 scans, other parameters are as in Fig. 2.2); dashed line: CP-MOIST enhanced SAMPI4 (128 scans). For select peaks the gain is up to 60% with an average gain of 35%.

2.5 Conclusion

In conclusion, the REP-CP cross-polarization scheme based on multiple equilibration-re-equilibrations of the high- and low-gamma reservoirs has yielded a significant gain in the signal-to-noise ratio as compared to conventional cross-polarization. Contrary to only a marginal (12%) enhancement expected from the conservation of energy argument under the assumption of thermodynamic equilibrium, and experimentally observed in single crystals (69), a two-fold enhancement has been obtained for Pf1 coat protein reconstituted in magnetically aligned bicelles. This is primarily due to a combination of thermodynamic bounds (finite ratios of the numbers of high- and low-gamma spins in proteins) and quantum mechanical bounds on spin dynamics resulting in reduced quasi-equilibrium magnetization transferred to the low-gamma spins in a single CP contact. Furthermore, Hartmann-Hahn mismatches due to rf field inhomogeneity, protein and bilayer dynamics, rf heating, and $T_{1\rho}$ relaxation, can further considerably reduce the amount of the transferred magnetization for fully hydrated biological samples. Regardless of the type of losses, however, repetitive CP contacts during the preparation period would still bring the two spin reservoirs to the spin temperature corresponding to the intact proton bath. The proposed REP-CP scheme can also be applied to other NMR samples where the $T_{1\rho}$ relaxation times are short.

CHAPTER 3

A SPECTROSCOPIC ASSIGNMENT TECHNIQUE FOR MEMBRANE PROTEINS RECONSTITUTED IN MAGNETICALLY ALIGNED BICELLS*

*This chapter is based on the publication entitled "A spectroscopic assignment technique for membrane proteins reconstituted in magnetically aligned bicelles" by Wenxing Tang, Robert W. Knox and Alexander A. Nevzorov.

3.1 Abstract

Oriented-sample NMR (OS-NMR) has emerged as a powerful tool for the structure determination of membrane proteins in their physiological environments. However, the traditional spectroscopic assignment method in OS NMR that uses the "shotgun" approach, though effective, is quite labor- and time- consuming as it is based on the preparation of multiple selectively labeled samples. Here we demonstrate that, by using a combination of the spin exchange under mismatched Hartmann-Hahn conditions and a recent sensitivity-enhancement REP-CP sequence, spectroscopic assignment of solid-state NMR spectra of Pf1 coat protein reconstituted in magnetically aligned bicelles can be significantly improved. This method yields a two-dimensional spin-exchanged version of the SAMPI4 spectrum correlating the ^{15}N chemical shift and ^{15}N-^{1}H dipolar couplings, as well as spin-correlations between the (i, $i\pm1$) amide sites. Combining the spin-exchanged SAMPI4 spectrum with the original SAMPI4 experiment makes it possible to establish sequential assignments, and this

technique is generally applicable to other uniaxially aligned membrane proteins. Inclusion of a ^{15}N-^{15}N correlation spectrum into the assignment process helps establish correlations between the peaks in crowded or ambiguous spectral regions of the spin-exchanged SAMPI4 experiment. Notably, unlike the traditional method, only a uniformly labeled protein sample is required for spectroscopic assignment with perhaps only a few selectively labeled "seed" spectra. Simulations for the magnetization transfer between the dilute spins under mismatched Hartmann Hahn conditions for various B_1 fields have also been performed. The results adequately describe the optimal conditions for establishing the cross peaks, thus eliminating the need for lengthy experimental optimizations.

3.2 Introduction

Magnetically oriented bicelles (38,47,48) provide a high degree of macroscopic alignment thus yielding sharp resonance lines that can be used for structure determination of bicelle-reconstituted membrane proteins. Moreover, bicelles provide a native-like environment for the embedded proteins including complete hydration, high lipid-to-protein ratios, and a near-physiological temperature range. In their natural aligned state, the DMPC/DHPC bicelles orient so that their membrane normals are perpendicular to the aligning magnetic field. Though it is possible to 'flip' the bicelles with the addition of lanthanide ions (73), thus making the bicelle normals parallel to the external magnetic field, unflipped bicelles yields sharper resonance lines. This is due to the fact that the range for the motionally averaged dipolar couplings and proton chemical shift anisotropy is narrower at

the perpendicular orientation, thus making proton decoupling more efficient and the effect of the mosaic spread less pronounced. Here the structural information is provided by the uniaxially averaged chemical shift anisotropies and dipolar couplings due to the fast rotational diffusion of membrane proteins about their alignment axis (the bilayer normal) (68,74). Previous studies (68,75) have estimated the correlation time of the uniaxial diffusion to be on the microsecond time scale.

Pf1 coat protein is composed of 46 amino acids (4.6 kDa), and is the major protein of Pf1 bacteriophage. It has a relatively simple structure: two alpha helices connected by a loop with the Q16–A46 region spanning the membrane (50). In its membrane-bound form, it assists the virus exit from the infected bacterial cells and its assembly by coating the phage virion (41). The structure of Pf1 coat protein reconstituted in magnetically aligned bicelles has been recently reported (50). Two-dimensional solid-state ^{15}N NMR spectra of Pf1 were found to contain resolved resonances for the residues Q16-A46 (50). Spectroscopic assignment of the ^{15}N NMR spectra has been accomplished by detecting the positions of the resonances for selectively labeled samples followed by the application of the “shotgun” approach (50). The latter still remains the current principal assignment method in oriented-sample NMR (OS NMR) as it provides nearly absolute assignment. However, it is generally restricted to the main secondary-structure elements such as alpha-helix (23,24) and beta-sheet (26). In addition, this method requires preparation of multiple selectively labeled samples, making it time consuming and expensive. Hence, a purely spectroscopic method of assignment utilizing uniformly labeled samples would greatly increase the value of OS NMR for structure determination of membrane proteins of arbitrary topology. A method involving

cross-referencing of the anisotropic chemical shifts at the perpendicular and parallel sample orientations has been proposed (34,76). However, this method requires the knowledge of the corresponding isotropic chemical shifts for each residue, thus necessitating additional solution NMR experiments. Alternatively, proton-driven spin diffusion (PDSD) (77) can be used to establish cross-correlations between the neighboring spins, thus providing a spectroscopic assignment method similar to those routinely used in solution and MAS NMR. In recent years, various spectroscopic methods based on dilute spin exchange (78,79) have been implemented to establish sequence-specific resonance assignments. Very recently, the ^{15}N OS NMR spectrum of sarcolipin has been assigned in "flipped" bicelles (80), where the membrane normal is parallel to the external magnetic field. In order to achieve higher spectral resolution, a three-dimensional pulse sequence employing PDSD was utilized. However, the PDSD-based methods suffer from the requirement of long mixing intervals (up to several seconds) in order to establish detectable spin-exchange signals among the weakly coupled dilute ^{15}N nuclei, thus potentially resulting in missing cross peaks. As an alternative to circumvent the above issue, an analog of the proton-assisted recoupling experiment (81) has been developed for aligned samples (82) with the potential of providing a general spectroscopic assignment method in OS NMR. This method is based on the transfer of the magnetization between the rare spins (^{15}N or ^{13}C) under mismatched Hartmann-Hahn (MMHH) conditions. The magnetization transfer utilizing MMHH conditions is accomplished with the assistance of the proton spin bath, and does not depend on the direct coupling between the low spins (82). Under the MMHH conditions, the Zeeman order of energy for an ^{15}N spin is transferred into the dipolar order of the proton bath and then back to

the Zeeman order of the neighboring ^{15}N spins (83), thus establishing cross peaks in a multidimensional NMR spectrum. Based on the results obtained for an *n*-acetyl leucine (NAL) single crystal, this scheme is capable of establishing correlations among the dilute spins (^{15}N) separated by as far as 6.7Å. Such an ability would be of great value for the spectroscopic assignment of solid-state NMR spectra of oriented membrane proteins. Additionally, the contact time in the MMHH scheme is only several milliseconds, which dramatically shortens the overall experiment time as compared to PDSD-based spin exchange, which require the contact times of several seconds. Furthermore, the MMHH method has been extended to the measurement of heteronuclear dipolar couplings by inclusion of the SAMPI4 pulse sequence (22) in the indirect dimension, thus yielding a spin-exchanged high-resolution separated local-field spectrum (84). In a previous study, the MMHH method has demonstrated its applicability for the uniformly labeled Pf1 phage when the axis of the sample alignment is parallel to the magnetic field (85). In principle, the method is applicable to any macroscopically aligned dilute-spin system bridged by a strong proton dipolar network, thus providing a general strategy for the sequential assignment of resonances in NMR spectra of oriented membrane proteins.

In the present work, we apply the MMHH technique to establish spin-correlations for membrane proteins at the perpendicular uniaxial alignment provided by magnetically oriented bicelles. Three (3) two-dimensional experiments have been performed using the bicelle-reconstituted Pf1 coat protein, including an ^{15}N-^{15}N correlation spectrum, a SAMPI4 spectrum (22) correlating the ^{15}N chemical shift and ^{1}H-^{15}N dipolar couplings, as well as the "spin-exchanged" version of the SAMPI4 spectrum (84). Intra-residue cross peaks have been

established by cross-referencing of the three spectra. The use of sensitivity-enhanced REP-CP pulse sequence (86) further increases the signal-to-noise ratio in these experiments, and makes it possible to detect all the cross peaks for the α-helical transmembrane region (i.e. residues I22-M42). Detailed many-spin simulations have been performed to establish the optimal Hartmann-Hahn mismatch for the amide backbone ^{15}N spin correlations.

3.3 Materials and Methods

A uniformly ^{15}N-labeled Pf1 phage sample was provided by Hyglos GmbH (Regensburg, Germany) at ca. 40 mg/mL total concentration of the protein. To purify Pf1 coat protein, a predefined amount of the phage was dissolved in 1 ml of TFE (50%)/TFA (0.1%) to precipitate the DNA, followed by lyophilization of the soluble fraction. Approximately 6 mg of the lyophilized protein was reconstituted in 180 μl solution of DMPC/DHPC (at q = 3:1 molar ratio) bicelles as previously described by Opella and co-workers (38). Alternatively, an ether-linked version of DHPC, 6-O-PC, can be used which yields no significant differences in the observed spectra, but a much longer lifetime of the sample (38,87). The lipid-to-protein ratio was maintained at around 55:1, and the optimal sample temperature T = 38°C was found by recording the linewidths of the ^{31}P NMR lipid spectra to determine the best bicelle alignment (results not shown). All experiments have been performed on a Bruker Avance II spectrometer operating at 500 MHz ^{1}H frequency and running Topspin™ 2.0 software. A Bruker 5 mm round-coil E-free™ probe was utilized in all experiments.

The pulse sequences used in the assignment process are shown in Fig. 3.1. Figure 3.1A depicts the homonuclear ^{15}N-^{15}N exchange experiment. Here the cross-polarization part is first applied to enhance sensitivity (either by means of a single-contact CP or repetitive, REP-CP). Next, the ^{15}N chemical shift evolves under the conditions of proton decoupling.

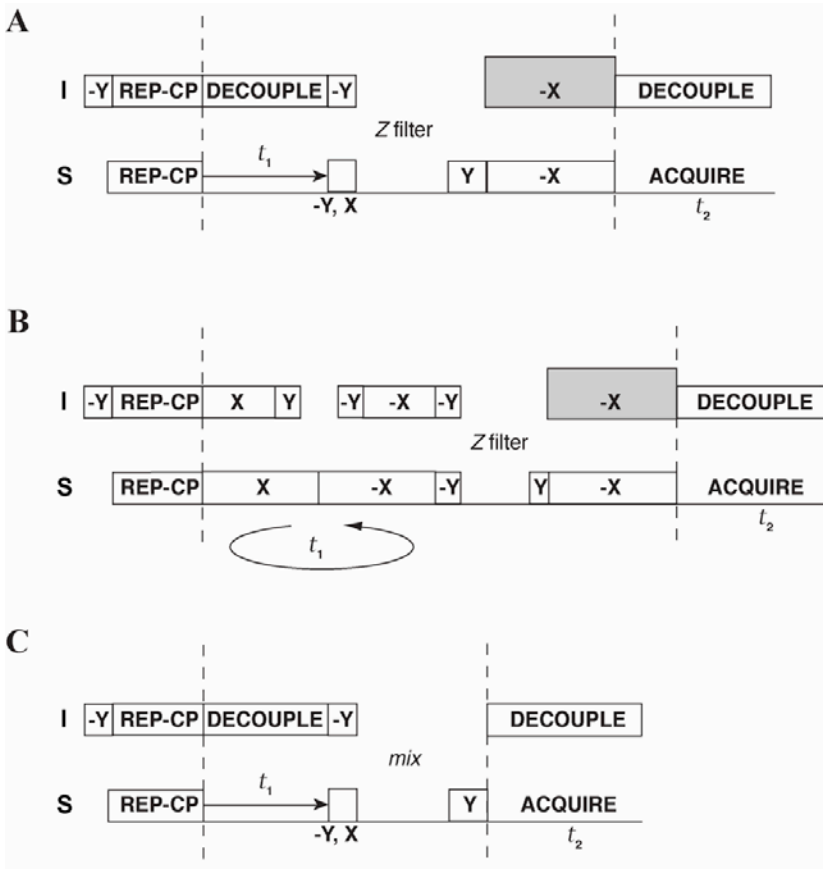

Figure 3.1 Pulse sequences used for NMR spectroscopic assignment of Pf1 coat protein reconstituted in magnetically aligned DMPC/DHPC bicelles. (A) ^{15}N-^{15}N correlation pulse sequence utilizing MMHH. (82,85) (B) Spin-exchanged SAMPI4 pulse sequence (84). (C) ^{15}N-^{15}N correlation pulse sequence utilizing PDSD (78). Either conventional cross-polarization, CP, or REP-CP (86) can be used to enhance the initial ^{15}N magnetization. A 5 ms contact time was chosen for all the MMHH-based experiments, whereas a mixing time of 3 seconds was used for the PDSD experiment. For further details of the pulse sequences cf. the text.

The proton magnetization is subsequently flipped along the *z*-direction, and an alternating 90° *-y/x* pulse on the ^{15}N site selects either the real or imaginary component of the chemical shift evolution. A wait time of typically less than one second is applied to eliminate any residual proton magnetization along the *x*-axis (the *Z*-filter). The proton-mediated transfer is achieved when the ^{15}N spins are brought back along the *x*-direction followed by simultaneous rf irradiation on both channels, with the rf amplitude on the ^{1}H site being higher than the Hartmann-Hahn match. Finally, the ^{15}N chemical shift is detected under the conditions of proton decoupling. Two-dimensional pulse sequence for the high-resolution separated local filed spectroscopy that simultaneously establishes internuclear correlations is depicted in Fig 3.1B. As in Fig. 3.1A, cross-polarization is used to enhance the magnetization on the ^{15}N side. The SAMPI4 pulse sequence (22) is applied to evolve the heteronuclear dipolar couplings. After the *Z*-filter, the stored ^{15}N magnetization is brought back along the *x*-axis, and the mismatched Hartmann-Hahn scheme is applied to establish intra-residue correlations. Finally, the ^{15}N chemical shift is detected. Fig. 3.1C shows the pulse sequence for the homonuclear exchange involving PDSD; it could also be thought as a variant of the sequence of Fig. 3.1A with a longer *Z*-filter, albeit without the MMHH spin exchange.

All many-spin simulations were performed using a script written in MATLAB (Mathworks, Inc.). The data have been processed using NMRPipe (88).

3.4 Results and Discussion

3.4.1 Simulations of spin dynamics for the perpendicular bicelles.

A theoretical framework for the magnetization exchange between two dilute spins surrounded by a proton bath under mismatched Hartmann-Hahn conditions has been previously described (82,84,89). Such a framework allows for theoretical simulations of the mismatch conditions, thus considerably shortening experimental optimizations. Using the crystal structures of NAL (84,89) and NAVL (89) simulations have been shown to accurately describe the experimental behavior such as the cross-peak intensity as a function of the B_1 field mismatch between the proton and ^{15}N rf fields, ^{15}N spin-lock rf field strengths, and the total irradiation time. Experiments performed on single crystals and the simulations demonstrate the capability of establishing cross peaks between the dilute spins separated by as far as 6.7 Å (82), which may give rise to long-distance (e.g. *i*, *i*+2) correlations in the spin-dense protein backbones and multiple cross peaks, thus potentially making the use of MMHH method difficult for sequence-specific assignment. Contrary to this expectation, however, it was shown experimentally (85), that the cross-peak resonances for a uniformly labeled sample generally follow the (*i, i*+1) pattern, thus making the MMHH scheme suitable for spectroscopic assignment. Here we have performed detailed many-spin simulations in order to optimize the experiment for the case of Pf1 coat protein reconstituted in bicelles, and to explore the potential evolution of the long-range cross peaks using the spectroscopic

assignment and structural coordinates from previous studies (45,50,90). Briefly, the spin system evolves under the Hamiltonian (82):

$$H = \omega_S S_x^{total} + \omega_I I_x^{total} + \sum_{k=1}^{N_S}\sum_{n=1}^{N_I} a_{kn} S_z^{(k)} I_z^{(n)} + \sum_{i<j}^{N_I} b_{ij}\left[I_z^{(i)} I_z^{(j)} - \frac{1}{4}\left(I_+^{(i)} I_-^{(j)} + I_-^{(i)} I_+^{(j)} \right) \right] \qquad \text{(Eqn. 3.1)}$$

And the magnetization transferred to the *k*'th nitrogen spin is obtained by using a trace metric expression:

$$\left\langle S_x^{(k)} \right\rangle = Trace\left(S_x^{(k)} e^{-iHt} \rho(0) e^{iHt} \right) \qquad \text{(Eqn. 3.2)}$$

where the initial density matrix corresponds to the "normalized" magnetization at the starting spin (denoted as the first nitrogen), and is given by:

$$\rho(0) = S_x^{(1)} / 2^{N-2} \qquad \text{(Eqn. 3.3)}$$

Two or three (N_S = 2, 3) nitrogen, or *S*, spins were considered in the simulations; N_I is the total number of protons, *I*. The radiofrequency (rf) irradiation amplitudes of the low (*S*) and high spins (*I*) are given by ω_S and ω_I , respectively. The interaction constants between the *S*-spins and N_I protons are given by a_n , and b_{ij} describe the interactions among the protons. To calculate the interaction constants, the atomic coordinates were taken from the three-dimensional structure of Pf1 coat protein (PDB ID 1ZN5) (45). Only the transmembrane residues were considered (i.e from I22 to M42), and the effect of the perpendicular orientation and uniaxial rotation in bicelles was treated by scaling the dipolar couplings by -0.4 (17). The amide protons and the alpha-protons were always included, and the other protons were retained if their dipolar couplings to the nitrogen spins of interest were greater than a certain cutoff value (generally around 100 Hz, depending on a residue) to yield the

desired number of protons for the simulation (N_I = 10 in the present study, thus making it a system of up to N = 13 spins total). The magnetization transfer amplitudes were calculated at various values of ω_S and ω_I for the mixing time 10 ms (sufficient to achieve a quasi-stationary equilibrium for the transfer). The magnetization amplitudes were normalized relative to the peak intensity in the absence of the exchange, cf. Eqn. 3.3. The transfers were calculated starting at each amide nitrogen in the sequence of Pf1 corresponding to the transmembrane region, (i.e from I22 to M42) and the transfer profiles were then averaged across the entire structure. The ^{1}H spin lock values were varied from -10 to +10 kHz relative to the ^{15}N spin lock. Figure 3.2A shows the simulations for the values of $\omega_S/2\pi$ equal to 20, 40, and 60 kHz. Here, only isolated pairs of the nitrogen spins were considered at a time (N_S = 2). The transfers calculated for the (i, i+1) and (i, i+2) magnetization pathways are shown in Fig. 3.2A for the various values of ω_S. The isolated-pair simulations predict that the average (i, i+2) transfer intensity is about half of that for the (i, i+1) cross peak (at its maximum value), which would imply that the experimental conditions can be adjusted accordingly by varying the mismatch rf amplitudes to minimize the evolution of long-range interactions. Moreover, a slight increase in the optimal transfer efficiency with decreasing ^{15}N spin-lock B_1 rf filed has been observed as in the previous crystal studies (89).

Furthermore, an important theoretical observation is unequal intensities of the cross peaks, which can be explained by spin competition owing to the non-commuting character of the dipolar interaction terms involved in the Hamiltonian, Eqn. 3.1. For instance, the amide nitrogen spin of residue L38 competes with that of A36 for the polarization originating at G37, while G37 competes with I39 for the polarization from L38, which can result in

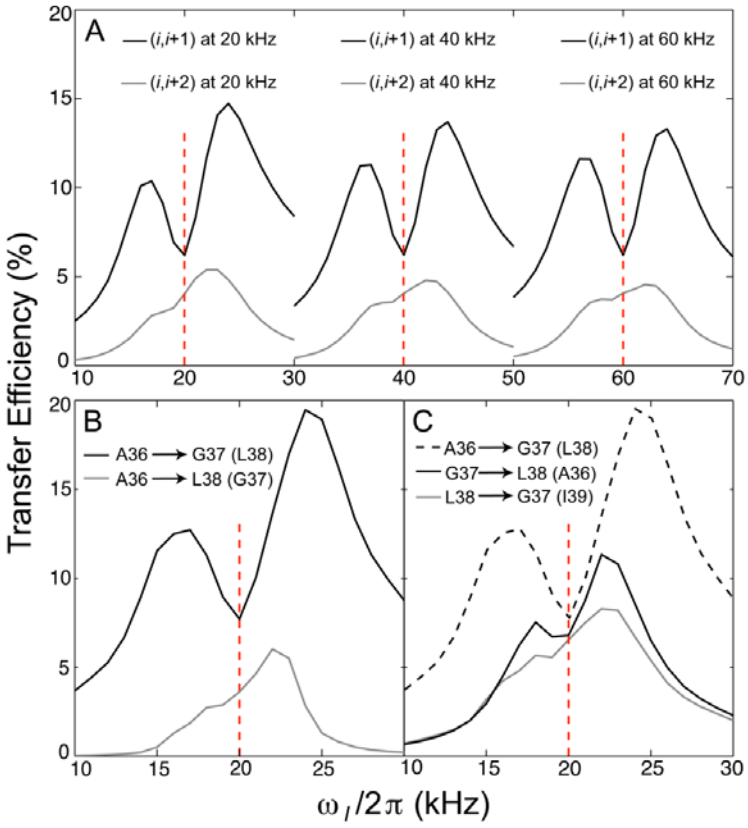

Figure 3.2 Simulations of the efficiency of magnetization transfer between the rare ^{15}N spins under the MMHH conditions. (A) N = 12 spin simulations including single pairs of amide ^{15}N spins for Pf1 reconstituted in bicelles (with the coordinates for residues I22-M42 taken from PDB ID 1ZN5, cf. the text) comparing the (i, i+1) and (i, i+2) magnetization exchange pathways at 20, 40, and 60 kHz ^{15}N spin-lock B_1 fields (marked by vertical dotted lines). Values were averaged across the transmembrane region (residues 22-42). At 20 kHz ^{15}N spin lock B_1 field, the optimal transfer is enhanced by ca. 5.5% and 7.5% over the 40 kHz and 60 kHz ^{15}N spin lock rf fields respectively (cf. Traaseth et al, 2010). (B) Three-^{15}N spin (N = 13) simulations examining the effects of spin competition on the long-range (i, i+2) magnetization transfer in the presence of the more preferential (i, i+1) pathway. The (i, i+2) magnetization transfer between two representative residues A36 and L38 (in the presence of a competing nitrogen spin at G37; gray line) is compared to the A36-G37 (i, i+1) transfer (black line). The efficiency of the (i, i+2) transfer in the presence of the competing (i, i+1) pathway is even lower than in part (A). (C) Three-^{15}N spin (N = 13 total number of spins) simulations comparing the magnetization build up and demonstrating the effect of competing spins on the (i, i+1) and (i+1, i) cross-peak intensities as a function of the rf amplitude mismatch. The transfer from the nitrogen spin at G37 to that of L38 (in the presence of A36; black line) and the transfer from L38 to G37 (in the presence of I39; gray line) have been considered. The A36-G37 transfer from part B is also shown here (black dashed line) to compare it to the L38-G37 transfer.

different cross peak intensities for the bi-directional exchange between the corresponding pairs of residues. The spin competition can be further used to explain the low probability of occurrence of long-range (e.g. i, $i\pm2$) correlations, considering that the (i, $i\pm2$) spin system would have to compete with the more preferential (i, $i+1$) or (i, $i-1$) transfer pathways. A series of simulations were run to explore the above effects of spin competition along the backbone of Pf1. However, within the computer memory limitations, only a single competing spin could be considered in addition to the main transfer pathway (yielding a $N = 13$ spin system total). Fig 3.2B shows the intensity profiles calculated for the (i, $i+2$) transfers from residue A36 to L38 (gray line) in the presence of the competing (i, $i+1$) pathway for the transfer from A36 to G37 (shown by the black line). It can be seen that the more predominant (i, $i+1$) pathway substantially lowers the efficiency of the long distance (i, $i+2$) transfer, thus making the differences between the (i, $i+1$) and (i, $i+2$) cross peaks even more pronounced than in Fig. 3.2A. This theoretical result shows that, for a uniformly ^{15}N labeled protein, most if not all of the crosspeaks are expected to be for an (i, $i\pm1$) transfer, thus making the MMHH scheme suitable for the sequential assignment of ^{15}N amide backbone resonances. Moreover, unequal intensities can be expected even for the (i, $i\pm1$) cross peaks, which may be due to different spin-density distributions of the side-chain protons participating in the MMHH transfer. To illustrate this effect, the profiles shown in Fig. 3.2C contain a representative (i, $i+1$) magnetization transfer from residue L38 to G37 in the presence of the amide nitrogen from residue I39 (black line), and from G37 to L38 in the presence of the competing (i, $i-1$) transfer to the amide nitrogen of A36 (gray line). As can be seen, the presence of a competing pathway may result in slightly unequal intensities of the cross peaks

that are symmetrically positioned with respect to the main diagonal in a homonuclear spin-exchange spectrum. In addition, shown in Fig. 3.2C by the black dashed line is the same A36-G37 transfer as in Fig 3.2B, but now it is to be compared to the L38-G37 transfer. It can be seen that even at the optimal MMHH conditions, the latter has a much lower intensity (about 12%) as compared to the A36-G37 transfer (about 20%). This unequal intensity of the cross peaks is fully supported by the experimental observations (see below). Such an intensity contrast can be used in disambiguation of the cross peaks during the assignment process.

3.4.2 Experimental Results.

Figure 3.3A shows the ^{15}N-^{15}N correlation spectrum of uniformly ^{15}N-labeled Pf1 coat protein reconstituted in magnetically aligned DMPC/DHPC bicelles acquired using the pulse sequence of Figure 3.1A (cf. figure captions for detailed listings of the experimental parameters). Figure 3.3B (red contours) shows the SAMPI4 (22) spectrum. The SAMPI4 spectrum is overlaid with its spin-exchanged version (blue contours) acquired using the pulse sequence shown in Figure 3.1B. The t_1 dimension of the latter is evolved using SAMPI4, followed by the *Z*-filter and the proton-mediated MMHH spin exchange, during which the proton rf amplitude is set above the Hartmann-Hahn matching condition (85). The choice for the optimal mismatch conditions is provided by the simulations as demonstrated in the previous section (cf. Fig. 3.2A). From the simulations, the optimal mismatch amplitude to evolve the (i, i+1) correlations was found to be at 5-6 kHz above the exact Hartmann-Hahn

match. Overlaying the spectra with and without spin exchange in Fig. 3.3B allows for the cross-peaks to be distinguished from the main peaks, and the sequential connectivity among the latter to be established. Note that the exchanged SAMPI4 spectrum exhibits somewhat broader linewidths in the dipolar (indirect) dimension than the SAMPI4, which may be due to the more prolonged sample heating during the MMHH exchange (5 ms). This, in turn, may change the B_1 rf fields at the sample, thus making the homonuclear decoupling during the dipolar evolution somewhat less efficient. In addition, some broader peaks may be due to the overlapping cross- and main-peaks.

As can be seen from Fig. 3.3 (where the red boxes are used to depict the *i*, *i*+1 connectivities) many of the spectral assignments can be established by associating the cross peaks with the corresponding main peaks. For clarity, the results for the sequential residues V35-A36, A36-G37, G37-L38, L38-I39, I39-Y40, Y40-S41 and S41-M42 are highlighted. Figure 3C and 3D show digitized versions of the experimental spectra of Figs. 3.3A and 3.3B to facilitate the visualization of the assignment process. It is important to note that the combination of the homonuclear ^{15}N-^{15}N spin-exchange spectrum (Figs. 3.3A, C) and the spin-exchange SAMPI4 spectrum (Figs. 3.3B, D) assists in resolving ambiguities when the main peaks in the latter spectrum have similar dipolar couplings. Furthermore, unequal relative intensities of the cross peaks can further aid in their disambiguation (see simulations in Fig 3.2C). For example, there are several assignment possibilities for the cross peak of G37, since there are three (3) main peaks that have the same dipolar couplings in the SAMPI4 spectrum (at around 2.1 kHz). However, upon the cross-referencing of the corresponding chemical shifts and the stronger cross peak in the ^{15}N-^{15}N exchange spectrum,

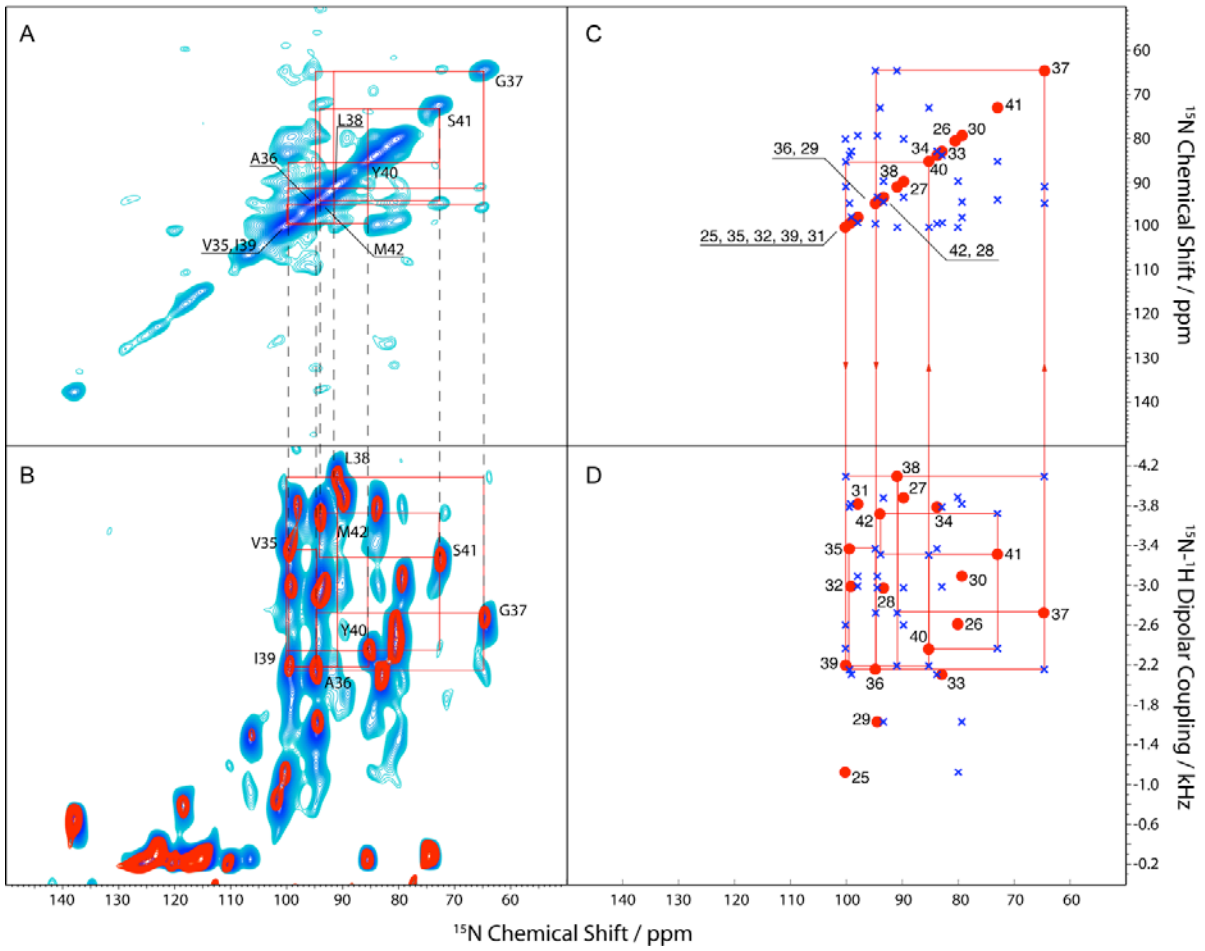

Figure 3.3 Spectra of Pf1 coat protein reconstituted in magnetically aligned DMPC/DHPC bicelles at T = 38°C. (A) Experimental ^{15}N-^{15}N spin correlation spectrum: 512 scans; MMHH at 45.5 kHz ^{15}N B_1 rf field and 51.5 kHz ^{1}H B_1 field, 0.5 s Z-filter and 5 ms mixing time; 64 complex t_1 points; (B) Experimental SAMPI4 spectrum (red) overlaid with its spin-exchange version (blue). SAMPI4: 128 scans, 45.5 kHz B_1 field (for CP match and decoupling), 80 real t_1 points (red contours); Spin-exchanged SAMPI4: 1024 scans, MMHH at 45.5 kHz ^{15}N B_1 rf field and 51.5 kHz ^{1}H B_1 field, 0.5 s Z-filter and 5 ms mixing time; 80 real t_1 points (blue contours). A single-contact CP of 1 ms, 10 ms total acquisition time in the indirect dimension, and a 6 s recycle delay were used in all experimental spectra. Darker shadows of blue in the spectra indicate higher intensity of the resonance lines, whereas lighter shadows correspond to less intense areas. (C) Digitized version of the ^{15}N-^{15}N spin correlation spectrum. (D) Digitized version of the SAMPI4 spectra. Cross-referencing among the three experimental spectra allows one to obtain connectivities between the consecutive residues as shown by the red boxes. For clarity, a representative assignment pathway for residues V35-M42 is shown in the digital versions of the spectra (parts C and D).

only one possibility remains, which leads to the assignment: A36-G37 (at 94.8 ppm and 64.6 ppm, respectively). All the other possibilities are ruled out. Note that the simulations of Fig 3.2C also predict that the intensity of the cross peak corresponding to the A36-G37 transfer is greater than that for the L38-G37 transfer, which may point at a role of the side-chain protons in the (*i*, *i*+1) MMHH transfer. Similar process can also be applied to other residues, thus establishing the sequential assignment of the transmembrane domain. This strategy, however, requires absolute assignment of at least one "seed" residue; G37, according to the result published by the Opella group (50,90), serves this purpose in the present illustrative case. Alternatively, a single selectively labeled spectrum including all Alanines, Glycines, and Leucines in the sequence could be used to immediately assign the residues A36-G37-L38 (there is only one such combination in the primary sequence for the Pf1 coat protein). This would serve as a starting point for the assignment; such a choice for selective labeling is clearly sequence-dependent. Notably, these assignments are in agreement with those obtained previously using a combination of selective isotopic labeling and the shotgun approach (50,90), and the cross-peaks generally follow the (*i*, *i* + 1) connectivity pattern. Similar process can also be applied to the remaining residues in the transmembrane domain, including Y25–G28 and others (cf. Fig. 3c). However, since the peaks for G28 and A29 have nearly identical 15N chemical shifts, detection of the cross peaks between these two residues using the two-dimensional spectra is not feasible, which breaks down the continuity of the assignment process. Therefore, complete assignment of NMR spectra of oriented membrane proteins would likely require performing three-dimensional double-resonance experiments, as done routinely in MAS and liquids NMR.

To further improve the quality of the spectra, the newly established REP-CP sequence (86) can be employed to significantly (up to 40%) increase the signal-to-noise ratio for the highly dynamic membrane proteins reconstituted in perpendicular bicelles. Moreover, with the enhanced signal-to-noise ratio, much longer (up to 20 ms) acquisition intervals in the direct dimension can be used to help eliminate the spectral crowdedness near the diagonal region in the homonuclear spin-exchanged spectra. As can be seen from Fig 3.4A, the resonance lines in the ^{15}N-^{15}N correlation spectrum are much narrower than those obtained in the previous spectra (cf. Fig. 3.3A), hence making the cross-peak detection more reliable. A side-by-side comparison was performed between two spin-exchange experiments involving

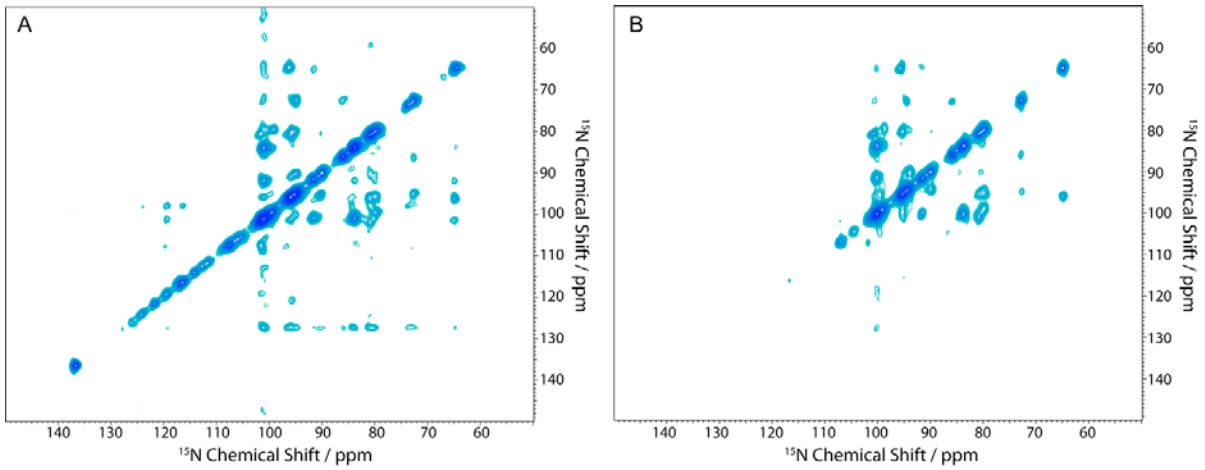

Figure 3.4 A comparison between (A) ^{15}N-^{15}N MMHH spin-exchange spectrum at 512 scans, 20 kHz ^{15}N B_1 rf field and 25 kHz ^{1}H B_1 field, and 0.5 s *Z*-filter; and (B) ^{15}N-^{15}N PDSD spectrum: 256 scans and 3 s mixing time. The REP-CP pulse sequence with 5 contacts of 300 μs length each was used to enhance magnetization on the ^{15}N spins (Tang and Nevzorov, 2011), 80 complex t_1 points, 20 ms total acquisition time in the direct dimension, and a 6 s recycle delay were used in both spectra. In part B, the peaks are slightly broader, and some of them (both the main and cross peaks) are missing in the spectrum.

either MMHH (Fig. 3.4A) or PDSD (Fig. 3.4B) during the mixing period (with the pulse sequence for the latter shown in Figure 3.1C). For the MMHH spin-exchange experiment, 512 transients were co-added, 5 ms contact time with a *Z* filter of 0.5 second were used (yielding the total time 6 d. 18 h.). For the PDSD spin-exchange experiment, 256 scans and a mixing time of 3 seconds were utilized (yielding the total time 4 d. 13 h.). In both experiments, 80 complex t_1 points, 5 repetitive contacts, and a 6 s recycle delay were employed. During the MMHH exchange, the absolute Hartmann-Hahn match amplitudes were lowered to the value of about 20 kHz, following the previous studies (83,89), while the B_1 amplitude mismatch for the protons was still kept at 5 kHz. An additional benefit of lowering the B_1 amplitudes is a reduced sample heating during the MMHH exchange and the subsequent 20 ms acquisition under the conditions of proton decoupling. A comparison of Figures 3.4A and 3.4B shows that the MMHH method yields a better resolution for both the main and cross peaks, especially near the main diagonal. The signal-to-noise ratio for the well-resolved representative cross peaks was estimated to be between 3:1 and 5:1 in both spectra. However, upon closer examination of the PDSD spectrum, it becomes clear that some of the cross peaks, such as that corresponding to G37 to L38, are not evolved at all when using the PDSD method. In addition, the main peaks corresponding to the more dynamic N-terminal region are entirely missing in the PDSD spectrum, cf. Figs. 3.4 A and B.

Shown in Fig. 3.5 is a symmetrized ^{15}N-^{15}N correlation experiment of Fig. 3.4A. Red crosses show the simulated cross peaks whose chemical shifts are taken from the corresponding SAMPI4 spectrum (the main peaks of Fig. 3.3D) using the previous assignment (34,50,90). As can be seen from Figure 5, all simulated cross peaks have an

underlying experimental intensity, which in turn, proves the correctness of the previous assignment (34,50,90). However, there are also additional weaker cross peaks that may correspond to the long-distance (i.e. *i*, *i*+2) correlations; the cross peak between G37 and I39 is one such example. We note that these extra peaks may not evolve when using higher B_1 rf fields and mismatches (cf. the simulations in Fig. 3.2A and the experimental spectrum of Fig. 3.3A); this issue merits further investigation.

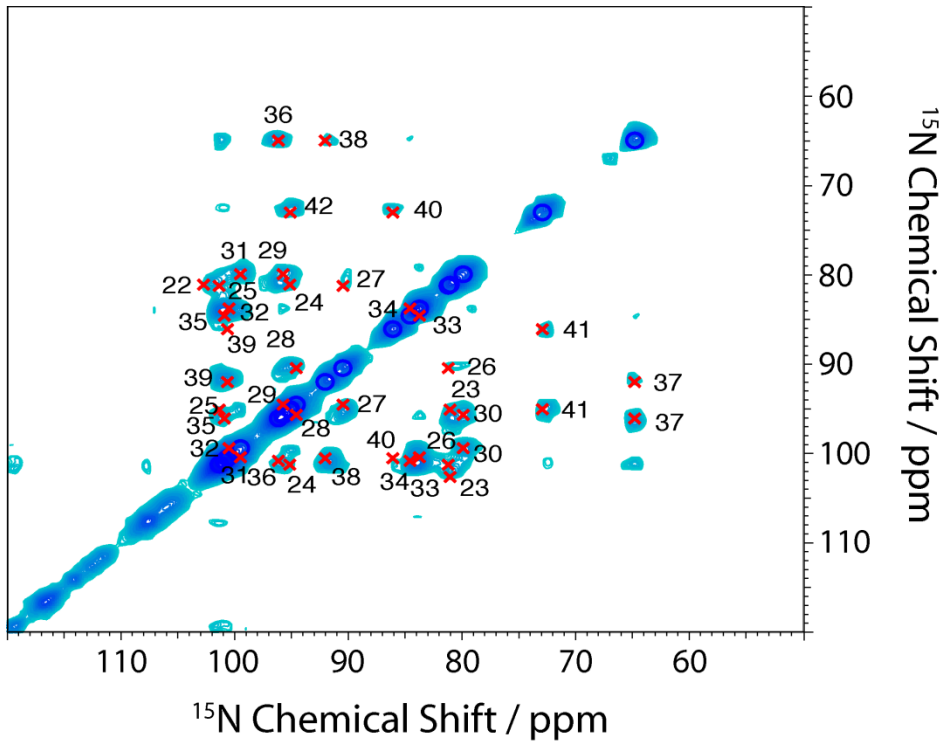

Figure 3.5 A zoomed-in view of the symmetrized ^{15}N-^{15}N MMHH exchange spectrum from Figure 3.4A overlaid with the simulated crosspeaks (red crosses) calculated using the chemical shifts from the main peaks of the SAMPI4 spectrum (from Fig. 3D) and the previous assignment (Opella et al, 2008; Park, 2010). All simulated cross peaks have underlying intensity, which proves the correctness of the previous assignment. Moreover, the cross peaks generally follow the (*i*, *i*+1) connectivity pattern.

3.5 Conclusions

Oriented-sample solid-state NMR represents a powerful technique for the structural studies of the conformations of membrane proteins in their native-like, fully hydrated lipid environment. In the present work, a purely spectroscopic method for establishment and validation of the NMR assignments for membrane proteins reconstituted in magnetically aligned bicelles has been presented. The quality of the spin-correlation spectra previously obtained for Pf1 reconstituted in magnetically aligned bicelles (85) have been significantly improved. Furthermore, we have provided an assignment strategy for the uniformly ^{15}N labeled Pf1 phage coat protein reconstituted in "perpendicular" bicelles by using three two-dimensional experiments that could greatly reduce the number of selectively labeled samples utilized in the assignment process. We have demonstrated the general applicability of the proton-mediated magnetization transfer under the MMHH conditions (82,85) for establishing predominantly the (i, i+1) spin correlations. Many-spin simulations accurately predict the optimal mismatch B_1 field amplitudes without the necessity of running lengthy experimental optimizations. The sample of Pf1 coat protein reconstituted in perpendicular bicelles provides sufficient resolution to resolve nearly all of the sequential cross peaks in the transmembrane region. Moreover, sensitivity enhancement afforded by the REP-CP sequence allows one to perform longer (up to 20 ms) acquisitions in the homonuclear ^{15}N-^{15}N exchange experiments. Since the MMHH exchange is driven by the dipolar couplings, its use is primarily restricted to the more rigid regions of the protein. The method has confirmed the previous assignment for the transmembrane region (34,90) that was performed using multiple selectively labeled

samples. Furthermore, with the ability to establish correlations among the dilute spins separated by as far as 6.7Å based on previous NAL crystal study, the MMHH scheme may be of great value for establishing intermolecular contacts between the neighboring alpha-helices and the elucidation of their packing structure, which calls for further investigation. Notably, the present assignment method allows one to use a uniformly ^{15}N labeled sample, with perhaps only a few selectively labeled "seed" spectra to initiate the assignment process. However, for structure determination and complete NMR assignment for membrane proteins of more complex topology, doubly labeled samples and three-dimensional pulse sequences incorporating the MMHH spin exchange may be necessary. Recent studies (91) correlating the ^{13}C and ^{15}N spins via the MMHH mechanism are especially encouraging in this regard.

CHAPTER 4

ANODIZED ALUMINUM OXIDE NANOPORES AS AN ALTERNATIVE ALIGNMENT MEDIA FOR THE STUDY OF MEMBRANE PROTEINS USING ORIENTED-SAMPLE NMR

4.1 Abstract

Substrate-supported phospholipid bilayers provide an adequate mimetic of cellular membranes. It has been shown that phospholipid vesicles transform into planar membranes when deposited on chemically treated surfaces. Such an arrangement closely mimics the native bilayer environment, and thus is suitable for the incorporation of transmembrane proteins (92). In 2003, a novel way of aligning membrane protein samples was reported by Smirnov and Poluektov (93). The lipids were placed inside nanoporous anodic aluminum oxide sheets (AAOs), and spontaneously assembled into nanotubular bilayers. The pores in AAOs are highly homogenous, and the pore size can be controlled from several nanometers to around 250 nm. These structures, which are called lipid nanotube arrays, have a high density of the nanoporous channels, thus, providing at least a 500 fold gain in the bilayer surface area as compared to similar sized planar substrates. These new substrate-supported bilayers have been proven to be quite similar to the unsupported lipid bilayers (94,95) and are suitable for aligning membrane proteins for the subsequent high-resolution solid-state NMR studies (96).

NMR studies of M2 protein of influenza A virus reconstituted in the lipid nanotube arrays have been previously reported (97). Here, we describe our solid-state NMR study of the Pf1 coat protein from bacteriophage, which is made possible with the improved method for preparing AAO supported lipid bilayers. The Pf1 coat protein was reconstituted in different lipid combinations which illustrates high flexibility of AAO-supported substrates for the incorporation and refolding of membrane proteins and studies of their lipid-induced conformational changes. One-dimensional ^{31}P NMR spectra demonstrate that both the lipids and membrane protein molecules are uniformly oriented within the nanotubes, whereas two-dimensional SAMPI4 spectra provide more insights about lipid-induced conformational changes of membrane proteins at atomic-resolution level.

4.2 Introduction

In the past decades, it has been widely recognized that solid-state NMR (SSNMR) has emerged as a powerful tool for the structural studies of membrane proteins in their native-like environment (98), which, due to the presence of lipids and water molecules, cannot be easily implemented via crystallization. The proteins whose structures have been successfully studied by Magic-Angle-Spinning (MAS) and Oriented-Sample (OS) NMR include, but are not limited to, gramicidin (11), rhodopsin (12), Pf1 phage coat protein (13), M2 domain of nAChR (14) and influenza A virus (15), phospholamban (16), Vpu from HIV-1 (17) and MerF (18). Most recently, the structure of CXCR1, a class A rhodopsin-like G-protein-

coupled receptor (GPCR) was fully solved by Opella and co-workers (99). Due to the fact that SSNMR normally has broader line widths, numerous methods have been developed over the past years in order to overcome, or at least to partially alleviate this problem. One of the most important techniques employed by OS NMR is the pursuit of higher spectral resolution by achieving higher degree of macroscopic sample alignment, which is normally done either mechanically with glass plates (100) or magnetically with bicelles (47).

Pioneered by McConnell and his coworkers (92,101) back in the 1980s, substrate-supported phospholipid bilayers represent a plausible mimetic of cellular membranes. Studies have shown that phospholipid vesicles transform into planar membranes when deposited on chemically treated surfaces (102-105), rendering the deposited lipids a very close approximation to the native bilayer environment, and thus suitable for the incorporation of transmembrane proteins (92). Although such a design brings several benefits, like the ease of manipulating certain parameters of the sample, the drawbacks are also quite obvious. First, the samples are rather delicate since the surface is exposed to the environment. In addition, it is hard to keep the surface of such an assembly fully hydrated, which is critical for maintaining the phospholipids in good structural order. In addition, the limited surface area restricts the maximum amount of the lipid molecules as well as the number density of membrane proteins that could be deposited. Bicelles, on the other hand, have gained their popularity in the research of membrane proteins by means of Oriented-Sample NMR over the past decade (106). Spectra obtained in such a system generally have sharper line widths due to the fast uniaxial rotation of membrane proteins about their alignment axis (74). In addition to the normal “perpendicular” orientation, bicelles could also be “flipped” by adding the

lanthanide ions, such as Yb^{3+} (35), giving rise to the possibility of investigating membrane proteins at a different alignment angle (73,80). However, bicelles are generally restricted to a rather limited repertoire of lipids. In other words, not any lipid mixture forms magnetically aligned bicelles, hence limiting the applicability of such a system. In 2003, a novel type of substrate-supported lipid bilayers that provided an alternative way to align membrane protein samples was reported (93). The same perpendicular orientation as in bicelles has been achieved mechanically by depositing the lipids inside highly homogeneous anodic aluminum oxide (AAO) substrates. A schematic representation of such a system is shown in Figure 4.1. Shown on the top left is a photo of the actual AAO slides. Top right is the Scanning Electron Microscopy (SEM) image of its surface, and the images on the bottom are the top and side view of the inner structure of the nanopores. Lipids were placed inside nanoporous anodic aluminum oxide sheets (AAOs), and spontaneously assembled into nanotubular bilayers. The pores in AAOs are highly homogenous and the pore size can be controlled from several nanometers to around 250 nm when different anodizing conditions are applied during the pore formation (107-109). These structures, which are called lipid nanotube arrays, have a high density of the nanoporous channels, thus, providing at least a 500 fold gain in the bilayer surface area as compared to a similar sized planar substrate. For example, 20 AAO strips of5×12 mm size having 100 nm pore diameter and 50 μm thickness yield the inner surface area of over 1 m^2.

In addition to their large surface area, lipid nanotube arrays represent several potential advantages over conventional planar bilayers. These include long-term stability of aligned

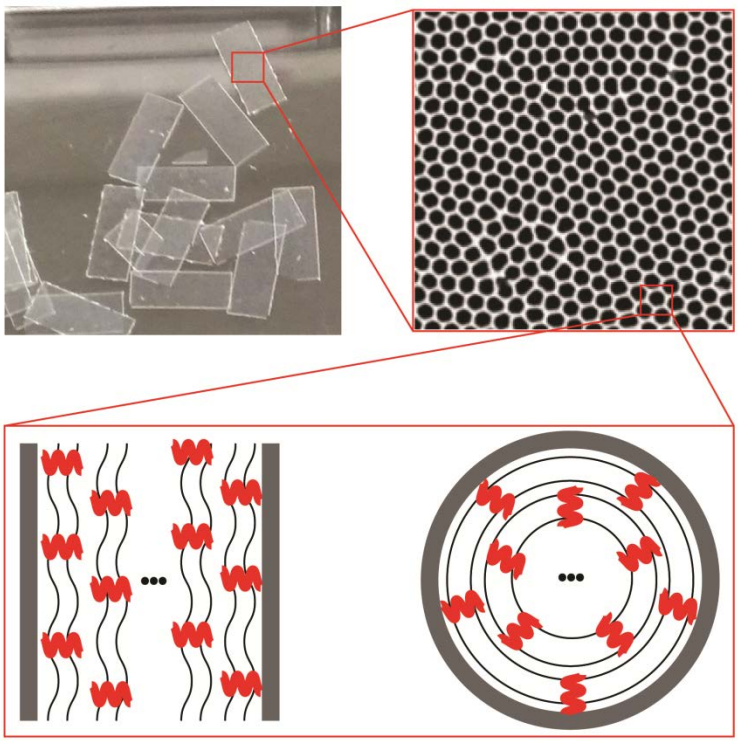

Figure 4.1 A schematic demonstration of membrane proteins reconstituted in lipid bilayers with the support of nanoporous AAO slides.

lipid assemblies under wide ranges of temperature, pH, and salt concentration. Moreover, AAO nanopores provide full hydration level of lipid bilayers, and protection from surface contaminations. Another feature is accessibility of the solute molecules to the bilayer surface. This makes it possible to expose membrane protein samples to different solution media, including ligand molecules, and repeat this procedure multiple times without changing the sample. Recent studies have demonstrated that these new substrate-supported bilayers are quite similar to the unsupported lipid bilayers (94,95) and are suitable for aligning membrane proteins for the subsequent high-resolution solid-state NMR studies (96).

In this work, we demonstrate the first two dimensional SSNMR study of uniformly ^{15}N labeled Pf1 phage coat protein reconstituted in lipid bilayers of various composition supported by AAO nanopores. The coat protein of Pf1 bacteriophage has been extensively studied by means of SSNMR (90), and hence serves as a model system in this case.

4.3 Materials and Methods

4.3.1 Preparation of AAO stripes

The AAO sheets have been prepared in a two-step process. High purity aluminum foil (99.997%, 0.127 mm x 100 mm) was purchased from Strem Chemicals, Inc. The foil was cut into rectangular pieces of around 10cm x 3cm, cleaned and electro-polished at 20V for 1 minute. The small pieces were then immersed into a solution of H_3PO_4:H_2SO_4 at 95:5 (v/v) with 20mg/l CrO_3 at 85°C. Immediately following this procedure, the aluminum pieces were anodized in 4% oxalic acid for 10min at 40V. A thin layer of nail polisher was then applied to one side of the foil in order to protect it from further anodization. Once thoroughly dried, the anodization step continued for at least 20h in the potentiostatic mode at 40V. The porous alumina oxide is then stripped down in a mixture of 3.5% H_3PO_4 and 45 g/l CrO_3 at 70°C, washed and then re-anodized for another 20-25 hours. Afterwards, the nail polisher could be removed by acetone, and the thin layer of aluminum was dissolved in 10% $CuCl_2$ solution at room temperature under mild sonication. In order to thoroughly open up the nanopores from

both ends, as well as to enlarge the pores to the desired diameter, the foil was subsequently treated with 5% H_3PO_4 solution for a controlled amount of time.

The product was then cut into desired sizes by in-house laser setup to fit the NMR tube.

4.3.2 Preparation of Pf1 coat protein and nanopore-supported lipid bilayers

Uniformly ^{15}N-labeled Pf1 phage was purchased from Hyglos GmbH (Regensburg, Germany). To purify Pf1 coat protein, a predefined amount of the phage was dissolved in 1 mL of TFE (50 %)/TFA (0.1 %) to precipitate the DNA, followed by lyophilization of the soluble fraction. Approximately 3 mg of the lyophilized protein was then dissolved in TFE, and mixed with DOPC/DOPG (w/w ratio = 10:1) in chloroform. The solvent was removed by rotary evaporation, and the sample was kept under vacuum overnight. Afterwards, the protein/lipid film was rehydrated in a 50mM sodium chloride solution. Vigorous vortex accompanied with freeze-thaw cycles was applied until the solution became uniform and non-viscous. Protein/lipid mixture was then deposited onto the nanoporous AAO structure by soaking and drying followed by re-hydration with small amount of water.

Around 30 deposited AAO stripes, in each case, were then collected and stacked to fit in the NMR sample tube.

A separate control sample containing Pf1 coat protein in DMPC/DHPC (at q = 3:1 molar ratio) bicelles was also prepared following the protocol published by Opella and co-workers (38).

4.3.3 NMR spectroscopy

All the NMR experiments have been performed on a Bruker Avance II spectrometer operating at 500 MHz ^{1}H frequency and running Topspin^{TM} 2.0 software. A static Bruker 5 mm round-coil E-free^{TM} probe was utilized in all experiments. The optimal sample temperature T = 45°C was found by recording the line widths of the ^{31}P NMR lipid spectra.

For acquiring two-dimensional separated local-field (SLF) experiments, the SAMPI4 pulse sequence (22) was used, yielding correlation spectra with ^{15}N chemical shift as one dimension and the ^{15}N-^{1}H dipolar coupling as the other. To further enhance the signal, a recently published pulse sequence, termed as REP-CP (86), was applied during the preparation period.

4.4 Results and Discussion

Shown in Figure 4.2 are the Scanning Electron Microscopy (SEM) images of our homemade AAO sheets, following the procedure described in the previous section. Compared to the commercial AAOs (images not shown), both the inner diameters and the alignment of the nanotubes are much more uniform, which plays a critical role in the line width of OS NMR, thus affecting the final resolution of the two-dimensional spectra.

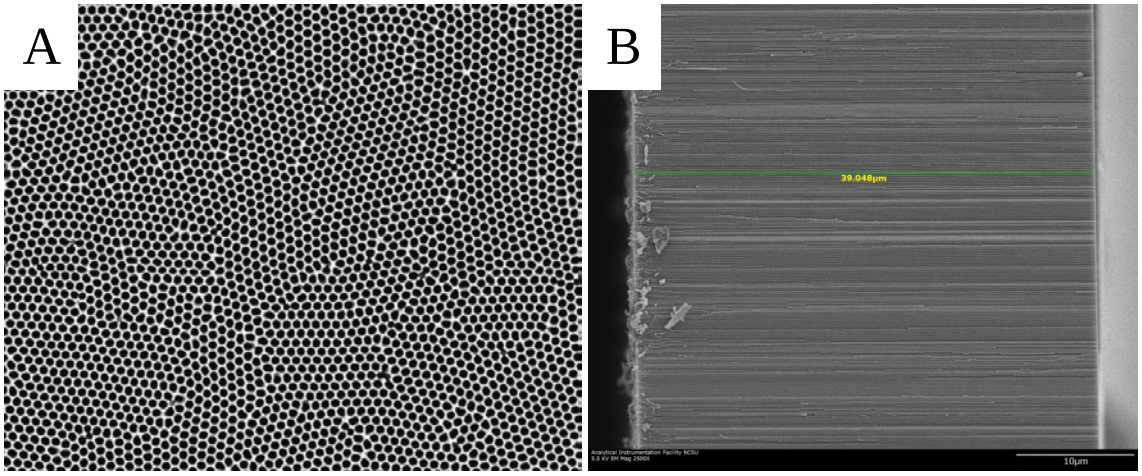

Figure 4.2 SEM images of the produced AAO sheets following the procedure as described in the text. A) The top view. B) The side view. (Photo courtesy of Dr. Antonin Marek)

Matlab (Mathworks, Inc. Natick, MA) scripts have been used to analyze the SEM micrographs, by identifying each of the pores followed by running statistical analysis on the whole assembly shown in the images. As a result, the pore size of the AAO sample in Figure 4.2A has been calculated to be 82.23 ± 4.2 nm with the thickness, as shown in Figure 4.2B, to be 39 µm. The distribution of the pore size of various homemade AAO samples, as compared to a commercially available AAO sample from Whatman™, has been calculated and is illustrated in Figure 4.3.

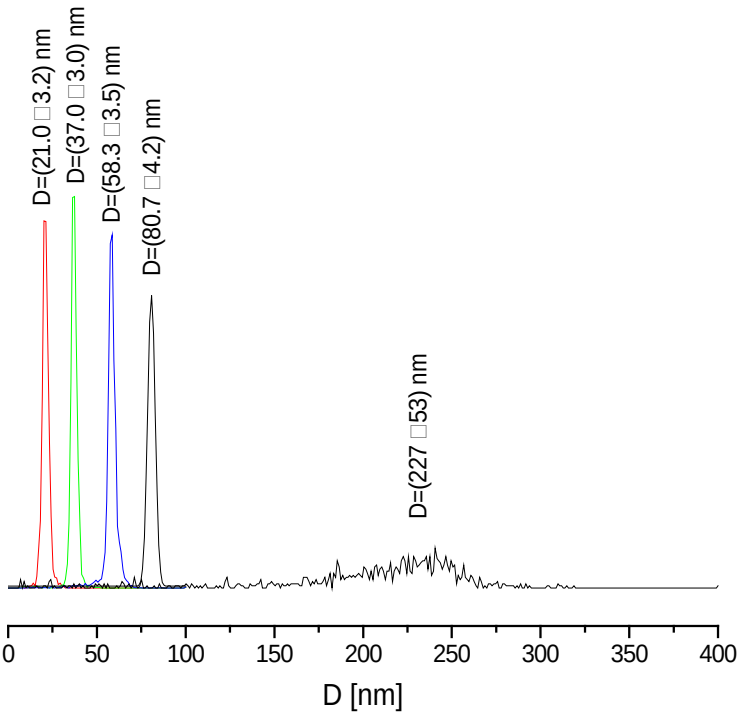

Figure 4.3 Distribution of the pore size of various homemade AAO samples as compared to the commercially available Whatman^{TM} AAOs at 200 nm diameter.

Circular dichroism (CD), which was invented in the first half of the 19th century, has a broad range of applications in various areas of research. It measures differences in the absorption of left-handed polarized light versus right-handed polarized light, which makes it a perfect tool for the investigation of the secondary structure of proteins. Figure 4.4 is the CD spectrum of the coat protein of Pf1 bacteriophage reconstituted in the lipid bilayers before the deposition into the AAO nanopores. From the appearance of the two peaks at around 210 nm and 225 nm, it is possible to say that the protein is correctly folded within the lipid bilayer, and is taking the alpha-helical form.

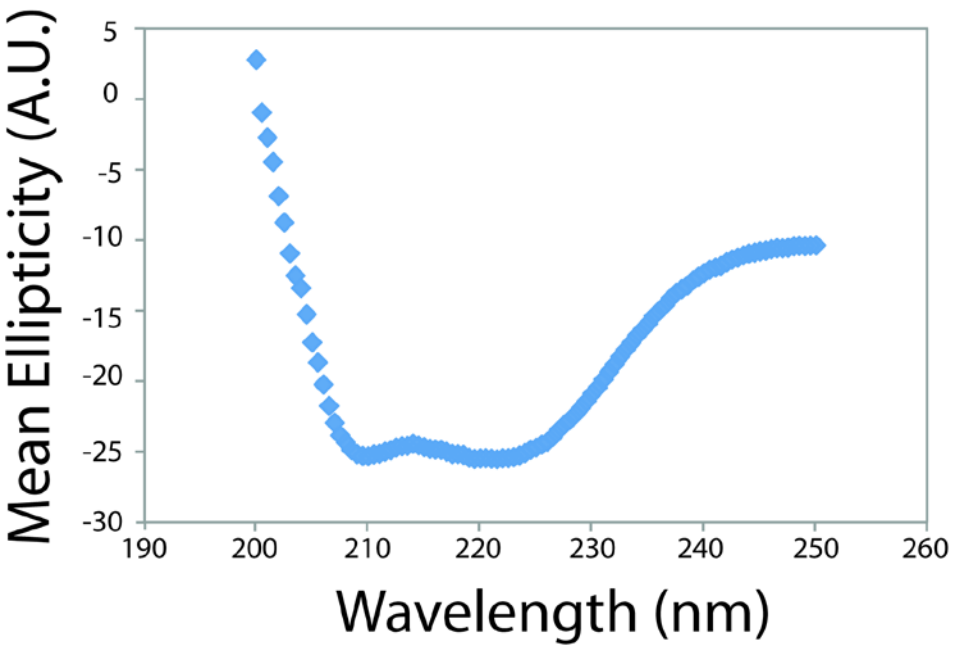

Figure 4.4 CD spectrum of the coat protein of Pf1 bacteriophage reconstituted in the lipid bilayers before the deposition into the AAO nanopores.

After the deposition of the membrane protein reconstituted in different lipid combinations, solid-state NMR experiments were carried out at 45°C as was described in the previous section. Figure 4.5 shows one-dimensional ^{1}H-decoupled ^{31}P NMR spectrum, as well as ^{15}N spectrum of Pf1 coat protein reconstituted in DOPC/DOPG in the ratio of 9:1. By integration of the peaks, the ratio of the areas between the 2 peaks has been found to be around 8:1, which is close to the originally deposited lipid amounts. The half-peak half-height width of the rightmost peak of around 170 Hz suggests that the lipid bilayers within the AAO nanopores are highly aligned. Figure 4.5B shows a one dimensional ^{1}H-decoupled ^{15}N spectrum of the same sample. The resolution of the peaks, especially those at around 60

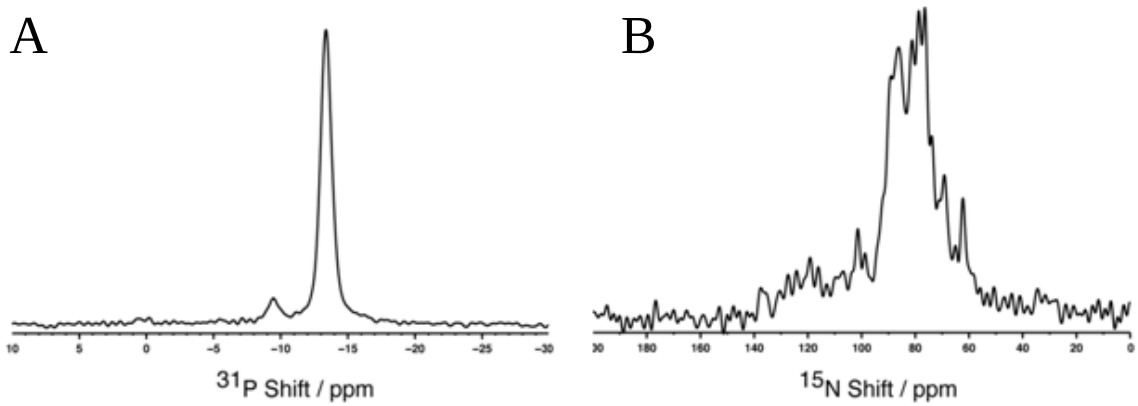

Figure 4.5 One dimensional ^{1}H-decoupled ^{31}P NMR spectrum (A) and ^{15}N CP spectrum (B) of Pf1 coat protein reconstituted in DOPC/DOPG lipid bilayers within the AAO nanopores. 1024 scans was used for the ^{31}P experiment, whereas 8192 scans with a 90° pulse duration of 4.9 μs was used for the ^{15}N experiment. More details are covered in the text.

ppm, suggests good alignment of the Pf1 coat protein within the DOPC/DOPG lipid bilayer. However, compared with the line widths of the corresponding spectra of Pf1 refolded in bicelles (51), the line widths in Figure 4.5 are somewhat broader. The reason might be that bicelles undergo fast uniaxial spinning about the bicelle normal in the aqueous solution, which provides additional line narrowing. On the other hand, the DOPC/DOPG lipid bilayers in the AAO nanopores are restricted by the local environment within the nanotubes, which prohibits the lipids from moving freely and hence lead to slower averaging of the uniaxial disorder (74). A greater uniaxial disorder could also arise from the wave-like conformations adopted by the surface of the lipid bilayer as proposed by Gaede et al. (110), cf. Figure 4.1.

Shown in Figure 4.6 are the two-dimensional separated local-field (SLF) spectra of Pf1 coat protein reconstituted in various lipid environments. SAMP4 (22) pulse sequence

was used in all the experiments, resulting in spectra correlating the ^{15}N chemical shifts with the ^{1}H-^{15}N dipolar coupling. To further enhance the signal, a recently developed CP scheme, termed as REP-CP (86), was utilized. Figure 4.6A is the SAMPI4 spectrum measured for Pf1 in DMPC/DHPC bicelles, which serves as a reference. 96 t_1 points was used with 256 transients for each point. The B_1 field was set to 40.3 kHz. The sample was maintained at 38°C based on previous optimization (data not shown). Polarity Index Slant Angle (PISA) wheels (23,24) are calculated using a Matlab script. The best fit for the spectrum (depicted in red circles in Fig. 4.6A) corresponds to an order parameter of 0.8 while the tilt angle of the helix is set to 22~24° relative to the bicelle normal. Shown in Fig. 4.6B is the SAMPI4 spectrum for Pf1 refolded in DMPC/DHPC lipid bilayers immobilized within the AAO nanopores. The experiment was carried out at 45°C, based on ^{31}P spectra line width under different temperatures. The B_1 field in this case was set to 50.3 kHz. 1024 scans were used for each of the 64 t_1 increment. The PISA wheel calculation yields the best fit when the order parameter is set to 0.95 with a tilt angle of 22~24°**.** Compared with Fig. 4.6A, there is a high similarity between the spectral patterns of the peaks, with the tilting angle being the same, which suggests that the conformation of Pf1 in these two lipid environments is very similar. However, the line widths in Fig. 4.6 B are noticeably broader presumably due to a larger degree of the uniaxial disorder within the DMPC nanopores (*vide supra*). Figure 4.6C is the SAMPI4 spectrum of Pf1 coat protein reconstituted in DOPC/DOPG lipid bilayers in AAO nanopores (at [DOPC]/[DOPG]=9:1 molar ratio). The spectrum was obtained under exactly the same condition as Fig. 4.6B. The best fit of the calculated PISA wheel in this case correspond to the order parameter of 0.95 with a tilt in the range of 18~20°. A slightly

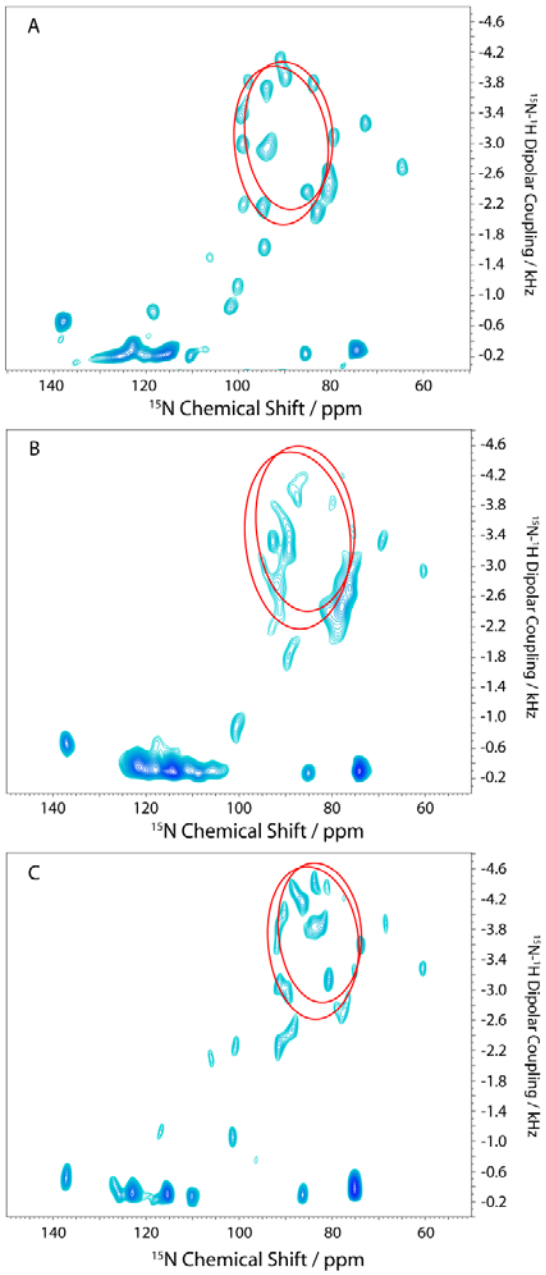

Figure 4.6 Two-dimensional separated local-field spectra of Pf1 coat protein reconstituted in various lipid environments overlaid with calculated PISA wheels. A) DMPC/DHPC bicelles. The B_1 field was set to 40.3 kHz. 96 t_1 points was obtained with 256 transients for each point. The experiment was done at 38°C**.** B) DMPC/DHPC in AAOs. The B_1 field was set to 50.3 kHz. 1024 scans were used for each of the 64 t_1 increment. The sample was maintained at 45°C during the experiment, which was optimized according to ^{31}P line width. C) DOPC/DOPG in AAOs (at 9:1 molar ratio). Experiment was carried out under the same condition as B.

different pattern in the spectral peaks, compared with the spectra shown in Fig. 4.6A and 4.6B, suggests a different orientation and conformation of the Pf1 coat protein in DOPC-based bilayers than in DMPC-based bilayers. This is expected because the length of the carbon chain in DOPC is longer than that of DMPC. As a result, the larger thickness of the hydrophobic core leads to a smaller tilt angle of the Pf1 coat protein with regard to the bilayer normal (90) in DOPC-based bilayers, cf. Fig. 4.6C.

4.5 Conclusion

Here we demonstrate the feasibility of high-resolution solid-state NMR spectroscopy of the Pf1 coat protein reconstituted in nanoporous AAO substrate-supported lipid bilayers. For the first time, a two-dimensional spectrum of a uniformly ^{15}N-labeled membrane protein has been acquired showing resolution comparable to that obtained in magnetically aligned bicelles. Moreover, AAO-supported substrates allow one to incorporate various lipid mimetics for the studies of lipid-induced conformational changes for membrane proteins. Different lipid combinations were used including DMPC, DOPC and DOPG. The two-dimensional SLF experiments on the DMPC-based AAO sample shows similarity to that of the spectrum obtained in magnetically aligned bicelles, whereas DOPC-based substrate shows marked deviations in the positions of the spectral peaks. This may indicate that the folding of the membrane-spanning proteins is lipid dependent (11), as well as provide a method for studying structural conformations of membrane proteins in different lipid environments. More importantly, the spectrum of DOPC/DOPG sample has broadened the

range of lipids as compared to magnetically aligned bicelles for the structural studies by OSNMR methods, since some membrane proteins may not be reconstituted in DMPC-based bicelle systems. By contrast, AAO supported lipid bilayers can incorporate any desired lipids for the refolding of membrane proteins.

Compared to glass plates, the nanoporous AAO-supported phospholipid bilayers have a much larger surface for lipid deposition. In addition, lipid nanotube arrays represent several potential advantages over the conventional planar bilayers. These include long-term stability of aligned lipid assemblies under wide ranges of temperature, pH, and salt concentration. Moreover, AAO nanopores provide full hydration level of lipid bilayers, and protection from surface contamination. Another feature is the excellent accessibility of solute molecules to the bilayer surface afforded by the nanopores. Furthermore, the diameter of the nanopores can be easily controlled during the anodization stage. Therefore, the AAO nanopores provide an alternative alignment media of flexible lipid mimetics for studying membrane proteins in their native like environments by solid-state NMR.

CHAPTER 5
SUMMARY AND FUTURE WORK

5.1 Summary

Membrane proteins are a class of proteins that have tremendous impact on any living creatures. They perform important functions related to almost every aspect of life, such as ion transport, signal transduction and molecular recognition, to name a few. For us human beings, they are the target of over 50% of modern drugs. Despite their vital importance, their structures are not well studied yet, as compared to the soluble proteins, due to their amphiphilic nature. Unique structures of membrane proteins reported so far represent only 1% of the total structures in the Protein Data Bank.

Over the past decades, solid-state NMR has emerged as a powerful tool for the structural research on membrane proteins reconstituted in their native environments. Most recently, the structure of CXCR1, a class A rhodopsin-like G-protein-coupled receptor with seven transmembrane domain was fully solved and reported. This study has not only proven the feasibility of SSNMR in the structural research of membrane proteins, but also broadened the range of research target to a greater molecular weight.

In this present work, three (3) critical aspects of oriented-sample NMR have been addressed, in hope to further facilitate its application in the structural-function of membrane proteins in their native-like lipid bilayer environment. The first is the intrinsic low sensitivity of solid-state NMR that every spectroscopist has to face. A repetitive-contact cross-

polarization scheme, termed as REP-CP, was developed that allows one to fully transfer the polarization from the abundant proton spins to the sparse low-gamma nuclei. As a result, a factor of two (2) enhancement in sensitivity was gained over the conventional single-contact CP, whereas 45% average intensity gain is achieved as compared to CP-MOIST. Secondly, a strategy for assigning solid-state NMR spectra of Pf1 coat protein reconstituted in magnetically aligned bicelles has been developed. A two-dimensional spin-exchanged version of the SAMPI4 spectrum correlating ^{15}N chemical shift and ^{15}N-^{1}H dipolar couplings is obtained under mis-matched Hartmann Hahn conditions. Combining the spin-exchanged version with the original SAMPI4 experiment makes it possible to establish sequence-specific assignments, and this technique is generally applicable to other membrane proteins. Of note, only a single uniformly labeled protein sample is required as opposed to multiple selectively labeled samples currently employed for spectroscopic assignment by the "shotgun" approach. Using sensitivity enhancement techniques such as REP-CP assists in further elucidating cross peaks and allows the establishment of correlations between the adjacent residues along the backbone. Simulation accurately predicts the optimal MMHH condition as well as explains experimental trends. Last but not least, we also established a new sample alignment method for OSNMR studies and successfully obtained high-resolution two-dimensional SLF spectra of the uniformly ^{15}N labeled transmembrane domain of Pf1 coat protein. Nanoporous anodic aluminum oxide (AAO) sheets have been proven to be an alternative alignment system for the study of membrane proteins in their native environments by means of solid-state NMR. AAO-supported bilayers have the potential of providing an

alternative membrane mimic of highly flexible composition for the structure-function studies of membrane proteins.

5.2 Future work

Through the work described in Chapter 2, REP-CP has been proven to be efficient in transferring magnetization from the abundant *I* spins to sparse *S* spins under high B_1 field. However, this rf irradiation at high power, together with the longer (20 ms) acquisition time might potentially heat up the sample under investigation, which is closely related to various problems, such as line broadening and peak shift. Hence, it would be of great interest to investigate magnetization transfer under ultra-low power by REP-CP. On the other hand, recent progress in the research of adiabatic cross-polarization has demonstrated that, unlike the traditional CP process where γ_I/γ_S is the theoretical limit for signal enhancement as compared to direct detection (~10 in the case of ^{15}N), one could get an extra amplification factor $(N_I/ N_S)^{1/2}$. In the case of membrane protein reconstituted in their native-like lipid bilayers, this factor could be around 3. In other words, if the magnetization is fully transferred from the proton bath to the sparse spins under adiabatic passage, one should be able to observe another 3 fold of signal enhancement as compared to the conventional single-contact CP. Hence, combining adiabatic-CP with the REP-CP scheme would be another promising way of enhance the sensitivity of SSNMR.

Apart from low sensitivity, SSNMR also suffer from lengthy experiment time. In a normal one-dimensional ^1H decoupled ^{15}N detection experiment, the contact time for CP is

around 1 ms (the “work” time), whereas the recycle delay during which the abundant spins reequilibrate is around 6 s (the “rest” time) due to long T_1 relaxation. As a result, a two-dimensional separated-local-field experiment, such as SAMPI4, could easily take days to be finished; and three-dimensional experiments would take weeks. To dramatically shorten the overall experiment time, it is natural to look into the mechanisms that affect T_1 relaxation. Paramagnetic Relaxation Enhancement (PRE), though originally designed to provide long range distance information, has been proven to be effective in shortening relaxation times, hence the overall duration of NMR experiments. In the case of membrane proteins in lipid bilayers, investigating the effect of different radicals based on their ability to participate between aqueous phase and the lipid phase may bring insights into membrane protein conformations while shortening the “idling” time.

In addition, non-linear sampling technique could also be an effective way to reduce the overall experiment time of SSNMR studies of membrane proteins. This is especially important for the three-dimensional NMR experiments correlating ^{15}N-^{13}C-^{1}H spins. These experiments are of great importance for assignment and structure determination of membrane protein of arbitrary topology. Such an ability would transform OSNMR as the ultimate tool for studies of structure and function of membrane proteins in their native-like environments.

REFERENCES

1. Hopkins, A. L. and C. R. Groom. 2002. The druggable genome. Nature Reviews Drug Discovery 1:727-730.

2. Wallin, E. and G. von Heijne. 1998. Genome-wide analysis of integral membrane proteins from eubacterial, archaean, and eukaryotic organisms. Protein Sci. 7:1029-1038.

3. Michel, H. 1983. Crystalization of membrane-proteins. Trends Biochem.Sci. 8:56-59.

4. Ostermeier, C. and H. Michel. 1997. Crystallization of membrane proteins. Curr Opin Struc Biol 7:697-701.

5. Watts, A. and P. J. R. Spooner. 1991. Phospholipid Phase-Transitions as Revealed by NMR. Chem. Phys. Lipids 57:195-211.

6. Arora, A. and L. K. Tamm. 2001. Biophysical approaches to membrane protein structure determination. Curr Opin Struc Biol 11:540-547.

7. Sanders, C. R. and G. C. Landis. 1995. Reconstitution of Membrane-Proteins into Lipid-Rich Bilayered Mixed Micelles for NMR-Studies. Biochemistry-Us 34:4030-4040.

8. Chou, J. J., J. D. Kaufman, S. J. Stahl, P. T. Wingfield, and A. Bax. 2002. Micelle-induced curvature in a water-insoluble HIV-1 Env peptide revealed by NMR dipolar coupling measurement in stretched polyacrylamide gel. J. Am. Chem. Soc. 124:2450-2451.

9. Barany-Wallje, E., A. Andersson, A. Graslund, and L. Maler. 2004. NMR solution structure and position of transportan in neutral phospholipid bicelles. Febs Letters 567:265-269.

10. Lindberg, M., H. Biverstahl, A. Graslund, and L. Maler. 2003. Structure and positioning comparison of two variants of penetratin in two different membrane mimicking systems by NMR. European Journal of Biochemistry 270:3055-3063.

11. Nicholson, L. K. and T. A. Cross. 1989. Gramicidin Cation Channel - An Experimental-Determination of the Right-Handed Helix Sense and Verification of Beta-Type Hydrogen-Bonding. Biochemistry-Us 28:9379-9385.

12. Smith, S. O. and R. G. Griffin. 1988. High-Resolution Solid-State NMR of Proteins. Annu Rev Phys Chem 39:511-535.

13. Opella, S. J. 1982. Solid-State Nmr of Biological-Systems. Annu Rev Phys Chem 33:533-562.

14. Opella, S. J., F. M. Marassi, J. J. Gesell, A. P. Valente, Y. Kim, M. Oblatt-Montal, and M. Montal. 1999. Structures of the M2 channel-lining segments from nicotinic acetylcholine and NMDA receptors by NMR spectroscopy. Nature Structural Biology 6:374-379.

15. Wang, J. F., S. Kim, F. Kovacs, and T. A. Cross. 2001. Structure of the transmembrane region of the M2 protein H+ channel. Protein Sci. 10:2241-2250.

16. Traaseth, N. J., J. J. Buffy, J. Zamoon, and G. Veglia. 2006. Structural dynamics and topology of phospholamban in oriented lipid bilayers using multidimensional solid-state NMR. Biochemistry-Us 45:13827-13834.

17. Park, S. H., A. A. De Angelis, A. A. Nevzorov, C. H. Wu, and S. J. Opella. 2006. Three-dimensional structure of the transmembrane domain of Vpu from HIV-1 in aligned phospholipid bicelles. Biophys. J. 91:3032-3042.

18. De Angelis, A. A., S. C. Howell, A. A. Nevzorov, and S. J. Opella. 2006. Structure determination of a membrane protein with two trans-membrane helices in aligned phospholipid bicelles by solid-state NMR spectroscopy. J. Am. Chem. Soc. 128:12256-12267.

19. Wu, C. H., A. Ramamoorthy, and S. J. Opella. 1994. High-Resolution Heteronuclear Dipolar Solid-State Nmr-Spectroscopy. J Magn Reson Ser A 109:270-272.

20. Goldburg, W. I. and M. Lee. 1963. Nuclear magnetic resonance line narrowing by a rotating rf field. Phys Rev Lett 11:255-&.

21. Nevzorov, A. A. and S. J. Opella. 2003. A "Magic Sandwich" pulse sequence with reduced offset dependence for high-resolution separated local field spectroscopy. J. Magn. Reson. 164:182-186.

22. Nevzorov, A. A. and S. J. Opella. 2007. Selective averaging for high-resolution solid-state NMR spectroscopy of aligned samples. J. Magn. Reson. 185:59-70.

23. Marassi, F. M. and S. J. Opella. 2000. A solid-state NMR index of helical membrane protein structure and topology. J. Magn. Reson. 144:150-155.

24. Wang, J., J. Denny, C. Tian, S. Kim, Y. Mo, F. Kovacs, Z. Song, K. Nishimura, Z. Gan, R. Fu, J. R. Quine, and T. A. Cross. 2000. Imaging membrane protein helical wheels. J. Magn. Reson. 144:162-167.

25. Schiffer, M. and A. B. Edmundson. 1967. Use of Helical Wheels to Represent Structures of Proteins and to Identify Segments with Helical Potential. Biophys. J. 7:121-135.

26. Marassi, F. M. 2001. A simple approach to membrane protein secondary structure and topology based on NMR spectroscopy. Biophys. J. 80:994-1003.

27. Seelig, J. and H. U. Gally. 1976. Investigation of phosphatidylethanolamine bilayers by deuterium and P-31 nuclear magnetic resonance. Biochemistry-Us 15:5199-5204.

28. Jones, D. H., K. R. Barber, and C. W. M. Grant. 1998. Sequence-related behaviour of transmembrane domains from class I receptor tyrosine kinases. Bba-Biomembranes 1371:199-212.

29. Da Costa, G., S. Chevance, E. Le Rumeur, and A. Bondon. 2006. Proton NMR detection of porphyrins and cytochrome c in small unilamellar vesicles: Role of the dissociation kinetic constant. Biophys. J. 90:L55-L57.

30. Marassi, F. M. and S. J. Opella. 2003. Simultaneous assignment and structure determination of a membrane protein from NMR orientational restraints. Protein Sci. 12:403-411.

31. Marassi, F. M., A. Ramamoorthy, and S. J. Opella. 1997. Complete resolution of the solid-state NMR spectrum of a uniformly N-15-labeled membrane protein in phospholipid bilayers. P Natl Acad Sci USA 94:8551-8556.

32. Gabriel, N. E. and M. F. Roberts. 1984. Spontaneous Formation of Stable Unilamellar Vesicles. Biochemistry-Us 23:4011-4015.

33. Sanders, C. R. and J. P. Schwonek. 1992. Characterization of Magnetically Orientable Bilayers in Mixtures of Dihexanoylphosphatidylcholine and Dimyristoylphosphatidylcholine by Solid-State Nmr. Biochemistry-Us 31:8898-8905.

34. Lu, G. J., W. S. Son, and S. J. Opella. 2011. A general assignment method for oriented sample (OS) solid-state NMR of proteins based on the correlation of resonances through heteronuclear dipolar couplings in samples aligned parallel and perpendicular to the magnetic field. J. Magn. Reson. 209:195-206.

35. Park, S. H., C. Loudet, F. M. Marassi, E. J. Dufourc, and S. J. Opella. 2008. Solid-state NMR spectroscopy of a membrane protein in biphenyl phospholipid bicelles with the bilayer normal parallel to the magnetic field. J. Magn. Reson. 193:133-138.

36. Durr, U. H. N., K. Yamamoto, S. C. Im, L. Waskell, and A. Ramamoorthy. 2007. Solid-state NMR reveals structural and dynamical properties of a membrane-anchored electron-carrier protein, cytochrome b(5). J. Am. Chem. Soc. 129:6670-+.

37. Triba, M. N., P. F. Devaux, and D. E. Warschawski. 2006. Effects of lipid chain length and unsaturation on bicelles stability. A phosphorus NMR study. Biophys. J. 91:1357-1367.

38. De Angelis, A. A. and S. J. Opella. 2007. Bicelle samples for solid-state NMR of membrane proteins. Nat. Protoc. 2:2332-2338.

39. Rakonjac, J., N. J. Bennett, J. Spagnuolo, D. Gagic, and M. Russel. 2011. Filamentous Bacteriophage: Biology, Phage Display and Nanotechnology Applications. Curr. Issues Mol. Biol. 13:51-75.

40. Lu, T. K. and M. S. Koeris. 2011. The next generation of bacteriophage therapy. Curr. Opin. Microbiol. 14:524-531.

41. Nambudripad, R., W. Stark, S. J. Opella, and L. Makowski. 1991. Membrane-Mediated Assembly of Filamentous Bacteriophage Pf1 Coat Protein. Science 252:1305-1308.

42. Gonzalez, A., C. Nave, and D. A. Marvin. 1995. Pf1 filamentous bacteriophage - refeinment of a molecular-model by simulated annealing using 3.3-angstrom resolution X-ray fiber diffraction data. Acta Crystallogr. Sect. D-Biol. Crystallogr. 51:792-804.

43. Welsh, L. C., M. F. Symmons, and D. A. Marvin. 2000. The molecular structure and structural transition of the alpha-helical capsid in filamentous bacteriophage Pf1. Acta Crystallogr. Sect. D-Biol. Crystallogr. 56:137-150.

44. Thiriot, D. S., A. A. Nevzorov, L. Zagyanskiy, C. H. Wu, and S. J. Opella. 2004. Structure of the coat protein in Pf1 bacteriophage determined by solid-state NMR Spectroscopy. J. Mol. Biol. 341:869-879.

45. Thiriot, D. S., A. A. Nevzorov, and S. J. Opella. 2005. Structural basis of the temperature transition of Pf1 bacteriophage. Protein Sci. 14:1064-1070.

46. Sharma, M., M. G. Yi, H. Dong, H. J. Qin, E. Peterson, D. D. Busath, H. X. Zhou, and T. A. Cross. 2010. Insight into the Mechanism of the Influenza A Proton Channel from a Structure in a Lipid Bilayer. Science 330:509-512.

47. Sanders, C. R., B. J. Hare, K. P. Howard, and J. H. Prestegard. 1994. Magnetically-Oriented Phospholipid Micelles as a Tool for the Study of Membrane-Associated Molecules. Progress in Nuclear Magnetic Resonance Spectroscopy 26:421-444.

48. Glover, K. J., J. A. Whiles, G. H. Wu, N. J. Yu, R. Deems, J. O. Struppe, R. E. Stark, E. A. Komives, and R. R. Vold. 2001. Structural evaluation of phospholipid bicelles for solution-state studies of membrane-associated biomolecules. Biophys. J. 81:2163-2171.

49. De Angelis, A. A., A. A. Nevzorov, S. H. Park, S. C. Howell, A. A. Mrse, and S. J. Opella. 2004. High-resolution NMR spectroscopy of membrane proteins in aligned bicelles. J. Am. Chem. Soc. 126:15340-15341.

50. Park, S. H., F. M. Marassi, D. Black, and S. J. Opella. 2010. Structure and Dynamics of the Membrane-Bound Form of Pf1 Coat Protein: Implications of Structural Rearrangement for Virus Assembly. Biophys. J. 99:1465-1474.

51. Park, S. H. and S. J. Opella. 2010. Triton X-100 as the "Short-Chain Lipid" Improves the Magnetic Alignment and Stability of Membrane Proteins in Phosphatidylcholine Bilayers for Oriented-Sample Solid-State NMR Spectroscopy. J. Am. Chem. Soc. 132:12552-12553.

52. Pines, A., M. G. Gibby, and J. S. Waugh. 1973. Proton-Enhanced Nmr of Dilute Spins in Solids. J. Chem. Phys. 59:569-590.

53. Hartmann, S. R. and E. L. Hahn. 1962. Nuclear Double Resonance in Rotating Frame. Phys Rev 128:2042-&.

54. Metz, G., X. L. Wu, and S. O. Smith. 1994. Ramped-Amplitude Cross-Polarization in Magic-Angle-Spinning NMR. J Magn Reson Ser A 110:219-227.

55. Levitt, M. H., D. Suter, and R. R. Ernst. 1986. Spin Dynamics and Thermodynamics in Solid-State NMR Cross Polarization. J. Chem. Phys. 84:4243-4255.

56. Levitt, M. H. 1991. Heteronuclear Cross Polarization in Liquid-State Nuclear-Magnetic-Resonance Mismatch Compensation and Relaxation Behavior. J. Chem. Phys. 94:30-38.

57. Wu, X. L. and K. W. Zilm. 1993. Cross-Polarization with High-Speed Magic-Angle-Spinning. J Magn Reson Ser A 104:154-165.

58. Peersen, O. B., X. L. Wu, and S. O. Smith. 1994. Enhancement of CP-MAS Signals by Variable-Amplitude Cross-Polarization - Compensation for Inhomogeneous B1 Fields. J Magn Reson Ser A 106:127-131.

59. Lopez, J. J., C. Kaiser, S. Asami, and C. Glaubitz. 2009. Higher Sensitivity through Selective C-13 Excitation in Solid-State NMR Spectroscopy. J. Am. Chem. Soc. 131:15970-+.

60. Kim, H., T. A. Cross, and R. Q. Fu. 2004. Cross-polarization schemes for peptide samples oriented in hydrated phospholipid bilayers. J. Magn. Reson. 168:147-152.

61. Fukuchi, M., A. Ramamoorthy, and K. Takegoshi. 2009. Efficient cross-polarization using a composite 0 degrees pulse for NMR studies on static solids. J. Magn. Reson. 196:105-109.

62. Dvinskikh, S. V., K. Yamamoto, U. H. N. Durr, and A. Ramamoorthy. 2007. Sensitivity and resolution enhancement in solid-state NMR spectroscopy of bicelles. J. Magn. Reson. 184:228-235.

63. Ernst, R. R., G. Bodenhausen, and A. Wokaun. 1987. Principles of nuclear magnetic resonance in one and two dimensions / Richard R. Ernst, Geoffrey Bodenhausen and Alexander Wokaun. Oxford : Clarendon Press.

64. Sorensen, O. W. 1990. A Universal Bound on Spin Dynamics. J. Magn. Reson. 86:435-440.

65. Bruschweiler, R. 1997. Nuclear spin relaxation and non-ergodic quasi-equilibria. Chem Phys Lett 270:217-221.

66. Tian, F. and T. A. Cross. 1997. Dipolar oscillations in cross-polarized peptide samples in oriented lipid bilayers. J. Magn. Reson. 125:220-223.

67. Alexander A. Nevzorov, Anna A. De Angelis, Sang Ho Park, and S. J. Opella. 2005. In NMR Spectroscopy of Biological Solids. A. Ramamoorthy, editor. CRC Press. 177-190.

68. Park, S. H., A. A. Mrse, A. A. Nevzorov, A. A. De Angelis, and S. J. Opella. 2006. Rotational diffusion of membrane proteins in aligned phospholipid bilayers by solid-state NMR spectroscopy. J. Magn. Reson. 178:162-165.

69. Nevzorov, A. A. 2011. Ergodicity and efficiency of cross-polarization in NMR of static solids. J. Magn. Reson. 209:161-166.

70. Gopinath, T. and G. Veglia. 2009. Sensitivity Enhancement in Static Solid-State NMR Experiments via Single- and Multiple-Quantum Dipolar Coherences. J. Am. Chem. Soc. 131:5754-+.

71. Gopinath, T., N. J. Traaseth, K. Mote, and G. Veglia. 2010. Sensitivity Enhanced Heteronuclear Correlation Spectroscopy in Multidimensional Solid-State NMR of Oriented Systems via Chemical Shift Coherences. J. Am. Chem. Soc. 132:5357-5363.

72. Wickramasinghe, N. P., M. Kotecha, A. Samoson, J. Past, and Y. Ishii. 2007. Sensitivity enhancement in C-13 solid-state NMR of protein microcrystals by use of paramagnetic metal ions for optimizing H-1 T-1 relaxation. J. Magn. Reson. 184:350-356.

73. Prosser, R. S., S. A. Hunt, J. A. DiNatale, and R. R. Vold. 1996. Magnetically aligned membrane model systems with positive order parameter: Switching the sign of S-zz with paramagnetic ions. J. Am. Chem. Soc. 118:269-270.

74. Nevzorov, A. A. 2011. Orientational and Motional Narrowing of Solid-State NMR Lineshapes of Uniaxially Aligned Membrane Proteins. J Phys Chem B 115:15406-15414.

75. Cady, S. D. and M. Hong. 2009. Effects of amantadine on the dynamics of membrane-bound influenza A M2 transmembrane peptide studied by NMR relaxation. J. Biomol. NMR 45:185-196.

76. De Angelis, A. A., S. C. Howell, and S. J. Opella. 2006. Assigning solid-state NMR spectra of aligned proteins using isotropic chemical shifts. J. Magn. Reson. 183:329-332.

77. Suter, D. and R. R. Ernst. 1985. Spin Diffusion in Resolved Solid-State NMR-Spectra. Physical Review B 32:5608-5627.

78. Marassi, F. M., J. J. Gesell, A. P. Valente, Y. Kim, M. Oblatt-Montal, M. Montal, and S. J. Opella. 1999. Dilute spin-exchange assignment of solid-state NMR spectra of oriented proteins: Acetylcholine M2 in bilayers. J. Biomol. NMR 14:141-148.

79. Xu, J. D., P. E. S. Smith, R. Soong, and A. Ramamoorthy. 2011. A Proton Spin Diffusion Based Solid-State NMR Approach for Structural Studies on Aligned Samples. J Phys Chem B 115:4863-4871.

80. Mote, K. R., T. Gopinath, N. J. Traaseth, J. Kitchen, P. L. Gor'kov, W. W. Brey, and G. Veglia. 2011. Multidimensional oriented solid-state NMR experiments enable the sequential assignment of uniformly (15)N labeled integral membrane proteins in magnetically aligned lipid bilayers. J. Biomol. NMR 51:339-346.

81. Lewandowski, J. R., G. De Paepe, and R. G. Griffin. 2007. Proton assisted insensitive nuclei cross polarization. J. Am. Chem. Soc. 129:728-729.

82. Nevzorov, A. A. 2008. Mismatched Hartmann-Hahn conditions cause proton-mediated intermolecular magnetization transfer between dilute low-spin nuclei in NMR of static solids. J. Am. Chem. Soc. 130:11282-11283.

83. Khitrin, A. K., J. D. Xu, and A. Ramamoorthy. 2011. Cross-correlations between low-gamma nuclei in solids via a common dipolar bath. J. Magn. Reson. 212:95-101.

84. Nevzorov, A. A. 2009. High-resolution local field spectroscopy with internuclear correlations. J. Magn. Reson. 201:111-114.

85. Knox, R. W., G. J. Lu, S. J. Opella, and A. A. Nevzorov. 2010. A Resonance Assignment Method for Oriented-Sample Solid-State NMR of Proteins. J. Am. Chem. Soc. 132:8255-8257.

86. Tang, W. X. and A. A. Nevzorov. 2011. Repetitive cross-polarization contacts via equilibration-re-equilibration of the proton bath: Sensitivity enhancement for NMR of membrane proteins reconstituted in magnetically aligned bicelles. J. Magn. Reson. 212:245-248.

87. Aussenac, F., B. Lavigne, and E. J. Dufourc. 2005. Toward bicelle stability with ether-linked phospholipids: Temperature, composition, and hydration diagrams by H-2 and P-31 solid-state NMR. Langmuir 21:7129-7135.

88. Delaglio, F., S. Grzesiek, G. W. Vuister, G. Zhu, J. Pfeifer, and A. Bax. 1995. NMRPipe - A Multidimensional spectral processing system based on Unix pipes. J. Biomol. NMR 6:277-293.

89. Traaseth, N. J., T. Gopinath, and G. Veglia. 2010. On the Performance of Spin Diffusion NMR Techniques in Oriented Solids: Prospects for Resonance Assignments and Distance Measurements from Separated Local Field Experiments. J Phys Chem B 114:13872-13880.

90. Opella, S. J., A. C. Zeri, and S. H. Park. 2008. Structure, dynamics, and assembly of filamentous bacteriophages by nuclear magnetic resonance spectroscopy. Annu Rev Phys Chem 59:635-657.

91. Lin, E. C. and S. J. Opella. 2011. (1)H assisted (13)C/(15)N heteronuclear correlation spectroscopy in oriented sample solid-state NMR of single crystal and magnetically aligned samples. J. Magn. Reson. 211:37-44.

92. Brian, A. A. and H. M. McConnell. 1984. Allogeneic Stimulation of Cyto-Toxic T-Cells by Supported Planar Membranes. P Natl Acad Sci-Biol 81:6159-6163.

93. Smirnov, A. I. and O. G. Poluektov. 2003. Substrate-supported lipid nanotube arrays. J. Am. Chem. Soc. 125:8434-8435.

94. Alaouie, A. M. and A. I. Smirnov. 2005. Cooperativity and kinetics of phase transitions in nanopore-confined bilayers studied by differential scanning calorimetry. Biophys. J. 88:L11-L13.

95. Alaouie, A. M. and A. I. Smirnov. 2006. Formation of a ripple phase in nanotubular dimyristoylphosphatidylcholine Bilayers confined inside nanoporous aluminum oxide substrates observed by DSC. Langmuir 22:5563-5565.

96. Chekmenev, E. Y., J. Hu, P. L. Gor'kov, W. W. Brey, T. A. Cross, A. Ruuge, and A. I. Smirnov. 2005. N-15 and P-31 solid-state NMR study of transmembrane domain alignment of M2 protein of influenza A virus in hydrated cylindrical lipid bilayers confined to anodic aluminum oxide nanopores. J. Magn. Reson. 173:322-327.

97. Chekmenev, E. Y., P. L. Gor'kov, T. A. Cross, A. M. Alaouie, and A. I. Smirnov. 2006. Flow-through lipid nanotube arrays for structure-function studies of membrane proteins by solid-state NMR spectroscopy. Biophys. J. 91:3076-3084.

98. Opella, S. J. and F. M. Marassi. 2004. Structure determination of membrane proteins by NMR spectroscopy. Chemical reviews 104:3587-3606.

99. Park, S. H., B. B. Das, F. Casagrande, Y. Tian, H. J. Nothnagel, M. Chu, H. Kiefer, K. Maier, A. A. De Angelis, F. M. Marassi, and S. J. Opella. 2012. Structure of the chemokine receptor CXCR1 in phospholipid bilayers. Nature.

100. Moll, F. and T. A. Cross. 1990. Optimizing and characterizing alignment of oriented lipid bilayers containing Gramicidin D. Biophys. J. 57:351-362.

101. McConnell, H. M., L. K. Tamm, and R. M. Weis. 1984. Periodic Structures in Lipid Monolayer Phase-Transitions. Proceedings of the National Academy of Sciences of the United States of America-Physical Sciences 81:3249-3253.

102. Sackmann, E. 1996. Supported membranes: Scientific and practical applications. Science 271:43-48.

103. Cremer, P. S. and S. G. Boxer. 1999. Formation and spreading of lipid bilayers on planar glass supports. J Phys Chem B 103:2554-2559.

104. Boxer, S. G. 2000. Molecular transport and organization in supported lipid membranes. Current Opinion in Chemical Biology 4:704-709.

105. Keller, C. A., K. Glasmastar, V. P. Zhdanov, and B. Kasemo. 2000. Formation of supported membranes from vesicles. Phys Rev Lett 84:5443-5446.

106. Durr, U. H., M. Gildenberg, and A. Ramamoorthy. 2012. The magic of bicelles lights up membrane protein structure. Chemical reviews 112:6054-6074.

107. Furneaux, R. C., W. R. Rigby, and A. P. Davidson. 1989. The Formation of Controlled-Porosity Membranes from Anodically Oxidized Aluminum. Nature 337:147-149.

108. Routkevitch, D., T. Bigioni, M. Moskovits, and J. M. Xu. 1996. Electrochemical fabrication of CdS nanowire arrays in porous anodic aluminum oxide templates. Journal of Physical Chemistry 100:14037-14047.

109. Routkevitch, D., T. L. Haslett, L. Ryan, T. Bigioni, C. Douketis, and M. Moskovits. 1996. Synthesis and resonance Raman spectroscopy of CdS nano-wire arrays. Chemical Physics 210:343-352.

110. Gaede, H. C., K. M. Luckett, I. V. Polozov, and K. Gawrisch. 2004. Multinuclear NMR studies of single lipid bilayers supported in cylindrical aluminum oxide nanopores. Langmuir 20:7711-7719.

APPENDICES

Appendix A Pulse sequences used in the study of REP-CP. A. Single CP contact; B. CP-MOIST; C. Multiple Contacts; D. REP-CP.

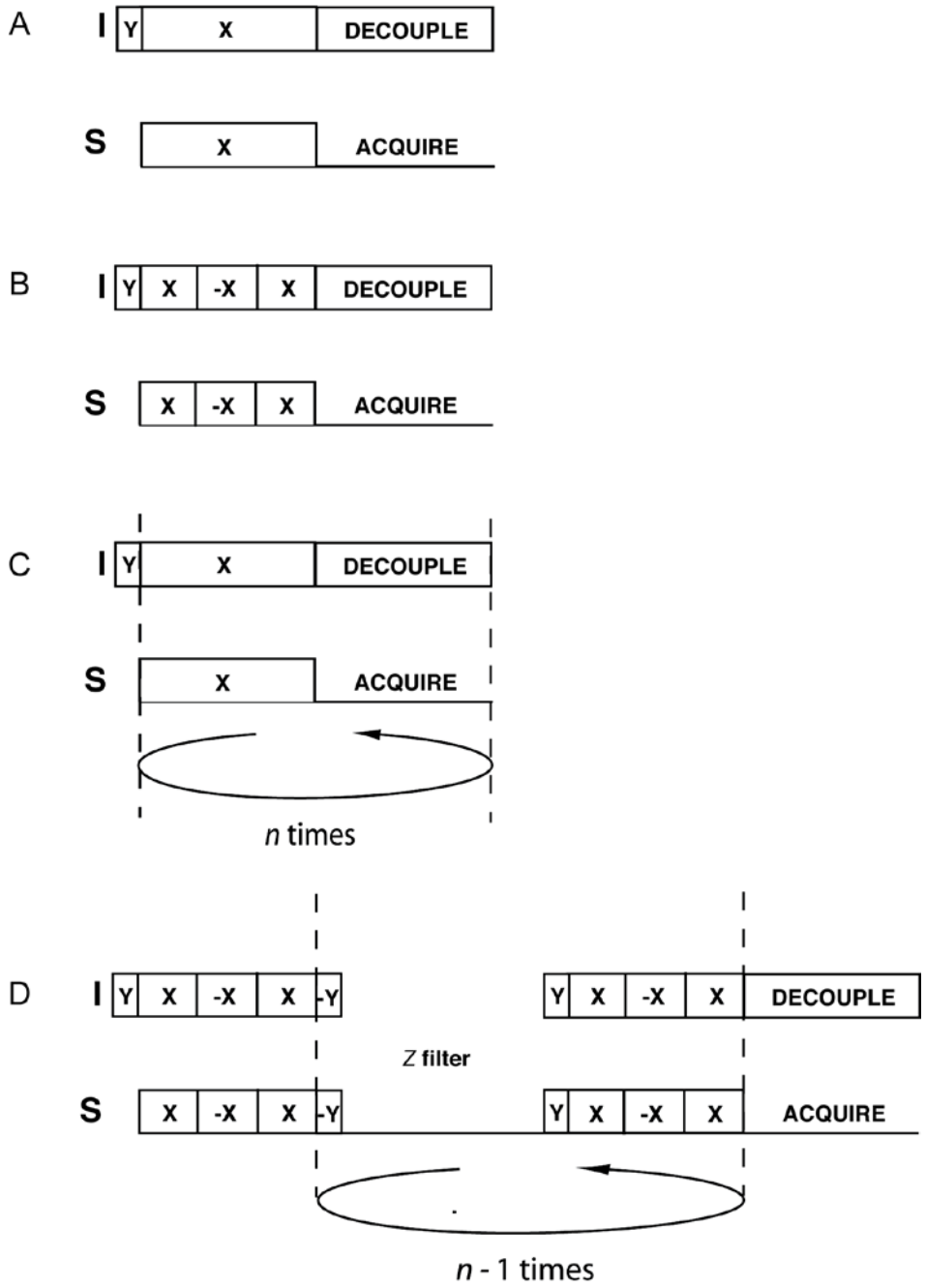

Appendix B Pulse program of one-dimensional ^{1}H decoupled ^{31}P experiment

```
; Created 01/15/08(an)
;Pulse on f1, decouple on f2 only

#include <Avance.incl>

1 ze
2 d1 do:f2
3 10u pl1:f1 pl2:f2
  (p3 ph1):f1

  1u cw:f2
  (4u pl2 ph2):f2
  go=2 ph1
  3m do:f2
  wr #0
exit

ph1=1 3
ph2=0

;pl1 : power level for X pulse (default)
;pl2 : power level for H pulse (default)
;pl14: power level for H mix
;pl15: power level for H decoupling
;p3 : 90 degree 1H pulse
;p30 : 35.60 degree 1H pulse
;p15 : mix pulse
;cnst0: set to 0
;cnst20: phase of compensation phase
;cnst21: LG shift frequency
;d1 : relaxation delay: 1.25 * T1(H1), but > 50 * aq
;NS: 2 * n
;DS: 0
;$Id: hxlgcp,v 1.1.8.5 2000/05/08 14:07:35 eng Exp $
```

Appendix C Pulse program of one-dimensional ^{1}H decoupled ^{15}N experiment

```
; multiple contact CP with spinal
; 08/23/10

#include <Avancesolids.incl>
#include <De.incl>
#include <trigg.incl>
#include <tppm.incl>

1 ze

2 d1 do:f2
3 10u pl1:f1 pl2:f2


  (p5 ph1 fq=cnst0):f2
  (p15*0.33 ph2):f1 (p15*0.33 ph2):f2
  (p15*0.33 ph4):f1 (p15*0.33 ph4):f2
  (p15*0.33 ph2):f1 (p15*0.33 ph2):f2

4 (p3 ph5):f1 (p3 ph7):f2
  (d4 p5 ph3):f1 (d4 p5 ph1):f2
  (p15*0.33 ph2):f1 (p15*0.33 ph2):f2
  (p15*0.33 ph4):f1 (p15*0.33 ph4):f2
  (p15*0.33 ph2):f1 (p15*0.33 ph2):f2

lo to 4 times l20

  ; detection
  1u cpds2:f2
  ACQ_START(ph30,ph31)
aq DWELL_GEN
1m do:f2
rcyc=2
  1m do:f2
  100m wr #0
exit


ph1=1 3
ph30=0
ph31=0 2
```

```
ph2=0
ph3=1
ph4=2
ph5=3
ph7=3 1
ph10=3

;pl1 : power level for X pulse (default)
;pl2 : power level for H pulse (default)
;pl14: power level for H mix
;pl12: power level for H decoupling
;p5 : 90 degree 1H pulse
;p30 : 35.60 degree 1H pulse
;p15 : mix pulse
;cnst0 : set to 0
;cnst1 : NN transfer 1H offset
;cnst21 : phase of compensation phase
;d1 : relaxation delay: 1.25 * T1(H1), but > 50 * aq
;d4 : multicontact relaxation delay
;NS: 2 * n
;DS: 0



;$Id: hxlgcp,v 1.1.8.5 2000/05/08 14:07:35 eng Exp $
```

Appendix D Pulse program of SAMPI4_multicont (for the SLF spectrum with only main peaks, REP-CP included).

```
; SAMPI4 with repetitive contacts
; Created 3/18/11 (AN)
; Uses SAMPI4 in the indirect dimension

;$OWNER=nmrsu
#include <Avancesolids.incl>
#include <De.incl>
#include <trigg.incl>
#include <tppm.incl>

define loopcounter t1count
"t1count=td1-1"

"p16=p3*4-p3*0.5"
define delay t1incr

"p17=p3*6-p3"

"d4=p17*0.5-p3"


1 ze
;  t1incr

2 d1 do:f2
  10u pl1:f1 pl2:f2
  1m rpp4
  1m rpp5
  1m rpp6
  1m rpp7

  (p5 ph1 fq=cnst0):f2
  (p15*0.33 ph3):f1 (p15*0.33 ph2):f2
  (p15*0.33 ph2):f1 (p15*0.33 ph3):f2
  (p15*0.33 ph3):f1 (p15*0.33 ph2):f2

  ; Multiple contacts with MOIST
3 (p3 ph8):f1 (p3 ph9):f2
  (d3 p5 ph10):f1 (d3 p5 ph1):f2
  (p15*0.33 ph3):f1 (p15*0.33 ph2):f2
```

```
  (p15*0.33 ph2):f1 (p15*0.33 ph3):f2
  (p15*0.33 ph3):f1 (p15*0.33 ph2):f2

lo to 3 times l22

; re-equilibration of the protons before SAMPI4 evolution

(p3 ph8):f1 (p3 ph9):f2
(d6 p5 ph10):f1 (d6 p5 ph1):f2

if "l20<1" goto 6

; Magic Sandwich starts here
4 (p16 ph4):f1 (p16 ph4):f2
  (p17*0.5 ph4):f1 (p3 ph6 ipp6 ipp4):f2
  (p17*0.5 ph5):f1 (d4 p3 ph7 ipp7):f2
  (p16 ph5):f1 (p16 ph5 ipp5):f2
lo to 4 times l20

6 0.3u fq=cnst0:f2
; detection
  1u cpds2:f2
  ACQ_START(ph30,ph31)
aq DWELL_GEN
1m do:f2
rcyc=2
  1m do:f2
  100m wr #0 if #0 iu20 zd

  lo to 2 times td1
exit


ph1=1 3
ph30=0
ph31=1 3

ph2=0
ph3=2

ph4=0 2
ph5=2 0 ; irradiation phases for the third part of the magic
sandwich
ph6=1 3 ; phases for the first +-90Y pulse on the high side
```

```
ph7=3 1

ph8=3
ph9=3 1
ph10=1

;pl1 : f1 channel - power level for X pulse (default)
;pl2 : f2 channel - power level for H pulse (default)
;pl11 : nitrogen power during TSAR
;pl12: f2 channel - power level for H decoupling
;p5 : f1 channel first 90 degree pulse
;p3 : f1 channel -  90 degree high power pulse
;p15 : cp time
;p16 : 2 * pi irradiation time for the magic sandwich
;p17 : total length of the window INCLUDING the +-90Y pulses
;d1 : relaxation delay: 1.25 * T1(H1), but > 50 * aq
;d3 : delay between miltiple contacts
;l22 : number of repetitive contacts - 1
;d6 : Z-filter length
;NS: 2 * n
;DS: 0
;l20 : number of points in the indirect dimension
```

Appendix E Pulse program of NN_TSAR2d_sammy_multicont (for the spin exchange version of SAMPI4, to get both main- and cross-peaks).

```
; NH-N correlation with TSAR
; Created 2/15/11 (AN)
; Uses SAMMY in the indirect dimension

#include <Avancesolids.incl>
#include <De.incl>
#include <trigg.incl>
#include <tppm.incl>

define loopcounter t1count
"t1count=td1-1"

"p16=p3*4-p3*0.5"
define delay t1incr
; "t1incr=8*p3"
; "in0=1.0927*t1incr"
"p17=p3*6-p3"

"d4=p17*0.5-p3"

;"p32=p3*165.0/90.0"

1 ze
; t1incr

2 d1 do:f2
  10u pl1:f1 pl2:f2
  1m rpp4
  1m rpp5
  1m rpp6
  1m rpp7

  (p5 ph1 fq=cnst0):f2
  (p15*0.33 ph2):f1 (p15*0.33 ph3):f2
  (p15*0.33 ph3):f1 (p15*0.33 ph2):f2
  (p15*0.33 ph2):f1 (p15*0.33 ph3):f2

; Multiple contacts with MOIST

3 (p3 ph8):f1 (p3 ph9):f2
```

```
  (d3 p5 ph10):f1 (d3 p5 ph1):f2
  (p15*0.33 ph2):f1 (p15*0.33 ph3):f2
  (p15*0.33 ph3):f1 (p15*0.33 ph2):f2
  (p15*0.33 ph2):f1 (p15*0.33 ph3):f2

lo to 3 times l22

; re-equilibration of the protons before the SAMPI4 evolution

(p3 ph8):f1 (p3 ph9):f2
(d3 p5 ph10):f1 (d3 p5 ph1):f2

if "l20<1" goto 6

; Magic Sandwich starts here
4 (p16 ph4):f1 (p16 ph4):f2
  (p17*0.5 ph4):f1 (p3 ph6 ipp6 ipp4):f2
  (p17*0.5 ph5):f1 (d4 p3 ph7 ipp7):f2
  (p16 ph5):f1 (p16 ph5 ipp5):f2
lo to 4 times l20

; TSAR
; Flip-back pulses
6 (p3 ph8):f1 (p3 ph9):f2

7 10u pl14:f2
; Y pulse to return the N-magnetization along X
  (d6 p5 ph10):f1
  (p18 ph2 pl11):f1 (p18 ph11):f2

0.3u fq=cnst0:f2
; detection
  1u cpds2:f2
  ACQ_START(ph30,ph31)
aq DWELL_GEN
1m do:f2
rcyc=2

  1m do:f2
  100m wr #0 if #0 iu20 zd

  lo to 2 times td1
exit
```

```
ph1=1 3
ph30=0
ph31=1 3

ph2=0
ph3=2

ph4=0 2
ph5=2 0 ; irradiation phases for the third part of the magic
sandwich
ph6=1 3 ; phases for the first +-90Y pulse on the high side
ph7=3 1

ph8=3
ph9=3 1
ph10=1
ph11=0

;pl1 : f1 channel - power level for X pulse (default)
;pl2 : f2 channel - power level for H pulse (default)
;pl11 : nitrogen power during TSAR
;pl12: f2 channel - power level for H decoupling
;pl14 : power level during TSAR
;p5 : f1 channel first 90 degree pulse
;p3 : f1 channel - 90 degree high power pulse
;p15 : cp time
;p16 : 2 * pi irradiation time for the magic sandwich
;p17 : total length of the window INCLUDING the +-90Y pulses
;p18 : total TSAR length
;d1 : relaxation delay: 1.25 * T1(H1), but > 50 * aq
;d3 : delay between miltiple contacts
;l22 : number of multiple contacts - 1
;d6 : Z-filter length
;NS: 2 * n
;DS: 0
;l20 : number of points in the indirect dimension
;cnst17 : decoupler frequency offset
;$Id: hxcp,v 1.1.8.5 2000/05/08 14:07:35 eng Exp $
```

Appendix F Pulse program of NN_TSAR2d_multicont (for the N-N correlation spectrum with both main- and cross-peaks).

```
; NN correlation with TSAR
; Created 02/15/11 (AN)
; Uses SPINAL in the indirect dimension
#include <Avancesolids.incl>
#include <De.incl>
#include <trigg.incl>
#include <tppm.incl>

define loopcounter t1count

"t1count=td1-1"
"l8=td1/2"
"d0=in0-2u"
; "cnst1=176776.7/p3"

1 ze

"l7=0"

;1m rpp7
;1m rpp8
;1m rpp13

2 d1 do:f2
3 10u pl1:f1 pl2:f2

  (p5 ph1 fq=cnst0):f2
  (p15*0.33 ph2):f1 (p15*0.33 ph2):f2
  (p15*0.33 ph4):f1 (p15*0.33 ph4):f2
  (p15*0.33 ph2):f1 (p15*0.33 ph2):f2

; Multiple contacts with MOIST
4 (p3 ph12):f1 (p3 ph7):f2
  (d3 p5 ph3):f1 (d3 p5 ph1):f2
  (p15*0.33 ph2):f1 (p15*0.33 ph2):f2
  (p15*0.33 ph4):f1 (p15*0.33 ph4):f2
  (p15*0.33 ph2):f1 (p15*0.33 ph2):f2

lo to 4 times l22
```

```
if "l7 < 1" goto 6
; 15N CSA evolution
1u cpds2:f2
d0
1u do:f2

; Quadrature Detection

6 (p5 ph5):f1 (p3 ph7):f2

7 10u pl14:f2

0.3u fq=cnst25:f2

; Y pulse
  (d4 p5 ph3):f1
  (p16 ph2 pl11):f1 (p16 ph8):f2

0.3u fq=cnst0:f2
; detection
  1u cpds2:f2
  ACQ_START(ph30,ph31)
aq DWELL_GEN
1m do:f2
rcyc=2
  1m do:f2
  100m wr #0 if #0 zd ip5

  lo to 2 times 2

  1m rp5
if "l7 < 1" goto 8

  10u id0

8 1m iu7

  lo to 2 times l8
exit


ph30=0
ph31=0 2
```

```
ph1=1 3 ; H 90
ph2=0 ; X initial CP
ph4=2 ; H initial CP

ph3=1
ph5=3
ph7=3 1
ph8=0 2
ph12=3
ph13=3 1

;pl1 : power level for X during CP
;pl11 : power level for X during TSAR
;pl2 : power level for H pulse (default)
;pl12 : power level for H decoupling
;pl14 : power level during TSAR
;p3 : 90 degree hot 1H pulse
;p5 : initial 90 degree 1H pulse
;p14 : dwell time for the indirect dimension
;p15 : mix pulse
;p16 : TSAR length
;cnst0: set to 0
;cnst25: 1H carrier upshift during TSAR
;d1 : relaxation delay: 1.25 * T1(H1), but > 50 * aq
;d3 : relaxation delay between multiple contacts
;d4 : Z-filter relaxation delay
;l22 : number of multiple contacts - 1
;NS: 2 * n
;DS: 0


;$Id: hxlgcp,v 1.1.8.5 2000/05/08 14:07:35 eng Exp $
```

Appendix G Pulse program of NN_PDSD_multicont (for the N-N correlation spectrum with PDSD instead of MMHH).

```
; NN correlation with TSAR
; Created 02/15/11 (AN)
; Uses SPINAL in the indirect dimension
#include <Avancesolids.incl>
#include <De.incl>
#include <trigg.incl>
#include <tppm.incl>

define loopcounter t1count

"t1count=td1-1"
"l8=td1/2"
"d0=in0-2u"
; "cnst1=176776.7/p3"

1 ze

"l7=0"

;1m rpp7
;1m rpp8
;1m rpp13

2 d1 do:f2
3 10u pl1:f1 pl2:f2

  (p5 ph1 fq=cnst0):f2
  (p15*0.33 ph2):f1 (p15*0.33 ph2):f2
  (p15*0.33 ph4):f1 (p15*0.33 ph4):f2
  (p15*0.33 ph2):f1 (p15*0.33 ph2):f2

; Multiple contacts with MOIST
4 (p3 ph12):f1 (p3 ph7):f2
  (d3 p5 ph3):f1 (d3 p5 ph1):f2
  (p15*0.33 ph2):f1 (p15*0.33 ph2):f2
  (p15*0.33 ph4):f1 (p15*0.33 ph4):f2
  (p15*0.33 ph2):f1 (p15*0.33 ph2):f2

lo to 4 times l22
```

```
if "l7 < 1" goto 6
; 15N CSA evolution
1u cpds2:f2
d0
1u do:f2

; Quadrature Detection

6 (p5 ph5):f1 (p3 ph7):f2

0.3u fq=cnst25:f2

; Y pulse
  (d4 p5 ph3):f1

0.3u fq=cnst0:f2
; detection
  1u cpds2:f2
  ACQ_START(ph30,ph31)
aq DWELL_GEN
1m do:f2
rcyc=2
  1m do:f2
  100m wr #0 if #0 zd ip5

  lo to 2 times 2

  1m rp5
if "l7 < 1" goto 8

  10u id0

8 1m iu7
  lo to 2 times l8
exit


ph30=0
ph31=0 2

ph1=1 3 ; H 90
ph2=0 ; X initial CP
ph4=2 ; H initial CP
```

```
ph3=1
ph5=3
ph7=3 1
ph8=0 2
ph12=3
ph13=3 1

;pl1 : power level for X during CP
;pl2 : power level for H pulse (default)
;pl12 : power level for H decoupling
;p3 : 90 degree hot 1H pulse
;p5 : initial 90 degree 1H pulse
;p14 : dwell time for the indirect dimension
;p15 : mix pulse
;cnst0: set to 0
;cnst25: 1H carrier upshift during TSAR
;d1 : relaxation delay: 1.25 * T1(H1), but > 50 * aq
;d3 : relaxation delay between multiple contacts
;d4 : Z-filter relaxation delay
;l22 : number of multiple contacts - 1
;NS: 2 * n
;DS: 0
;$Id: hxlgcp,v 1.1.8.5 2000/05/08 14:07:35 eng Exp $
```

Appendix H Table S1 Crosspeaks from the N-N homonuclear exchange experiment for Figure 3.3A, C.

Index	CSA_X / ppm	CSA_Y / ppm	Comment
1	100.252	80.091	26 to 25
2	94.458	79.377	30 to 29
3	94.458	93.396	28 to 29
4	82.944	99.191	32 to 33
5	82.944	83.811	34 to 33
6	94.818	64.639	37 to 36
7	94.818	99.462	35 to 36
8	100.139	85.265	40 to 39
9	100.139	90.982	38 to 39
10	85.265	100.139	39 to 40
11	85.265	73.001	41 to 40
12	80.091	100.252	25 to 26
13	80.091	89.784	27 to 26
14	64.639	94.818	36 to 37
15	64.639	90.982	38 to 37
16	99.191	82.944	33 to 32
17	99.191	97.967	31 to 32
18	79.377	94.458	29 to 30
19	79.377	97.967	31 to 30
20	73.001	85.265	40 to 41
21	73.001	93.976	42 to 41
22	99.462	94.818	36 to 35
23	99.462	83.811	34 to 35
24	93.976	73.001	41 to 42
25	83.811	82.944	33 to 34
26	83.811	99.462	35 to 34
27	97.967	99.191	32 to 31
28	97.967	79.377	30 to 31
29	89.784	80.091	26 to 27
30	89.784	93.396	28 to 27
31	90.982	100.139	39 to 38
32	90.982	64.639	37 to 38
33	93.396	94.458	29 to 28
34	93.396	89.784	27 to 28

Appendix I Table S2 Main peaks from the SAMPI4 experiment (Figs. 3.3B, D) and their assignment.

Index	CSA / ppm	DC / Hz	Assignment
1	100.252	-1128.645	Y25
2	94.458	-1634.957	A29
3	82.944	-2109.572	L33
4	94.818	-2161.768	A36
5	100.139	-2197.91	I39
6	85.265	-2364.952	Y40
7	80.091	-2624.857	I26
8	64.639	-2722.601	G37
9	99.191	-2990.646	I32
10	79.377	-3094.715	L30
11	73.001	-3307.684	S41
12	99.462	-3369.772	V35
13	93.976	-3719.332	M42
14	83.811	-3788.857	A34
15	97.967	-3821.15	V31
16	89.784	-3881.893	V27
17	90.982	-4097.554	L38
18	93.396	-2978.368	G28

Appendix J Table S3 Cross-peaks from the spin-exchanged SAMPI4 experiment (Figs. 3.3B, D).

Index	CSA / ppm	DC / Hz	Comment
1	100.252	-2624.857	26 to 25
2	94.458	-3094.715	30 to 29
3	94.458	-2978.368	28 to 29
4	82.944	-2990.646	32 to 33
5	82.944	-3788.857	34 to 33
6	94.818	-2722.601	37 to 36
7	94.818	-3369.772	35 to 36
8	100.139	-2364.952	40 to 39
9	100.139	-4097.554	38 to 39
10	85.265	-2197.91	39 to 40
11	85.265	-3307.684	41 to 40
12	80.091	-1128.645	25 to 26
13	80.091	-3881.893	27 to 26
14	64.639	-2161.768	36 to 37
15	64.639	-4097.554	38 to 37
16	99.191	-2109.572	33 to 32
17	99.191	-3821.15	31 to 32
18	79.377	-1634.957	29 to 30
19	79.377	-3821.15	31 to 30
20	73.001	-2364.952	40 to 41
21	73.001	-3719.332	42 to 41
22	99.462	-2161.768	36 to 35
23	99.462	-3788.857	34 to 35
24	93.976	-3307.684	41 to 42
25	83.811	-2109.572	33 to 34
26	83.811	-3369.772	35 to 34
27	97.967	-2990.646	32 to 31
28	97.967	-3094.715	30 to 31
29	89.784	-2624.857	26 to 27
30	89.784	-2978.368	28 to 27
31	90.982	-2197.91	39 to 38
32	90.982	-2722.601	37 to 38
33	93.396	-1634.957	29 to 28
34	93.396	-3881.893	27 to 28

Appendix K Matlab (Mathworks, Inc.) script to simulate spectra from assigned PISEMA data

```
%06/23/11
%PROGRAM FOR SIMULATING SPECTRA FROM ASSIGNED PISEMA DATA

clear all

[A1, A2]=xlsread('pf1_bic_sim_25to42.xls');

index1=A1(:,2);
CSA=A1(:,3);
DIP=-A1(:,4);
[N,M]=size(A1);

%SIMULATION OF THE 1H-15N DIPOLAR COUPLING AND 15N CORRELATION
SAMPI4 SPECTRUM
figure(1)
clf

plot(CSA, DIP, 'o')

hold on
i=1;
for n1=1:N
    for n2=1:N
        if abs(index1(n1)-index1(n2))==1
            plot(CSA(n1), DIP(n2), 'x r')
            text(CSA(n1), DIP(n1), num2str(index1(n1)))
            text(CSA(n1), DIP(n2), num2str(i))
            i=i+1;
        end
    end
end

axis([50 150 0 4.4e3])

set(gca, 'XDir', 'reverse')

%SIMULATION OF THE 15N-15N EXCHANGE SPECTRUM
figure(2)
clf

plot(CSA,CSA, 'o')
```

```
hold on
j=1;
for n3=1:N
    for n4=1:N

        if abs(index1(n3)-index1(n4))==1
            plot(CSA(n3),CSA(n4),'x r')
            text(CSA(n3), CSA(n3), num2str(index1(n3)))
            text(CSA(n3), CSA(n4), num2str(j))
            j=j+1;
        end

    end
end


set(gca, 'XDir', 'reverse')
set(gca, 'YDir', 'reverse')

axis([50 150 50 150])

%SIMULATION OF THE 3D SAMPI4-15N-15N SPECTRUM
figure(3)
clf

plot3(CSA, DIP, CSA, 'o')

hold on

for n5=1:N
    for n6=1:N
        if abs(index1(n5)-index1(n6))==1
            plot3(CSA(n5), DIP(n6), CSA(n6), 'x r')
        end
    end
end

axis([50 150 0 4.4e3 50 150])
set(gca, 'XDir', 'reverse')
%set(gca, 'YDir', 'reverse')
set(gca, 'ZDir', 'reverse')
```

Appendix L Matlab (Mathworks, Inc.) script to simulate PISA wheels

```
%04/10/03
%PLOT OF THE 3D PISA wheels
%HNCH experiment

clear all
clf

N=18;

s11N=64;
%s11N=77;
s22N=77;
s33N=222;

s11H=3;
s22H=8;
s33H=17;


%ORDER PARAMETER
So=.97;

%CONSTANTS
gamma1=pi/180*18.5;
gamma2=-90*pi/180;
gamma3=-118.2*pi/180;
%gamma3=119.5*pi/180;

ga=2.718e7; gb=2.675e8; hbar=1.055e-34; d=1.07e-10;
gc=6.7283e7; rCH=1.1e-10; rNC=1.45e-10;
chi0=1e-7*ga*gb*hbar/d^3/2/pi;
chi1=1e-7*gc*gb*hbar/rCH^3/2/pi;
chi2=1e-7*ga*gc*hbar/rNC^3/2/pi;


PHI=-61;
PSI=-45;
OMEGA1=pi/180*[151.8, PHI, 110.5];
OMEGA2=pi/180*[0, -PSI-180, 34.9];
```

```
%DEFINING ORIENTATION OF FIRST PEPTIDE PLANE RELATIVE TO THE
HELIX AXIS
P=wigner1(OMEGA1)*wigner1(OMEGA2);

x1=(1-P(2,2))/(P(2,1)-P(3,2));


    u4=([x1, 1, -conj(x1)].')/sqrt(1+2*x1*conj(x1));

    theta_p=acos(u4(2));

    phi_p=pi+log(-u4(1)*sqrt(2)/sin(theta_p))/i;

x=linspace(1, N, 100*N);

%ordering of plots
order_wheel=[1,2,3,4,5,11,12,13,14,15];

%TILT ANGLES - DEGREES
tilts=[10 12 14 16];
tilt_color=['rgbc'];
Npz=4;
for pz=1:Npz

D=1;
R=0;

psi=0;
%theta=(pz-1)/(Npz-1)*90*pi/180; %helix tilt
theta=tilts(pz)*pi/180;
phi=-120*pi/180; %helix twist

for n=1:100*N

wigner_LM=wigner1([psi, theta, phi])*wigner1([0, theta_p,
phi_p])*P^(x(n)-1);

wigner_tot1=wigner_LM*wigner1([gamma1, pi/2, pi/2]);
wigner_tot2=wigner_LM*wigner1([0, pi/2, 0]);
wigner_tot3=wigner_LM*wigner1([151.8, PHI-60, 90-
109.47]*pi/180)*wigner1([0, -pi/2, 0]);
wigner_tot4=wigner_LM*wigner1([gamma2, -pi/2, pi/2]);
wigner_tot5=wigner_LM*wigner1([gamma3, pi/2, pi/2]);
```

```
beta_tot1=acos(wigner_tot1(2,2));
alpha_tot1=real(log(wigner_tot1(3,2)*sqrt(2)/sin(beta_tot1))/i
);
gamma_tot1=-
real(log(wigner_tot1(2,1)*sqrt(2)/sin(beta_tot1))/i);

beta_tot2=acos(wigner_tot2(2,2));
alpha_tot2=real(log(wigner_tot2(3,2)*sqrt(2)/sin(beta_tot2))/i
);
gamma_tot2=-
real(log(wigner_tot2(2,1)*sqrt(2)/sin(beta_tot2))/i);

%15N CSA
beta_tot3=acos(wigner_tot3(2,2));
alpha_tot3=real(log(wigner_tot3(3,2)*sqrt(2)/sin(beta_tot3))/i
);
gamma_tot3=-
real(log(wigner_tot3(2,1)*sqrt(2)/sin(beta_tot3))/i);


term1=D*((3*cos(beta_tot1)^2-
1)/2+3/4*R*sin(beta_tot1)^2*cos(2*alpha_tot1));

term2=D*(sin(beta_tot1)^2*cos(2*gamma_tot1)+R/4*((1+cos(beta_t
ot1))^2*cos(2*(alpha_tot1+gamma_tot1))+(1-
cos(beta_tot1))^2*cos(2*(alpha_tot1-gamma_tot1))));

field(n, 1)=real((s11N+s22N+s33N)/3+(2*s33N-s11N-
s22N)/3*term1+(s11N-s22N)/2*term2);
field(n, 1)=(1+So/2)*(s11N+s22N+s33N)/3-So/2*field(n,1);
%1H-15N dipolar coupling
field(n, 2)=abs(real(chi0*D*((3*cos(beta_tot2)^2-
1)/2+3/4*R*sin(beta_tot2)^2*cos(2*alpha_tot2))));
field(n,2)=So/2*field(n,2);
%Ca-Ha dipolar coupling
field(n, 3)=real(chi1*D*((3*cos(beta_tot3)^2-
1)/2+3/4*R*sin(beta_tot3)^2*cos(2*alpha_tot3)));

%1H CSA
beta_tot4=acos(wigner_tot4(2,2));
alpha_tot4=real(log(wigner_tot4(3,2)*sqrt(2)/sin(beta_tot4))/i
);
gamma_tot4=-
real(log(wigner_tot4(2,1)*sqrt(2)/sin(beta_tot4))/i);
```

```
term3=D*((3*cos(beta_tot4)^2-
1)/2+3/4*R*sin(beta_tot4)^2*cos(2*alpha_tot4));

term4=D*(sin(beta_tot4)^2*cos(2*gamma_tot4)+R/4*((1+cos(beta_t
ot4))^2*cos(2*(alpha_tot4+gamma_tot4))+(1-
cos(beta_tot4))^2*cos(2*(alpha_tot4-gamma_tot4))));

field(n, 4)=real((s11H+s22H+s33H)/3+(2*s33H-s11H-
s22H)/3*term3+(s11H-s22H)/2*term4);

%15N-Ca dipolar coupling

beta_tot5=acos(wigner_tot5(2,2));
alpha_tot5=real(log(wigner_tot5(3,2)*sqrt(2)/sin(beta_tot5))/i
);
gamma_tot5=-
real(log(wigner_tot5(2,1)*sqrt(2)/sin(beta_tot5))/i);

field(n, 5)=real(chi2*D*((3*cos(beta_tot5)^2-
1)/2+3/4*R*sin(beta_tot5)^2*cos(2*alpha_tot5)));

end


%CALCULATION OF THE BACKBONE

wigner_i=wigner1([psi, theta, phi])*wigner1([0, theta_p,
phi_p]);
th1=pi/180*90;
th2=pi/180*90;
th3=pi/180*90;

f1=pi/180*(-124.9);
f2=pi/180*(-60.5);
f3=pi/180*(-118.2);

r1=1.52;
r2=1.33;
r3=1.45;

Y_p=[-sin(th1)*exp(i*f1)/sqrt(2), cos(th1), sin(th1)*exp(-
i*f1)/sqrt(2);
```

```
     -sin(th2)*exp(i*f2)/sqrt(2), cos(th2), sin(th2)*exp(-
i*f2)/sqrt(2);
     -sin(th3)*exp(i*f3)/sqrt(2), cos(th3), sin(th3)*exp(-
i*f3)/sqrt(2)];

 k=1;
 R=zeros(3*N);

for n=1:N

    u=wigner_i*Y_p';

    u_tot(k+0, :)=r1*[real(-u(1,1)*sqrt(2)),
imag(u(1,1)*sqrt(2)), real(u(2,1))];
    u_tot(k+1, :)=r2*[real(-u(1,2)*sqrt(2)),
imag(u(1,2)*sqrt(2)), real(u(2,2))];
    u_tot(k+2, :)=r3*[real(-u(1,3)*sqrt(2)),
imag(u(1,3)*sqrt(2)), real(u(2,3))];
    k=k+3;


wigner_i=wigner_i*wigner1(OMEGA1)*wigner1(OMEGA2);

end

for k=1:3*N
R=R+diag(ones(3*N-k+1,1), -(k-1));
end

B(1,:)=[0,0,0];
B(2:3*N+1,:)=R*u_tot;

%subplot(4,5,order_wheel(pz)+5)

plot(field(:, 1), field(:, 2)/1000, ['-', tilt_color(pz)])
hold on
%plot(field(1, 1), field(1, 2)/1000, 'o r', 'MarkerSize', 4,
'MarkerFace', 'r')


axis([50 150 0e4 4.8])
set(gca, 'XDir', 'reverse')
xlabel('15N Shift (ppm)')
ylabel('1H-15N Dipolar Cplg (kHz)')
```

```
daspect([1 .055 1])
hold on

freqcalc=field(:,1:2);
% for n=1:N
%
%  if freqcalc(n, 1)<200
%  text(freqcalc(n, 1), freqcalc(n, 2)/1000, [' ',
num2str(n)], 'FontSize', 8, 'HorizontalAlignment','left',
'Clipping', 'on', 'FontName','Times');
%  hold on
%  end
%  if freqcalc(n, 1)>=200
%  text(freqcalc(n, 1), freqcalc(n, 2)/1000, [num2str(n),' '],
'FontSize', 8, 'HorizontalAlignment','right', 'Clipping',
'on', 'FontName','Times');
%  hold on
%  end
%
% end

%text(100, 4.7, [num2str(theta*180/pi), '^{o} tilt']);
pz



%subplot(4,5,order_wheel(pz))

%plot3(B(:, 1), B(:, 2), B(:, 3), '- ', 'MarkerSize', 10)
hold on

%plot3(B(3, 1), B(3, 2), B(3, 3), 'o r', 'MarkerSize', 4,
'MarkerFace', 'r')

% axis([-10 30 -10 30 -10 30])
% axis off
% daspect([1, 1, 1])
% view([0 0])
hold on

end
```

Appendix M Protocol for reconstituting Pf1 bacteriophage coat protein into the DMPC/DHPC (q=3.2) bicelles

^{15}N uniformly labeled Pf1 bacteriophage was purchased from Hyglos GmbH (Regensburg, Germany). To get Pf1 coat protein reconstituted in the DMPC/DHPC (q=3.2) bicelles:

1. Measure a calculated amount of Pf1 (normally around 5~6mg), and dissolve in 1ml of TFE(50%)/TFA(0.1%) solution, to remove the DNA.
2. The soluble fraction is then isolated and lyophilized over night.
3. A second round of lyophilization with H_2O is highly recommended to thoroughly remove any residual TFA.
4. Measure 38mg of DMPC and 7mg of DHPC separately, and lyophilize them in different micro centrifuge tubes over night to remove the chloroform.
5. Rehydrate DHPC in 160 μL H_2O, or low strenghth phosphate buffer at around pH6.7.
6. Transfer the solution into the container with Pf1 coat protein. To fully dissolve all the proteins, some mild vortex/heat cycles would be helpful.
7. Adjust the pH of the fully transparent solution to around 6.7.
8. Transfer the solution into the tube with DMPC power. Extensive freeze-thaw cycles (hot water bath at 45 °C to ice to liquid nitrogen) followed by vortex would be necessary.
9. Adjust the pH to 6.7.
10. Some more freeze-thaw cycles until the solution becomes clear and uniform.

The final volume is around 180 μL to fit the NMR tube. Ideally, the final product should be transparent at all temperatures (from 0°C to 45°C), fluid at 0°C, fluid-like at room temperature and glue-like with limited mobility at 45°C.

Appendix N Protocol for reconstituting Pf1 bacteriophage coat protein into DOPC/DOPG (9:1) lipid bilayers inside AAO nanopores

^{15}N uniformly labeled Pf1 bacteriophage was purchased from Hyglos GmbH (Regensburg, Germany). To get Pf1 coat protein reconstituted in the DOPC/DOPG bilayers within the AAO nanopores:

1. Measure a calculated amount of Pf1 (normally around ~3mg), and dissolve in 1ml of TFE(50%)/TFA(0.1%) solution, to remove the DNA.
2. The soluble fraction is then isolated and lyophilized over night.
3. A second round of lyophilization with H_2O is highly recommended to thoroughly remove any residual TFA.
4. Dissolve the Pf1 protein power in TFE.
5. Measure a total weight of 25mg of DOPC and DOPG in the w/w ratio of 10:1 (in chloroform) into a round bottom flask.
6. Transfer the solution in Step 4 into the flask as well, mix well.
7. Subject the mixture to rotary evaporation to remove the solvent and form a thin film.
8. Keep the sample in a desiccator under vacuum over night to thoroughly remove the residual solvent.
9. The next day, remove the sample from the desiccator and add 300 μL H_2O, or low strength buffers at desired pH, with 50mM NaCl.
10. Rotate the flask at a low rate until the film on the wall is ‘melted’ into inhomogeneous liquid.

11. Subject the mixture to water-bath sonication for around 2 hrs.
12. Extensive freeze-thaw cycles followed by vortex until the solution is white and uniform.
13. Take around 30 pieces of the pre-cut AAO slides, and wash them in both water and organic solvent alternatively.
14. After the slides are dry, keep them on a clean surface.
15. Manually deposit 5 μL of the Pf1/lipid solution onto the surface of each slide.
16. Wait until the surface are dried, and flip them over.
17. Deposit another 5 μL of the Pf1/lipid solution onto the other side.
18. Wait for several minutes, and wipe the surface of each AAO slides clean. (Optional)
19. Transfer all the AAO slides back into H_2O or buffer solution that was used in Step 9.
20. Stack the slides together and pack the pile into a NMR tube with spacers.
21. Seal the tube with wax or nail polisher.